

land surface  
temperature  
cci



CCI Land Surface Temperature

## Climate Assessment Report

WP5.1 – DEL-5.1

Ref.: LST-CCI-D5.1-CAR

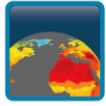
Date: 25-May-2024

Organisation: LST\_cci Consortium



## Signatures

	Name	Organisation	Signature
Written and Edited	Lizzie Good	Met Office	
Written contributions	Josh Blannin	Met Office	
	Ioanna Karagali	DMI	
	Panagiotis Sismanidis	RUB	
	Sorin Cheval, Alexandru Dumitrescu, Dana Micu	MeteoRomania	
	R. Niclòs, M. Perelló, S. Arribas, & J. Puchades	U. Valencia	
	Bethan Harris	CEH	
	Shaerdan Shataer	U. Reading	
	Elody Fluck	ESA	
	Francisco José Cuesta Valero	Helmholtz-Centre for Environmental Research	
	Amina Maroini	ESA	
Reviewed by	Darren Ghent	ULeic	
Approved by	Darren Ghent	ULeic	
Authorized by	Simon Pinnock	ESA	



## Change log

Version	Date	Changes
1.0	17-Dec-2020	First version of Phase 1
2.0	20-Dec-2021	Second version of Phase 1
3.0	25-May-2024	First version of Phase 2

## Table of Content

<b>EXECUTIVE SUMMARY</b> -----	<b>1</b>
<b>1. INTRODUCTION</b> -----	<b>3</b>
1.1. Purpose and scope -----	3
1.2. Structure of the document-----	4
1.3. Definition of terms -----	7
<b>2. LST_CCI USER CASE STUDY REPORTS</b> -----	<b>11</b>
<b>2.1. UCS#1: Development of moderate extreme indices based on LST (Lizzie Good &amp; Josh Blannin, Met Office) 11</b>	
2.1.1. Key Messages -----	11
2.1.2. Scientific Analysis -----	11
2.1.3. Feedback on scientific utility of the LST_cci products -----	22
<b>2.2. UCS#2: Impact of CCI LST IST products from MODIS and SLSTR on the Arctic SST/IST Multi-Year (MY) Product of the Copernicus Marine Service (Ioanna Karagali, Adrien Combelles and Pia Englyst, DMI) 25</b>	
2.2.1. Key Messages -----	25
2.2.2. Scientific Analysis -----	25
2.2.3. Feedback on scientific utility of the LST_cci products -----	31
<b>2.3. UCS#3: Global SUHI Trend Analysis (Panagiotis Sismanidis, RUB) -----</b>	<b>32</b>
2.3.1. Key Messages -----	32
2.3.2. Scientific Analysis -----	32
2.3.3. Feedback on scientific utility of the LST_cci products -----	38
<b>2.4. UCS#5: Evaluating the Surface Urban Heat Island Intensity using the SENTINEL3x_SLSTR_L3C_0.01 products (Sorin Cheval, Alexandru Dumitrescu and Dana Micu, MeteoRomania): -----</b>	<b>38</b>
2.4.1. Key Messages -----	38
2.4.2. Scientific Analysis -----	39
2.4.3. Feedback on scientific utility of the LST_cci products -----	46
<b>3. OTHER CRG STUDY REPORTS</b> -----	<b>47</b>
<b>3.1. Evaluation of v4 LST_cci products and study of LST trends in Spain (R. Niclòs, M. Perelló, S. Arribas, &amp; J. Puchades, University of Valencia) -----</b>	<b>47</b>
1.1.1 Key Messages -----	47
1.1.2 Scientific Analysis -----	48
1.1.3 Feedback on scientific utility of the LST_cci products-----	56
<b>3.1. SUBDROUGHT: Subseasonal-to-seasonal drought and heatwave evolution via land-atmosphere interactions (Bethan Harris, ESA CCI fellowship, UK Centre for Ecology &amp; Hydrology/National Centre for Earth Observation) -----</b>	<b>56</b>
3.1.1. Scientific Analysis -----	56
3.1.2. Feedback on scientific utility of the LST_cci products -----	57
<b>4. NON-CRG STUDY REPORTS</b> -----	<b>59</b>
<b>4.1. Downscaling Daily Land Surface Temperature (Shaerdan Shataer, University of Reading)-----</b>	<b>59</b>
4.1.1. Scientific Analysis -----	59
4.1.2. Feedback on scientific utility of the LST_cci products -----	59
<b>4.1. 25 years assessment of Hot and Dry Weather Compound Events in Europe (Elody Fluck, ESA) ----</b>	<b>60</b>
4.1.1. Scientific Analysis -----	60
4.1.2. Feedback on scientific utility of the LST_cci products -----	61
<b>4.2. AI4GHEObs: Ground Heat Flux from satellite data (Francisco José Cuesta Valero, Helmholtz-Centre for Environmental Research – UFZ) -----</b>	<b>61</b>
4.2.1. Scientific Analysis -----	61
4.2.2. Feedback on scientific utility of the LST_cci products -----	62

<b>4.3. Evaluating heat extremes in the Sahel using LST_cci data (Amina Maroini, ESA Graduate Trainee project)</b> -----	<b>64</b>
4.3.1. Scientific Analysis -----	64
4.3.2. Feedback on scientific utility of the LST_cci products -----	69
<b>5. SUMMARY OF USER FEEDBACK AND RESPONSE FROM THE SCIENCE TEAM</b> -----	<b>70</b>
<b>5.1. General Feedback</b> -----	<b>70</b>
<b>5.2. Product-Specific Feedback</b> -----	<b>70</b>
5.2.1. MODIS/Aqua v4.aa-----	70
5.2.2. SLSTR/Sentinel-3B v3.0 -----	71
5.2.3. SLSTR/Sentinel-3A & -B v4.aa -----	72
5.2.4. IRMGP v1.00 -----	73
5.2.5. SSM/I & SSMIS MW product v2.33-----	74

## List of Figures

Figure 2-1: Stations used to produce the HadEX3 data set using the 1981-2010 baseline period (left; see [RD-01] Figure A1 for the 1961-1990 baseline period). -----12

Figure 2-2: AR6 regions (top: figure source [https://regionmask.readthedocs.io/en/stable/defined\\_scientific.html#ar6-regions](https://regionmask.readthedocs.io/en/stable/defined_scientific.html#ar6-regions) and references therein) and the GHCNd stations that fall within each of the 45 land regions (colours have no meaning other than to denote different AR6 regions) Note that not all stations on this map provide Tmin/Tmax data over the study period. -----16

Figure 2-3: Distributions of spatially and temporally colocated T2m and LST observations over AR6 regions 1 (top) and 16 (bottom). The LST\_cci6am distribution represents minimum LST where there are two LST overpasses and the LST at 6 am for days and locations with only one overpass. Similarly, the LST\_cci6pm distribution represents maximum LST where there are two LST overpasses and the LST at 6 pm for days and locations with only one overpass. -----17

Figure 2-4: Distributions of LST values for days where the threshold-based indices are triggered by the T2m observations in AR6 region 1 (left: maximum LST or LST at 6pm, right: minimum LST or LST at 6 am). ---19

Figure 2-5: Distributions of LST values for days where the threshold-based indices are triggered by the T2m observations in AR6 region 16 (left: maximum LST or LST at 6pm, right: minimum LST or LST at 6 am). --19

Figure 2-6: Timeseries of T2m (blue) and LST (orange) mean percentage of days per month that are above (below) the 90th (10th) percentiles averaged over all stations in the bespoke test region. Plots show a) TX10p, b) TX90p, c) TN10p, and d) TN90p (see Table 2-3).-----21

Figure 2-7: Average seasonal MW LST data availability over Asia as a percentage of the complete timeseries for the ascending overpass between 1996-2012. Data availability refers to the percentage of data points in a time series not labelled as “missing” because of either no measurements being taken or having been removed by applying quality flags. MAM is March/April/May, JJA is June/July/August, SON is September/October/November and DJF is December/January/February. -----23

Figure 2-8: Average seasonal MW LST data availability over the USA as a percentage of the complete timeseries for the ascending overpass between 1996-2012. Data availability refers to the percentage of data points in a time series not labelled as “missing” because of either no measurements being taken or having been removed by applying quality flags. MAM is March/April/May, JJA is June/July/August, SON is September/October/November and DJF is December/January/February. -----24

Figure 2-9: USA rice yields in 2012 for the US Department of Agriculture. Regions of high rice yield show marked similarity to regions with stippled, low data availability in Figure 2-3. (Source: USDA Census of Agriculture Historical Archive - Ag Atlas (census year: 2012) – Crops and Plants – Rice, Harvested Acres. Retrieved at: [https://agcensus.library.cornell.edu/census\\_parts/2012-agricultural-atlas/](https://agcensus.library.cornell.edu/census_parts/2012-agricultural-atlas/). Last access: 29/03/2023).-----24

Figure 2-10: Schematic diagram illustrating the processing steps of the DMIOI L4 Processing System. ---27

Figure 2-11: In situ observation data obtained during 2021 used in the study. -----28

Figure 2-12: 2-d plots of the mean bias between various IST products: MODIS/Aqua minus MODIS/Terra on top left, MODIS/Aqua minus AASTI on top middle, MODIS/Terra minus AASTI on top right, SLSTR/S3-A minus SLSTR/S3-B on bottom left, SLSTR/S3-A minus AASTI on bottom middle and SLSTR/S3-A minus MODIS/Terra on bottom right. All spatially averaged biases are for 2021. -----29

Figure 2-13: Time-series of mean daily biases between MODIS/Aqua and AASTI (left) and SLSTR/S3-A and AASTI (right) for 2021. -----29

Figure 2-14: Time-series of spatially averaged daily mean temperature (top left), median temperature (top right), standard deviation of the temperature (bottom left) and number of points used in the spatial averaging (bottom right) for MODIS/Aqua (red), MODIS/Terra (blue), SLSTR/S3-A (magenta), SLSTR/S3-B (grey) and AASTI (yellow) for 2021. -----30

Figure 2-15: Example of L3S and L4 OI IST/SST product along with the surface mask and uncertainty estimates. Observed stability:  $-0.0001$  °C/year and  $0.0047$  °C/year against drifters (SST) and North Pole (NP) drifting buoys (IST) observations. -----31

Figure 2-16: The distribution of nighttime LST trends (2002-2021) across the globe. -----35

Figure 2-17: The distribution of the LST trends per climate zone (a) and as function of latitude (b). -----35

Figure 2-18: The LST observations, monthly means, monthly anomalies, and Thei-Sen slope (trend) for a) Doha, Qatar; b) Hafar Al Batin (Saudi Arabia); and c) Kirkuk, Iraq. -----36

Figure 2-19: Agreement between the 2002-2021 nighttime LST, Tair (a) and SKT (b) trends for the urban areas included in this analysis. The dashed line is the  $y=x$ . The dots are plotted with the same hue of blue and some level of transparency; darker blues imply that several dots overlap. -----37

Figure 2-20: Location of the 156 weather stations of the National Meteorological Network delivering T2m values. -----39

Figure 2-21: Average monthly night-time LST (°C) over Romania in 2020, derived from L3C-LST-SLSTRA-0.01. -----40

Figure 2-22: Correlation (COR) and Mean Absolute Errors (MAE) between L3C-LST-SLSTRA-0.01deg and weather station air temperature (WS T2m) for the different altitude categories (top of each column, in m above sea level). -----41

Figure 2-23: Correlation (COR) and Mean Absolute Errors (MAE) between LST\_cci retrieved from L3C-LST-SLSTRB-0.01deg and weather station air temperature (WS T2m) for the different altitude categories (top of each column, in m above sea level). -----42

Figure 2-24: Summary statistics for LST\_cci retrieved from L3C-LST-SLSTRA-0.01 and weather station air temperature (WS T2m) for each year. -----42

Figure 2-25: Summary statistics for LST\_cci retrieved from L3C-LST-SLSTRB-0.01 and weather station air temperature (WS T2m) for each year. -----43

Figure 2-26: Spatial distribution of the correlation coefficients (COR) between the LST\_cci retrieved from L3C-LST-SLSTRx-0.01 and weather station air temperature (WS T2m). -----43

Figure 2-27: Spatial distribution of the mean absolute error (MAE) between the LST\_cci retrieved from L3C-LST-SLSTRx-0.01, and weather station air temperature (WS T2m). -----43

Figure 2-28: Land Cover Classes over Craiova city (Romania) retrieved from the L3C-LST-SLSTRA-0.01 product, for 13 June 2016 and 16 June 2016. The figures in the legend stand for: 10 - cropland\_rainfed, 11 - cropland\_rainfed\_herbaceous\_cover, 12 - cropland\_rainfed\_tree\_or\_shrub\_cover, 30 - mosaic\_cropland, 60 - tree\_broadleaved\_deciduous\_closed\_to\_open, 130 - grassland, 190 – urban. ---44

Figure 2-29: Daily range of the L3C-LST-SLSTRA-0.01 and L3C-LST-SLSTRB-0.01 at the country level in each season. -----44

Figure 2-30: Delimitation of areas for computing LST\_cci<sub>urban</sub> and LST\_cci<sub>rural</sub>. The example is for Braşov City (Romania). The rural buffer is drawn at  $\frac{1}{2}$  \* average distance between the city centroid (blue dot) and nodes of the urban administrative perimeter (red dots). -----45

Figure 2-31: Web-based interface for visualising and analysing the SUHII of the Bucharest city. -----46

Figure 3-1: Comparison of LSTs obtained for the Valencia Test site coordinates from the EOS Aqua – MODIS products against ground LSTs. Results for versions 1 to 4 AQUA\_MODIS\_L3C products and v061 MYD11\_L2 and MYD21 operational products are shown for daytime only, when ground measurements along transects were acquired.-----52

Figure 3-2: Comparison of LSTs obtained for the Valencia Test coordinates from the EOS Terra – MODIS products against ground LSTs. Results for versions 1 to 4 TERRA\_MODIS\_L3C products and v061 MOD11\_L2 and MOD21 operational products are shown for daytime only, when ground measurements along transects were acquired.-----52

Figure 3-3: Annual AQUA MODIS LST\_cci v4 trends in the Iberian Peninsula for (a) daytime and (b) nighttime mean seasonal temperatures. -----55

Figure 4-1: LST (left half of each image above) and maximum daily T2m from the HadUK-Grid dataset [RD-31] (right half of each image shown) showing data scarcity (white space) and cloud contamination (cold temperatures shown in blue) in the LST data. -----60

Figure 4-2: Example of the LST\_cci MW LST product for a day in 1996 in ASC and DES mode. Some regions in Europe are covered twice by the swaths; but some other regions in Europe are not covered at all. ---61

Figure 4-3: Plot of ESACCI-LST-L3S-LST-IRMGP\_-0.05deg\_1MONTHLY-20180701120000-fv1.00.nc showing valid LSTs in the ocean off the coast of S. America. -----62

Figure 4-4: (Top) Time series of mean global monthly actual LST from the MW LST\_cci product v2.33. The numerical values of the trends are also shown on the plot where ‘raw’ refers to the MW LST data without applying the LST correction for orbital drift and ‘fixed’ refers to the MW LST data where the orbital drift LST correction has been applied. (Bottom) Geographical distribution of trends in the actual MW LST monthly data where the orbital drift LST correction has been applied. Red indicates positive trends and blue negative trends in the data. The units of the trend are in K per month. -----63

Figure 4-5: Distribution of the 75 GSOD NOAA stations in the Sahel region. -----65

Figure 4-6: Monthly anomalies of Tx during 2010 with respect to the 1996-2020 baseline for ERA5 T2m (left) and MW LST\_cci (right) -----67

Figure 4-7: Monthly climatology of the Number of Hot Days (NHD) over the Sahel for the period 1996-2020 using ERA5 data (left) and using MW LST\_cci data (right).-----68

Figure 4-8: Monthly anomaly of maximum temperature (TX) over Diiori Hamani (Niger) station for the period 1996-2020-----68

Figure 4-9: Monthly Number of Hot Days (NHD) over Diiori Hamani (Niger) station for the period 1996-2020-----68

### List of Tables

Table 1-1: Proposed LST products for both LST\_cci Phase-1 (2018-2022) and LST\_cci Phase-2 (2022-2025). For instrument (e.g. ATSR-2), satellite (e.g. ERS-2) and product (e.g. L2P) acronyms, please see Section 1.3. ----- 5

Table 2-1: List of threshold-based Climpect indices tested in the study (see <https://climpect-sci.org/>).--13

Table 2-2: List of value-based Climpect indices tested in the study (see <https://climpect-sci.org/>). -----14

Table 2-3: List of percentile-based Climpect indices tested in the study (see <https://climpect-sci.org/>). -15

Table 2-4: A summary of LST\_cci products used for this study. -----15



Table 2-5: Mean Climact Index values for the threshold- and value-based indices across all station locations in AR6 region 1 (NW North America).-----18

Table 2-6: Mean Climact Index values for the threshold- and value-based indices across all station locations in AR6 region 16 (Northern Europe).-----18

Table 2-7: Unadjusted and adjusted thresholds for LST for selected threshold-based Climact indices. -20

Table 2-8: Results using unadjusted and adjusted thresholds for LST for selected threshold-based Climact indices for the bespoke test region.-----21

Table 2-9: A summary of LST\_cci products used in this study. -----26

Table 2-10: Validation results for 2021 between ESA LST\_cci products from MODIS and SLSTR for IST and in situ stations. The metrics for the AASTI v2.1 IST dataset and the L4 SST/IST MY product are also shown for reference. Note that the in situ data represent T2m while the satellite data are IST. Therefore, a non-zero difference is expected in this comparison due to the inherent differences between IST/LST and T2m (see text). -----27

Table 2-11: The LST\_cci products used for this study. -----33

Table 2-12: A summary of LST\_cci products used in this study.-----39

Table 3-1: A summary of LST\_cci products used for this study. -----49

Table 3-2: Results of the evaluation of the different versions of the AQUA MODIS LST\_cci products.----51

Table 3-3: Results of the evaluation of the operational v006 and v061 products for EOS Aqua - MODIS. 51

Table 3-4: Results of the evaluation of the different versions of the TERRA MODIS LST\_cci products. ----51

Table 3-5: Results of the evaluation of the operational v006 and v061 products for EOS Terra - MODIS. No v006 MOD21 product was available for the study period. -----51

Table 3-6: Results of the evaluation of the SENTINEL3A\_SLSTR\_L3C LST\_cci product and the operational one together with the alternative E-SWA proposed for the SLSTR data in Sentinel-3A. -----53

Table 3-7: Results of the evaluation of the SENTINEL3B\_SLSTR\_L3C LST\_cci product and the operational one together with the alternative E-SWA proposed for the SLSTR data in Sentinel-3B. -----54

Table 3-8: LST trends results obtained for the whole year using the full v4 AQUA MODIS LST\_cci dataset. -----54

Table 3-9: A summary of LST\_cci products used for this study. -----57

Table 4-1: A summary of LST\_cci products used for this study. -----59

Table 4-2: A summary of LST\_cci products used for this study. -----60

Table 4-3: A summary of LST\_cci products used for this study. -----62

Table 4-4: A summary of LST\_cci products used for this study. -----64

## Applicable Documents

Identity	Reference
AD-01	LST_cci (2021) Product User Guide, Reference LST-CCI-D4.3-PUG

## Reference Documents

Identity	Reference
RD-01	Dunn, R. J. H., et al. (2020), Development of an updated global land in-situ-based dataset of temperature and precipitation extremes: HadEX3, JGR-A, 125, e2019JD032263
RD-02	IPCC, 2021: Climate Change 2021: The Physical Science Basis. Contribution of Working Group I to the Sixth Assessment Report of the Intergovernmental Panel on Climate Change [Masson-Delmotte, V., P. Zhai, A. Pirani, S.L. Connors, C. Péan, S. Berger, N. Caud, Y. Chen, L. Goldfarb, M.I. Gomis, M. Huang, K. Leitzell, E. Lonnoy, J.B.R. Matthews, T.K. Maycock, T. Waterfield, O. Yelekçi, R. Yu, and B. Zhou (eds.)]. Cambridge University Press, Cambridge, United Kingdom and New York, NY, USA, In press, doi: <a href="https://doi.org/10.1017/9781009157896">10.1017/9781009157896</a> .
RD-03	Menne, M.J., Durre, I., Vose, R.S., Gleason, B.E. and Houston, T.G., 2012. An overview of the global historical climatology network-daily database. <i>Journal of atmospheric and oceanic technology</i> , 29(7), pp.897-910, doi: <a href="https://doi.org/10.1175/JTECH-D-11-00103.1">https://doi.org/10.1175/JTECH-D-11-00103.1</a> . Last access 07/02/2023
RD-04	Good, E. J., et al. (2022). An analysis of the stability and trends in the LST_cci Land Surface Temperature datasets over Europe. <i>Earth and Space Science</i> , 9, e2022EA002317. <a href="https://doi.org/10.1029/2022EA002317">https://doi.org/10.1029/2022EA002317</a>
RD-05	Nielsen-Englyst et al. (2023), 'A combined sea and sea-ice surface temperature climate dataset of the Arctic, 1982–2021', <i>Remote Sensing of Environment</i> , 284, 113331, <a href="https://doi.org/10.1016/j.rse.2022.113331">https://doi.org/10.1016/j.rse.2022.113331</a>
RD-06	Nielsen-Englyst et al. (2019), 'In situ observed relationships between snow and ice surface skin temperatures and 2 m air temperatures in the Arctic', <i>Cryosphere</i> , 13 (2019), pp. 1005-1024, <a href="https://doi.org/10.5194/tc-13-1005-2019">https://doi.org/10.5194/tc-13-1005-2019</a>
RD-07	Krelaus, L., Apfel, J., Bechtel, B., & Sismanidis, P. (2023). Surface and canopy-layer urban heat island intensities in Europe—Quantifying differences in the diurnal cycle for three summer periods. In <i>2023 Joint Urban Remote Sensing Event (JURSE)</i> (pp. 1-4). <a href="https://doi.org/10.1109/JURSE57346.2023.10144174">https://doi.org/10.1109/JURSE57346.2023.10144174</a> .
RD-08	Bulgin, C.E., Embury O., and Merchant C.J.. (2016). "Sampling Uncertainty in Gridded Sea Surface Temperature Products and Advanced Very High Resolution Radiometer (AVHRR) Global Area Coverage (GAC) Data." <i>Remote Sensing of Environment</i> 177 (May): 287–94. <a href="https://doi.org/10.1016/j.rse.2016.02.021">https://doi.org/10.1016/j.rse.2016.02.021</a> .
RD-09	Sutton AJ, Battisti R, Carter B, Evans W, Newton J, Alin S, Bates NR, Cai W-J, Currie K, Feely RA, Sabine C, Tanhua T, Tilbrook B and Wanninkhof R (2022) Advancing best practices for assessing trends of ocean acidification time series. <i>Front. Mar. Sci.</i> 9:1045667. doi: 10.3389/fmars.2022.1045667
RD-10	Sen, P. K. (1968), Estimates of the regression coefficient based on Kendall's tau, <i>J. Am. Stat. Assoc.</i> , 63, 1379–1389.

Identity	Reference
RD-11	Weatherhead, E. C., Reinsel, G. C., Tiao, G. C., Meng, X.-L., Choi, D., Cheang, W.-K., et al. (1998). Factors affecting the detection of trends: Statistical considerations and applications to environmental data. <i>Journal of Geophysical Research: Atmospheres</i> , 103(D14), 17149–17161. <a href="http://dx.doi.org/10.1029/98JD00995">http://dx.doi.org/10.1029/98JD00995</a>
RD-12	Hersbach H, Bell B, Berrisford P, et al. The ERA5 global reanalysis. <i>Q J R Meteorol Soc.</i> 2020; 146: 1999–2049. <a href="https://doi.org/10.1002/qj.3803">https://doi.org/10.1002/qj.3803</a>
RD-13	Cheval, S., Dumitrescu, A., Iraşoc, A., Paraschiv, M.-G., Perry, M., & Ghent, D. (2022). MODIS-based climatology of the Surface Urban Heat Island at country scale (Romania). <i>Urban Climate</i> , 41, 101056. <a href="https://doi.org/10.1016/j.uclim.2021.101056">https://doi.org/10.1016/j.uclim.2021.101056</a>
RD-14	Coll, C., Caselles, V., Galve, J.M., Valor, E., Niclòs, R., Sánchez, J.M., Rivas, R. (2005). Ground measurements for the validation of land surface temperatures derived from AATSR and MODIS data. <i>Rem. Sens. Environ.</i> 97, 288–300.
RD-15	Niclòs, R., Pérez-Planells, Ll., Valiente, J.A., Coll, C., Valor, E., 2018. Evaluation of the S-NPP VIIRS Land Surface Temperature product using ground data acquired by an autonomous system at a rice paddy. <i>ISPRS J. Photogramm. Remote Sens.</i> 135, 1-12.
RD-16	Niclòs, R., Galve, J.M., Valiente, J.A., Estrela, M.J., Coll, C. 2011. Accuracy assessment of land surface temperature retrievals from MSG2-SEVIRI data. <i>Remote Sens. Environ.</i> 115, 2126–2140.
RD-17	Niclòs, R., Perelló, M., Puchades, J., Coll, C., Valor, E., 2023. Evaluating Landsat-9 TIRS-2 calibrations and land surface temperature retrievals against ground measurements using multi-instrument spatial and temporal sampling along transects, <i>International Journal of Applied Earth Observation and Geoinformation</i> , 125, 103576.
RD-18	Pérez-Planells, L., Niclòs, R., Puchades, J., Coll, C., Götsche, F.-M., Valiente, J.A., Valor, E., Galve, J.M. 2021. Validation of Sentinel-3 SLSTR Land Surface Temperature Retrieved by the Operational Product and Comparison with Explicitly Emissivity-Dependent Algorithms. <i>Remote Sens.</i> , 13, 2228.
RD-19	Wan, Z., Dozier, J., 1996. A generalized split-window algorithm for retrieving land-surface temperature from space. <i>IEEE Trans. Geosci. Remote Sens.</i> 34, 892–905.
RD-20	Wan, Z., 2014. New refinements and validation of the collection-6 MODIS land-surface temperature/emissivity product. <i>Remote Sens. Environ.</i> 140, 36–45.
RD-21	Gillespie, A.R., Matsunaga, T., Rokugawa, S., Hook, S.J., 1998. Temperature and emissivity separation from Advanced Spaceborne Thermal Emission and Reflection Radiometer (ASTER) images. <i>IEEE Trans. Geosci. Rem. Sens.</i> 36, 1113–1125.
RD-22	Hulley, G. C., S. J. Hook, and A. M. Baldridge (2011), Generating consistent land surface temperature and emissivity products between ASTER and MODIS data for Earth science research, <i>IEEE Trans. Geosci. Remote Sens.</i> , 49(4), 1304–1315, doi:10.1109/TGRS.2010.2063034.
RD-23	Ghent, D.J., Remedios, J.J. Dodd, E., 2021. Sentinel-3 optical products and algorithm definition. SLSTR ATBD land surface temperature. S3-L2-SD-03-T03-ULNILU-ATBD_L2LST.
RD-24	Coll, C., Niclòs, R., Puchades, J., García-Santos, V., Galve, J.M., Pérez-Planells, Ll., Valor, E., Theocharous, E. (2019). Laboratory calibration and field measurement of land surface temperature and emissivity using thermal infrared multiband radiometers. <i>Int. J. Appl. Earth Obs. Geoinformation</i> , 78, 227-239.
RD-25	Theocharous, E., N. P. Fox , I. Barker-Snook , R. Niclòs, V. Garcia Santos, P. J. Minnett, F. M. Götsche, L. Poutier, N. Morgan , T. Nightingale, W. Wimmer, J. Høyer , K. Zhang , M. Yang , L. Guan, M. Arbelo, and C. J. Donlon (2019). The 2016 CEOS Infrared Radiometer Comparison: Part II: Laboratory Comparison of Radiation Thermometers. <i>Journal of Atmospheric and Oceanic Technology</i> , 1079–1092. 10.1175/JTECH-D-18-0032.1.

Identity	Reference
RD-26	Yamada, Y., Harris, S., Hayes, M., Simpson R., Wimmer, W., Holmes, R., Nightingale, T., Lee, A., Jepsen, N., Morgan, N., Götsche, F.M., Niclòs, R., Perelló, M., Donlon, C., Fox, N., 2024. 2022 CEOS International Thermal Infrared Radiometer Comparison. Part I: Laboratory Comparison of Radiometers and Blackbodies. <i>Journal of Atmospheric and Oceanic Technology</i> , 41(3), 295–307.
RD-27	Guillevic, P., Götsche, F., Nickeson, J., Hulley, G., Ghent, D., Yu, Y., Trigo, I., Hook, S., Sobrino, J.A., Remedios, J., Román, M., Camacho, F. (2018). Land surface temperature product validation best practice protocol version 1.1. <i>Best Pract. Satell. L. Prod. Valid.</i> (p. 60) <i>L. Prod. Valid. Subgr.</i> doi, 58. <a href="https://doi.org/10.5067/doc/ceoswgc/lpv/lst.001">https://doi.org/10.5067/doc/ceoswgc/lpv/lst.001</a> .
RD-28	Hulley, G.C., Hook, S.J., 2009. The North American ASTER Land Surface Emissivity Database (NAALSED). Version 2.0. <i>Remote Sens. Environ.</i> , 113, 1967–1975.
RD-29	Hirsch, R.M., Slack, J.R., 1984. A Nonparametric Trend Test for Seasonal Data with Serial Dependence. <i>Water Resources Research</i> , 20(6), 727-732
RD-30	Liu, J., Hagan, D.F.T., Liu, Yi, 2021. Global Land Surface Temperature Change (2003–2017) and Its Relationship with Climate Drivers: AIRS, MODIS, and ERA5-Land Based Analysis. <i>Remote Sens.</i> , 13(1), 44.
RD-31	Met Office; Hollis, D.; McCarthy, M.; Kendon, M.; Legg, T.; Simpson, I. (2018): HadUK-Grid gridded and regional average climate observations for the UK. Centre for Environmental Data Analysis, date of citation. <a href="http://catalogue.ceda.ac.uk/uuid/4dc8450d889a491ebb20e724debe2dfb">http://catalogue.ceda.ac.uk/uuid/4dc8450d889a491ebb20e724debe2dfb</a>
RD-32	Thom, E. C. (1959). The Discomfort Index. <i>Weatherwise</i> , 12(2), 57–61. <a href="https://doi.org/10.1080/00431672.1959.9926960">https://doi.org/10.1080/00431672.1959.9926960</a>
RD-33	Epstein Y, Moran DS. Thermal comfort and the heat stress indices. <i>Ind Health</i> . 2006 Jul;44(3):388-98. doi: 10.2486/indhealth.44.388. PMID: 16922182.
RD-34	Oueslati, B. , B. Pohl , V. Moron , S. Rome , and S. Janicot , 2017: Characterization of heat waves in the Sahel and associated physical mechanisms. <i>J. Climate</i> , 30, 3095–3115, <a href="https://doi.org/10.1175/JCLI-D-16-0432.1">https://doi.org/10.1175/JCLI-D-16-0432.1</a>

## Executive Summary

This document represents the first Climate Assessment Report (CAR) for the European Space Agency (ESA) Climate Change Initiative (CCI) for Land Surface Temperature (LST) LST\_cci project Phase-2 (<https://climate.esa.int/en/projects/land-surface-temperature/>). It comprises reports from the funded LST\_cci project User Case Studies (UCS) and other studies that have used LST\_cci data sets that have been produced in both Phase-1 and Phase-2 of the project. These studies demonstrate that the LST\_cci products can be used for a wide range of climate applications and include the following areas of research:

- ❖ Development of moderate extreme indices based on LST
- ❖ Impact of LST\_cci Ice Surface Temperature (IST) products from MODIS and SLSTR on the Arctic SST/IST Multi-Year (MY) Product of the Copernicus Marine Service
- ❖ Global Surface Urban Heat Island Intensity (SUHI) Trend Analysis
- ❖ Evaluating the Surface Urban Heat Island Intensity using the SENTINEL3 SLSTR LST\_cci products
- ❖ Evaluation of v4 LST\_cci products and study of LST trends in Spain
- ❖ Subseasonal-to-seasonal drought and heatwave evolution via land-atmosphere interactions
- ❖ Downscaling Daily Land Surface Temperature
- ❖ 25 years assessment of Hot and Dry Weather Compound Events in Europe
- ❖ Ground Heat Flux from satellite data
- ❖ Evaluating heat extremes in the Sahel using LST\_cci data

Some of these studies are still underway, but the feedback collected here is made available to the LST\_cci Science Team to further develop and improve the LST\_cci data sets and plan for the next phases of the project. This document will be updated towards the end of the LST\_cci Phase-2, which will include final results from the UCS conducted within the project and other studies wherever possible.

Overall user feedback on the LST\_cci products is generally very positive. In particular:

- ❖ The data are generally easy to use and the NetCDF formatting of the data files is widely appreciated.
- ❖ The provision of multiple LST datasets in a common format from a single source is a major strength of the LST\_cci project.
- ❖ The data are generally high quality.
- ❖ The provision of uncertainty information is useful and some users are now using these data in their applications.
- ❖ The provision of colocated auxiliary data in some of the LST\_cci products significantly enhances the user experience (e.g. reanalysis 2m air temperature & skin temperature, land cover classification and Normalised Difference Vegetation Index). It is a strong recommendation of this report that provision of these data is extended to all LST\_cci products.

However, some improvements to the products and related documentation are also noted. In particular:

- ❖ The Product User Guide (PUG) could be updated to provide more detailed information on data availability (or coverage), as a few studies have reported problems in using data as data availability is sparser than expected and there is a lack of information on how missing whole days of data are handled in the products.

- ❖ While the data quality is generally considered high, there are some localised issues with the product accuracy, in particular the newly added ice surface temperatures in the Arctic are found to be several K too cold.
- ❖ Users report that the significant cloud contamination problem in the Phase-1 MODIS LST\_cci products has been improved in the updated versions produced in Phase-2. However, there seems to be significant cloud contamination issues in the SLSTR products from Phase-1 and Phase-2.

The studies presented here provide highly relevant feedback for the Science Team to improve the performance of the LST\_cci products from both Phase-1 and Phase-2. The Science Team have, in parallel, been working on improvements to these products and have taken on board feedback from users throughout the project. A new 'issues and updates log' is being trialled in the project via public folder on Jasmin ('The UK's data analysis facility for environmental science': <https://jasmin.ac.uk/>), where the LST\_cci Phase-2 beta products are also made available to trailblazer users. This log provides a record of new beta product releases and dataset issues, reported by both the Science Team and users, to keep all parties informed about the datasets and related feedback, and how this feedback is being addressed. While the focus of this report is on an independent climate assessment of the LST\_cci products, detailed information on the wider context of how the project is responding to the feedback is also provided.

# 1. Introduction

## 1.1. Purpose and scope

The European Space Agency's (ESA's) Climate Change Initiative (CCI) project aims to provide a comprehensive and timely response to the challenging requirements set by the Global Climate Observing System (GCOS) and the Committee on Earth Observation Satellites (CEOS) for highly stable, long-term, satellite-based products for climate research.

Space observations provide unique information that cannot be obtained from traditional ground stations – they can provide better spatial coverage and resolution, and records are now approaching the time periods required for climate research. As part of the CCI project, a total of 26 Essential Climate Variables (ECVs) have been targeted. The Land Surface Temperature (LST) ECV was added during the second phase of the CCI programme. Now in its seventh year, the LST\_cci project aims to deliver a significant improvement on the capability of current satellite LST data records to meet the GCOS requirements for climate applications and realise the full potential of long-term LST data for climate science (<https://climate.esa.int/en/projects/land-surface-temperature/>).

The LST\_cci project has developed new LST products for a range of satellites that include instruments operating at both infrared (IR) and microwave (MW) wavelengths, and in polar-orbiting and geostationary orbit (Table 1-1). During LST\_cci Phase-1 (2018-2022), 14 new LST\_cci products were produced. A further nine LST\_cci products are currently under development in LST\_cci Phase-2 (2022-2025), in addition to extending and improving the products from Phase-1. Throughout the project, early (beta) versions of these products have been made available to selected users who are (i) performing dedicated user case studies (UCS) that are funded through the LST\_cci project, (ii) users from other CCI projects (e.g. CCI for Vegetation) and the CCI Climate Modelling User Group (CMUG), and (iii) other users who are in direct contact with the LST\_cci science team. These trailblazer users are critical to the success of the project as they can provide early feedback and assessment of the LST\_cci data that can be used to improve the products while they are being developed and before they are officially released to the wider public. Once tested and validated, the LST\_cci products are made publicly available through the ESA CCI Open Data Portal (ODP; <https://climate.esa.int/en/data/#/dashboard>). Many of the improvements made to LST\_cci products between the beta versions and official products released via the ODP have resulted from feedback from the trailblazer users.

As ESA's CCI programme targets the production of data sets that can be used for climate research, a crucial requirement is to assess the suitability and utility of these data from a climate-science perspective. Across CCI, this is performed through the Climate Assessment Reports (CAR) that are produced by each CCI ECV project. This document presents the CAR version 1 (v1) for Phase-2 of the LST\_cci project; the CAR v2 will be produced at the end of Phase-2 in mid-2025. The objective of the report is to demonstrate how the LST\_cci data can be used in scientific studies and provide information on their suitability for use in climate applications. The CAR focuses on both climate-critical aspects of the data, such as stability and homogeneity, and the utility and presentation of the data in a way that is useful for climate applications. The assessment is based on reports from the User Case Studies (UCS) funded through the LST\_cci project and other studies that are not directly funded through the project. Some of these non-funded studies



have been performed by members of the LST\_cci Climate Research Group (CRG), which comprises a group of early LST\_cci data users, including the LST\_cci UCS partners. At the time of writing, the members of the LST\_cci CRG are:

- ❖ Lizzie Good (Met Office, LST\_cci CRG lead & LST\_cci project)
- ❖ Josh Blannin (Met Office & LST\_cci project)
- ❖ Ioanna Karagali (DMI & LST\_cci project)
- ❖ Panagiotis Sismanidis (RUB & LST\_cci project)
- ❖ Sorin Cheval, Alexandru Dumitrescu and Dana Micu (MeteoRomania & LST\_cci project)
- ❖ Kaniska Mallick and Tian Hu (LIST & LST\_cci project)
- ❖ Rob King (Met Office and CMUG)
- ❖ Racquel Niclòs (U. Valencia)
- ❖ Bethan Harris (ESA Fellow & CEH)
- ❖ Sophia Walther (MPI)
- ❖ Jakub P. Walawender (Independent Researcher)

This LST\_cci Phase-2 CAR v1 represents the initial findings of the Phase-2 CRG and includes reports from four of the six funded LST\_cci UCS, four other ESA-funded studies (not funded through LST\_cci) and two studies that are not funded through LST\_cci or ESA. Findings from the two funded UCS that are not included in this LST\_cci Phase-2 CAR v1 will be included in the CAR v2 (these studies have yet to start at the time of writing). These two studies are:

- ❖ UCS#4 (Met Office): ‘Comparison between LST and reanalysis “skin” temperature time series’ (Met Office)
- ❖ UCS#6 (LIST): ‘Evaluating Diurnal Dynamics of Evaporation and Temporal Integration Impacts in Evaporation Modelling’

## 1.2. Structure of the document

---

This document consists of three sections. Section 2 presents the reports from the LST\_cci UCS, while Section 3 includes reports from two other CRG studies that have used LST\_cci products. Section 4 provides the reports from other external users who are not current members of the CRG. For the UCS and other CRG study reports, the scientific objectives are outlined together with a brief description of the study approach and results. Feedback on the utility of the LST\_cci data from each study is also provided. Where possible, these details are also provided for the external study reports, although the emphasis of this Section of the report is more focused on the product feedback. Section 5 of the report synthesises the findings from all studies presented in Sections 2, 3 and 4 and summarises the main outcomes of this CAR, including any feedback and response from the LST\_cci project Science Team.



**Table 1-1: Proposed LST products for both LST\_cci Phase-1 (2018-2022) and LST\_cci Phase-2 (2022-2025). For instrument (e.g. ATSR-2), satellite (e.g. ERS-2) and product (e.g. L2P) acronyms, please see Section 1.3.**

Instrument	Satellite(s)	LST_cci Phase-1		LST_cci Phase-2		Products	Comments	
		Year 1	Year 3	Year 1	Year 3			
ATSR-2	ERS-2	1995-2003	1995-2003	1995-2003	1995-2003	1 km L2P 0.01° Daily L3C		
AATSR	Envisat	2002-2012	2002-2012	2002-2012	2002-2012			
AVHRR/3	NOAA-15 to 19		2010-2020	2010-2020	1998-2020		GAC (4km)	
	Metop-A to C		2010	2007-2021	2007-2023		FRAC (1km)	
MODIS	Terra	1999-2018	1999-2018	1999-2021	1999-2021			
	Aqua	2002-2018	2002-2018	2002-2021	2002-2021			
SLSTR	Sentinel-3A	2016-2018	2016-2020	2016-2021	2016-2023			
	Sentinel-3B		2018-2020	2018-2021	2018-2023			
SEVIRI	MSG-1-4	2008-2010	2004-2020	2004-2021	2004-2023		MVIRI done by CM SAF	
Imager	GOES 12-16		2004-2020	2004-2021	2004-2023		0.05° Hourly L3U	
JAMI	MTSAT-2		2009-2015	2009-2015	2009-2015			
SSM/I	DMSF F-13,17	1998-2018	1995-2020	1995-2021	1995-2023		0.25° Daily L3C	
ATSR-S3 CDR	ATSR, MODIS, SLSTR	1995-2012	1995-2020	1995-2021	1995-2023		0.05° Daily + Monthly L3S	ATSR-2 to SLSTR (+ sea ice)
Merged IR CDR	LEO+GEO IR above		2009-2020	2009-2021	2009-2023		0.05° 3-hourly L3S	3-hr Merged GEO+LEO
VIIRS	Suomi-NPP + JPSS-1				2012-2023		750m / 1 km L2P 0.01° Daily L3C	
AHI	Himawari 8-9				2015-2023		0.05° Hourly L3U	
AMSR-E	Aqua			2002-2011	2002-2011	~0.1° Daily L3C		
AMSR2	GCOM-W				2012-2023			

Instrument	Satellite(s)	LST_cci Phase-1		LST_cci Phase-2		Products	Comments
		Year 1	Year 3	Year 1	Year 3		
Downscaled MW	SSMIS + AMSR2 + Merged IR CDR above				2012-2023	0.05° 10-day L3S	Sub-daily composites
Prototype HR	Landsat			2013-2021	2013-2023	100m select areas	
Prototype Downscaled HR	Landsat + Sentinel-3A/B				2002-2021	100m select areas	Downscaled from 1km
Prototype IR+MW	Multiple				2010		

### 1.3. Definition of terms

The terms used in this report are listed below, together with their definitions.

Term	Definition
AASTI	Arctic and Antarctic ice Surface Temperatures from thermal Infrared satellite sensors
AATSR	Advanced Along-Track Scanning Radiometer
AHI	Advanced Himawari Imager
AMSR2	Advanced Microwave Scanning Radiometer - 2
AMSR-E	Advanced Microwave Scanning Radiometer for EOS
ATSR	Along-Track Scanning Radiometer
ATSR-2	Second ATSR instrument
AVHRR	Advanced Very High Resolution Radiometer
BGA	Boundary Generation Algorithm
C3S	Copernicus Climate Change Service
CAR	Climate Assessment Report
CCI	Climate Change Initiative
CDR	Climate Data Record
CEH	Centre for Ecology & Hydrology
CEOS	Committee on Earth Observation Satellites
CERES	Clouds and the Earth's Radiant Energy System
CM-SAF	Satellite Application Facility for Climate Monitoring
CMEMS	Copernicus Marine and Environment Monitoring Service (now usually just referred to as Copernicus Marine Service)
CMUG	Climate Modelling User Group
COR	Pearson's coefficient of correlation
CRG	Climate Research Group
DI_Thoms	Thom's Discomfort Heat Stress Index
DMI	Danmarks Meteorologiske Institut (Danish Meteorological Institute)
DMIOI	Danmarks Meteorologiske Institut (Danish Meteorological Institute) Optimal Interpolation
DMSP	Defense Meteorological <i>Satellite</i> Program
E-SWA	Emissivity-dependent Split Window Algorithm
ECMWF	European Centre for Medium-Range Weather Forecasts

ECV	Essential Climate Variable
EO	Earth Observation
EO-SIP	EO Submission Information Package (a data format type)
EOS	Earth Observing System
ERA5	ECMWF Reanalysis 5
ERS-2	Second European Remote Sensing satellite
ESA	European Space Agency
FRAC	Full Resolution Area Coverage
GAC	Global Area Coverage
GEO	Geostationary
GCOM-W	Global Change Observation Mission for Water
GCOS	Global Climate Observing System
GHDNd	Global Historical Climate Network daily
GLEAM	Global Land Evaporation Amsterdam Model
GSOD	Global Summary Of the Day
HR	High-Resolution
IPCC	Intergovernmental Panel on Climate Change
IR	InfraRed
IST	Ice Surface Temperature
ISH	Integrated Surface Hourly
JAMI	Japanese Advanced Meteorological Imager
JPSS-1	Joint Polar Satellite System-1
K	Kelvin
L2P	Level 2 Pre-Processed data (orbit/swath data at full resolution from a single sensor)
L3	Level 3 data (gridded data)
L3C	Level 3 Collated data (multiple L2P files from one sensor are gridded)
L3S	Level 3 Super-collated data (multiple L2P files from more than one sensor are gridded)
L3U	Level 3 Uncollated (gridded single L2P product from one sensor)
L4	Level 4 gap-free gridded products
LC	Land Cover
LC_cci	Land Cover Climate Change Initiative
LCC	Land Cover Class
LE	Latent heat flux

LEO	Low Earth Orbiting
LST	Land Surface Temperature
LIST	Luxemburg Institute of Science and Technology
LST_cci	Land Surface Temperature Climate Change Initiative
MAE	Mean Absolute Error
MK	Mann-Kendall
MeteoRomania	National Meteorological Administration of Romania
MIZ	Marginal Ice Zone
MODIS	Moderate Resolution Imaging Spectroradiometer
MSG	Meteosat Second Generation
MTSAT	Multifunction Transport SATellite
MVIRI	Meteosat Visible Infra-Red Imager
MW	MicroWave
NASA	National Aeronautics and Space Administration (USA)
NetCDF	Network Common Data Format
NHD	Number of Hot Days
NMS	National Meteorological Service(s)
NOAA	National Oceanic and Atmospheric Administration (USA)
OI	Optimal Interpolation
ODP	Open Data Portal
PUG	Product User Guide
r	Pearson correlation coefficient
RCM	Regional Climate Model
RH	Relative Humidity
RMS	Root Mean Square
RMSD	Root Mean Square Difference
RUB	Ruhr-University Bochum
S3	Sentinel-3
SD	Standard Deviation
SEVIRI	Spinning Enhanced Visible and Infra-Red Imager
SIC	Sea Ice Concentration
SIMB3	Seasonal Ice Mass Balance Buoy 3
SKT	Skin Temperature

SLSTR	Sea and Land Surface Temperature Radiometer
SM_cci	Soil Moisture Climate Change Initiative
SSM/I	Special Sensor Microwave/Imager
SSMIS	Special Sensor Microwave Imager Sounder
SST	Sea Surface Temperature
SU	Subsampling Uncertainty
Suomi-NPP	Suomi National Polar-orbiting Partnership
SUHI	Surface Urban Heat Island
SUHII	Surface Urban Heat Island Intensity
SW	Split Window
T2m or Tair	2m air temperature
TAC	Thematic Assembly Centre
TDT	Trend Detection Time
TES	Temperature Emissivity Separation
TS	Theil-Sen slope estimator
UCS	User Case Study
UHI	Urban Heat Island
UNLCCS	United Nations Land Cover Classification System
USAF	United States Air Force
VIIRS	Visible/Infrared Imager Radiometer Suite
WBGT	Wet Bulb Globe Temperature
WMO	World Meteorological Organisation
WLS	Weighted Least Squares
WS	Weather Station

## 2. LST\_cci User Case Study Reports

### 2.1. UCS#1: Development of moderate extreme indices based on LST (Lizzie Good & Josh Blannin, Met Office)

---

#### 2.1.1. Key Messages

- ❖ A selection of the moderate extreme 2m-air temperature (T2m)-based ‘Climpact’ indices are applied to the LST\_cci SSM/I & SSMIS MW LST product (v2.33) and are compared with the equivalent station T2m-based indices to establish whether similar information can be provided using both data types.
- ❖ The study finds that the Climpact indices cannot be applied in most geographical regions due to sparse MW LST data availability as the Climpact indices require near-daily observations. Therefore, LST-based indices can only be calculated reliably above ~50° latitude due to the more frequent orbits at higher latitudes.
- ❖ Climpact indices calculated using MW LST data provide comparable results to those calculated using spatio-temporally colocated station T2m data for some of the indices tested in the study. For example, good results are obtained using the percentile-based indices. For other indices, the agreement between the LST-based results and T2m-based results is poor.
- ❖ Further work is required to establish which indices are most suitable to be used with the MW LST data and whether some of the Climpact threshold-based indices can be adapted to work with the MW LST data. For example, by using different ‘adjusted’ LST-based thresholds that account for the inherent physical differences between LST and T2m.

#### 2.1.2. Scientific Analysis

##### 2.1.2.1. Aims of the study

The objective of this study is to investigate the feasibility of developing a satellite-based, moderate temperature extremes data set. This data set would be designed to complement the HadEX3 moderate extremes data set that is based on in situ data [RD-01] and is reported in the Intergovernmental Climate Change Panel (IPCC) report 2021 [RD-02].

The HadEX3 data set provides the suite of Climpact indices (<https://climpact-sci.org/>) for both precipitation and 2m air temperature (T2m) from 1901 at a spatial resolution of 1.875° x 1.25° longitude-latitude, which can be used to investigate how the frequency of moderate extremes are changing over time as well as to evaluate models. For example, HadEX3 shows that number of summer days (maximum daily T2m>25°C) and tropical nights (minimum daily T2m>20°C) has increased significantly since 1950 and particularly in the past 40 years. This is consistent with an increase in the frequency of heat wave events, which can have serious health implications for humans, livestock and plants, as well as impacts on agriculture and infrastructure.

Although HadEX3 benefits from station data that have been provided by private agreement with various national meteorological services (NMS) and individual researchers, and therefore has a high density of observations compared with many other in-situ based data sets, there are still large gaps in the network (Figure 2-1). This results in a number of large regions that are represented in HadEX3 by extrapolated extremes indices that may have large uncertainties or have no data, e.g. parts of Africa, Mongolia, and Greenland. The density of station data also limits the spatial resolution of HadEX3. Using satellite data

could provide additional information on temperature extremes in these data-sparse regions as well as data at a higher spatial resolution.

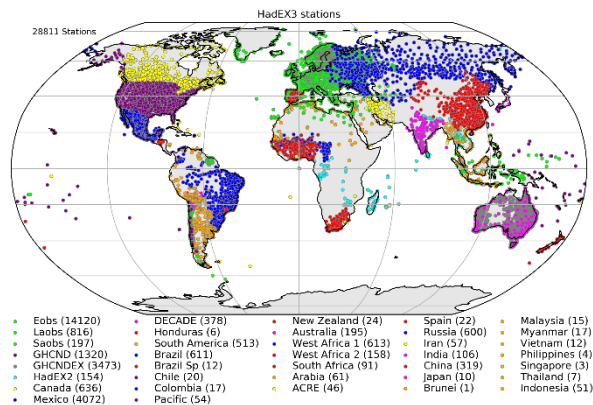


**Figure 2-1: Stations used to produce the HadEX3 data set using the 1981-2010 baseline period (left; see [RD-01] Figure A1 for the 1961-1990 baseline period).**

### 2.1.2.2. Data and methods

The approach taken in the study is to compare Climpect Indices derived for both station T2m and satellite LST data that are collocated in space and time. The period 1996-2020 is used in the study (to be extended to 2022 in future). The success of the satellite data in matching the station-based indices can then be assessed. A selection of the Climpect temperature indices is used in the study. These can be categorised as

- ❖ *Threshold-based indices*, where a specific exceedance threshold is used, such as the number of summer days, i.e. where the number of days with a daily maximum temperature above 25°C are counted (Table 2-1).
- ❖ *Value-based indices*, where certain temperatures are used to define the index, for example, the monthly maximum value of daily maximum temperature (Table 2-2).
- ❖ *Percentile-based indices*, where exceedances of a specific percentile are counted, for example, the percentage of days when maximum daily temperature exceeds the 90th percentile (Table 2-3).

The station dataset used in the study is the Global Historical Climate Network daily (GHCNd) [RD-03]. GHCNd is a multivariate dataset consisting of 80,000 stations over 180 countries compiled by the National Oceanic and Atmospheric Administration (NOAA). Minimum T2m (Tmin) and maximum T2m (Tmax) are used in this study.

The LST\_cci data used in the study are from the MW LST daily dataset (Table 2-4). This dataset was selected as the Climpect indices require close to daily coverage, which cannot be achieved with the infrared LST\_cci products due to cloud coverage. Even with the near-all sky MW LST data, >80% daily coverage may only be achieved at latitudes above ~47° latitude owing to the swath width. The MW LST data correspond to ~6 am/pm (after applying the orbital drift LST correction provided). In this study, maximum LST from either the 6am/pm overpass is compared with Tmax, and the minimum LST with Tmin. In almost 90% of cases where both overpasses are available, the maximum LST occurs at 6 pm and the minimum LST at 6 am. For locations where only one overpass is available, the LST at 6 am is compared



with  $T_{min}$  and the LST at 6 pm with  $T_{max}$ , following the approach of [RD-04]. The MW LST data are also quality controlled/filtered following [RD-04].

Application of the Climpact indices to the daily observations requires a maximum number of missing days during a given period. A month is rejected if there are more than three missing days of data, and a year is rejected if there are more than 15 missing days of data or if any month is rejected. However, using these official Climpact missing data thresholds resulted in no annual indices and very few monthly indices being calculated for the colocated station and satellite data, owing to too many missing days of data in the MW LST product. Therefore, for the purposes of this study to assess the feasibility of creating a HadEX3-like product using satellite data, these thresholds are relaxed to allow up to 36 missing days of data per year and to retain years with any whole months that would have been rejected.

**Table 2-1: List of threshold-based Climpact indices tested in the study (see <https://climpact-sci.org/>).**

Climpact Index	Name	Climpact Definition
SD	Number of summer days	Annual count of days when $T_X$ (daily maximum temperature) $> 25^\circ\text{C}$ . Let $T_{X_{ij}}$ be daily maximum temperature on day $i$ in year $j$ . Count the number of days where $T_{X_{ij}} > 25^\circ\text{C}$ .
ID	Number of icing days	Annual count of days when $T_X$ (daily maximum temperature) $< 0^\circ\text{C}$ . Let $T_{X_{ij}}$ be daily maximum temperature on day $i$ in year $j$ . Count the number of days where $T_{X_{ij}} < 0^\circ\text{C}$ .
TR	Number of tropical nights	Annual count of days when $T_N$ (daily minimum temperature) $> 20^\circ\text{C}$ . Let $T_{N_{ij}}$ be daily minimum temperature on day $i$ in year $j$ . Count the number of days where $T_{N_{ij}} > 20^\circ\text{C}$ .
FD	Number of frost days	Annual count of days when $T_N$ (daily minimum temperature) $< 0^\circ\text{C}$ . Let $T_{N_{ij}}$ be daily minimum temperature on day $i$ in year $j$ . Count the number of days where $T_{N_{ij}} < 0^\circ\text{C}$ .
TNlt2	TN below $2^\circ\text{C}$	Annual count of the number of days when $T_N$ (daily minimum temperature) $< 2^\circ\text{C}$ .
TNltm2	TN below $-2^\circ\text{C}$	Annual count of the number of days when $T_N$ (daily minimum temperature) $< -2^\circ\text{C}$ .
Tltm20	TN below $-20^\circ\text{C}$	Annual count of the number of days when $T_N$ (daily minimum temperature) $< -20^\circ\text{C}$ .
TXge30	TX of greater than or equal to $30^\circ\text{C}$	Annual count of the number of days when $T_X$ (daily maximum temperature) $\geq 30^\circ\text{C}$ .
TXge35	TX of greater than or equal to $35^\circ\text{C}$	Annual count of the number of days when $T_X$ (daily maximum temperature) $\geq 35^\circ\text{C}$ .

**Table 2-2: List of value-based Climpect indices tested in the study (see <https://climpect-sci.org/>).**

Climpect Index	Name	Climpect Definition
TXx	Monthly maximum value of daily maximum temperature	Let $TX_x$ be the daily maximum temperatures in month $k$ , period $j$ . The maximum daily maximum temperature each month is then $TX_{xkj} = \max(TX_{xkj})$ .
TXn	Monthly minimum value of daily maximum temperature	Let $TX_n$ be the daily maximum temperatures in month $k$ , period $j$ . The minimum daily maximum temperature each month is then $TX_{nkj} = \min(TX_{nkj})$ .
TNx	Monthly maximum value of daily minimum temperature	Let $TN_x$ be the daily minimum temperatures in month $k$ , period $j$ . The maximum daily minimum temperature each month is then $TN_{xkj} = \max(TN_{xkj})$ .
TNn	Monthly minimum value of daily minimum temperature	Let $TN_n$ be the daily minimum temperatures in month $k$ , period $j$ . The minimum daily minimum temperature each month is then $TN_{nkj} = \min(TN_{nkj})$ .
TXm	Mean TX	The mean daily maximum temperature (monthly)
TNm	Mean TN	The mean daily minimum temperature (monthly)
DTR	Daily temperature range	Let $TX_{ij}$ and $TN_{ij}$ be the daily maximum and minimum temperature respectively on day $i$ in period $j$ . If $i$ represents the number of days in $j$ , then:  $DTR_j = \frac{\sum_{i=1}^I (TX_{ij} - TN_{ij})}{I}$

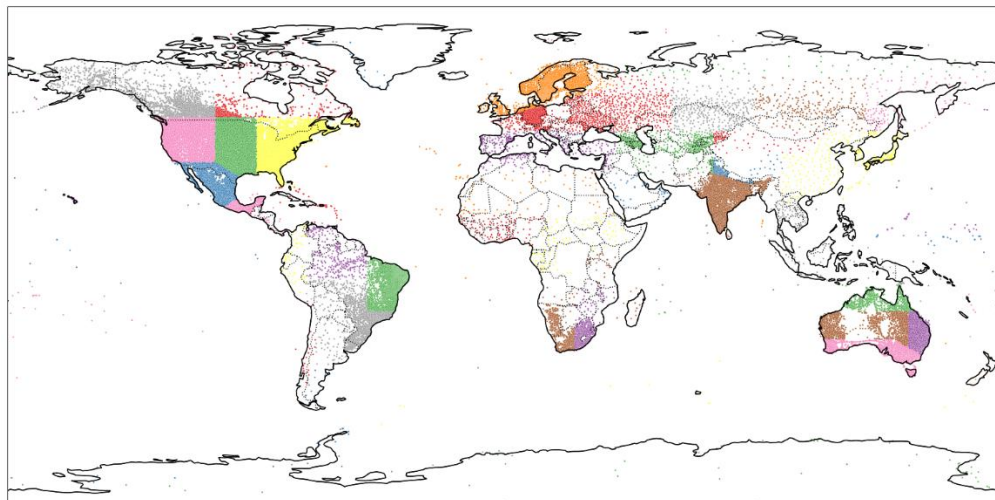
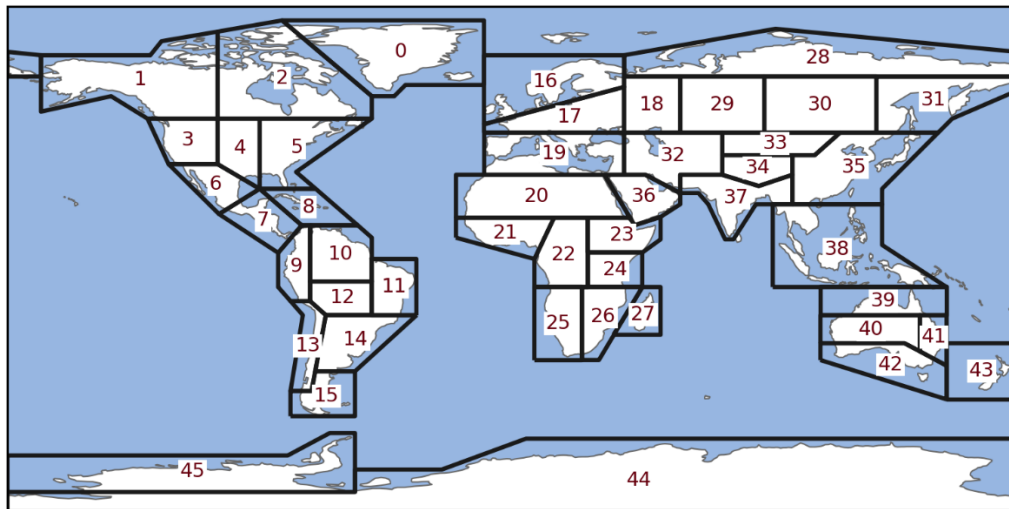
The analysis of colocated T2m/LST indices is performed by region, using the IPCC 6th Assessment Report (AR6) regions [RD-02] (Figure 2-2). Most AR6 regions do not produce any meaningful results owing to the data availability, even with the reduced Climpect missing data thresholds. Further investigation is required to ascertain whether these thresholds can be reduced further, so for the purposes of this report, results are only presented for two higher-latitude AR6 regions as proof of concept. These are AR6 regions 1 in NW North America (n stations with valid T2m/LST indices = 1608) and 16 in Northern Europe (number of stations with valid T2m/LST indices = 1308). Some results for a bespoke test region in Northern/Central Asia and Russia (longitude>50°N, latitude>45°E) between 1996 and 2012 that were obtained earlier in the study are also presented, hereafter referred to as the ‘bespoke test region’. However, it should be noted that the missing data thresholds described above were not applied to this bespoke test region. Instead, a threshold of >80% observational coverage was applied to the MW LST data and >90% for the GHCNd data.

**Table 2-3: List of percentile-based Climpect indices tested in the study (see <https://climpect-sci.org/>).**

Climpect Index	Name	Climpect Definition
TX90p	Percentage of days when TX > 90th percentile	Let $TX_{ij}$ be the daily maximum temperature on day $i$ in period $j$ and let $TX_{in90}$ be the calendar day 90 <sup>th</sup> percentile centred on a 5-day window for the base period 1961-1990. The percentage of time for the base period is determined where $TX_{ij} > TX_{in90}$ . To avoid possible inhomogeneity across the in-base and out-base periods, the calculation for the base period (1961-1990) requires the use of a bootstrap procedure.
TX10p	Percentage of days when TX < 10th percentile	Let $TX_{ij}$ be the daily maximum temperature on day $i$ in period $j$ and let $TX_{in10}$ be the calendar day 10 <sup>th</sup> percentile centred on a 5-day window for the base period 1961-1990. The percentage of time for the base period is determined where $TX_{ij} < TX_{in10}$ . To avoid possible inhomogeneity across the in-base and out-base periods, the calculation for the base period (1961-1990) requires the use of a bootstrap procedure.
TN90p	Percentage of days when TN > 90th percentile	Let $TN_{ij}$ be the daily minimum temperature on day $i$ in period $j$ and let $TN_{in90}$ be the calendar day 90 <sup>th</sup> percentile centred on a 5-day window for the base period 1961-1990. The percentage of time for the base period is determined where $TN_{ij} > TN_{in90}$ . To avoid possible inhomogeneity across the in-base and out-base periods, the calculation for the base period (1961-1990) requires the use of a bootstrap procedure.
TN10p	Percentage of days when TN < 10th percentile	Let $TN_{ij}$ be the daily minimum temperature on day $i$ in period $j$ and let $TN_{in10}$ be the calendar day 10 <sup>th</sup> percentile centred on a 5-day window for the base period 1961-1990. The percentage of time for the base period is determined where: $TN_{ij} < TN_{in10}$ . To avoid possible inhomogeneity across the in-base and out-base periods, the calculation for the base period (1961-1990) requires the use of a bootstrap procedure.

**Table 2-4: A summary of LST\_cci products used for this study.**

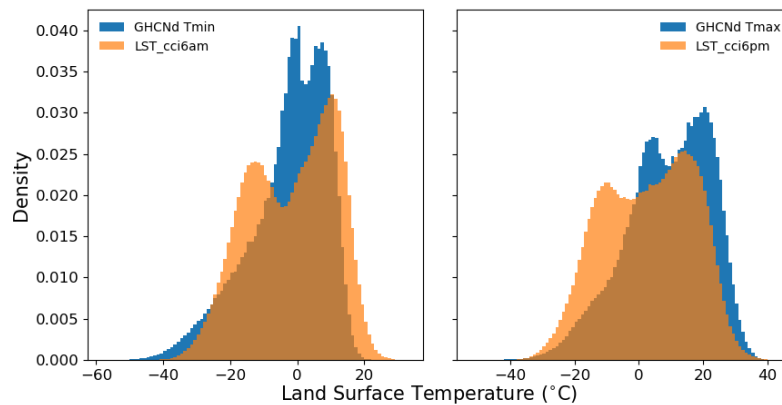
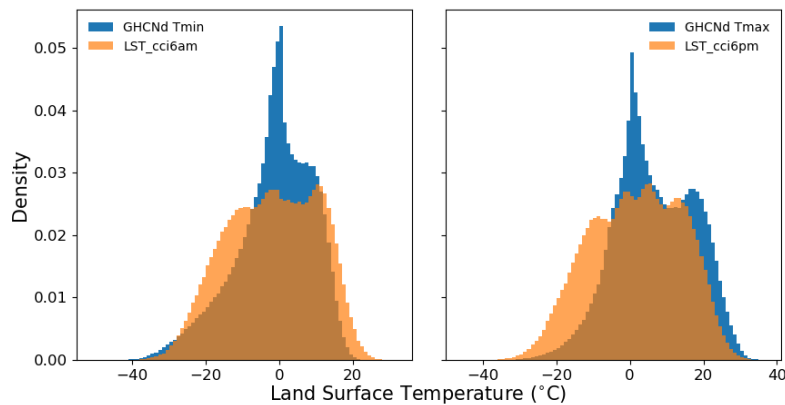
Product String and version	Sensor type	Resolution	Data availability	Local time of ascending node
ESACCI-LST-L3C-LST-SSMI13/ ESACCI-LST-L3C-LST-SSMI17 Daily (v2.23)	MW	0.25°	January 1996 – December 2020	~17:30-19:30 but corrected to 18:00



**Figure 2-2:** AR6 regions (top: figure source [https://regionmask.readthedocs.io/en/stable/defined\\_scientific.html#ar6-regions](https://regionmask.readthedocs.io/en/stable/defined_scientific.html#ar6-regions) and references therein) and the GHCND stations that fall within each of the 45 land regions (colours have no meaning other than to denote different AR6 regions) Note that not all stations on this map provide Tmin/Tmax data over the study period.

### 2.1.2.3. Results

Figure 2-3 shows the distributions of spatially and temporally colocated station T2m and satellite LST observations for the AR6 regions 1 and 16. As reported by [RD-04] the temperature distributions from both datasets show good agreement, despite the different observation times. (The LST represents 6 am/pm local time, while Tmax and Tmin can occur at any time of the day, for example, ~3 pm local time for Tmax and ~5 am local time for Tmin.) However, in both regions there are at least two modes of distribution where the colder peak in the LST distribution (i.e. the left-most peak of the orange distribution in each panel) falls outside the T2m distributions. This pattern requires further investigation but is likely to be related to the strong seasonal climate in both regions. It should be noted that the LST distributions may also include contamination from convective clouds and errors due to the adjustment applied to the LST data to correct for orbital drift (Section 2.1.2.2.). However, there is no obvious feature in the MW LST distributions (orange) that can be attributed to these issues.

**N.W.North-America (AR6 id = 1)**

**N.Europe (AR6 id = 16)**


**Figure 2-3: Distributions of spatially and temporally colocated T2m and LST observations over AR6 regions 1 (top) and 16 (bottom). The LST\_cci6am distribution represents minimum LST where there are two LST overpasses and the LST at 6 am for days and locations with only one overpass. Similarly, the LST\_cci6pm distribution represents maximum LST where there are two LST overpasses and the LST at 6 pm for days and locations with only one overpass.**

Table 2-5 and Table 2-6 show the mean Climptact index values across all station locations for T2m and LST in regions 1 and 16, respectively. For some indices, there is quite good agreement between the results for T2m and LST. For region 1, the differences for the FD, TNlt2, TNltm2 and TNn indices are within 10% (with respect to the T2m index value). The TR, FD, TXge35, TNx, TNn, and TNm are also numerically similar for region 1, agreeing within 5 days/2°C (depending on the index). For region 16, none of the indices agree to within 10%. However, the TR, TXge30 and TXge35 are numerically similar, agreeing to within 5 days.

**Table 2-5: Mean Climpect Index values for the threshold- and value-based indices across all station locations in AR6 region 1 (NW North America).**

Climpect Index (unit)	T2m index mean value	LST index mean value	Difference (LST-T2m)	% Difference with respect to T2m (%)
SU (ndays)	27.5	9.6	-17.9	65.1
ID (ndays)	89.7	156.9	67.2	74.9
TR (ndays)	0.1	2.7	2.6	2600.0
FD (ndays)	187.5	189.9	2.4	1.3
TNI <sub>t2</sub> (ndays)	214.4	205.7	-8.7	4.1
TNI <sub>tm2</sub> (ndays)	159.7	174.9	15.2	9.5
TNI <sub>tm20</sub> (ndays)	39.5	32.5	-7.0	17.7
TX <sub>ge30</sub> (ndays)	6.8	1.5	-5.3	77.9
TX <sub>ge35</sub> (ndays)	0.7	0.2	-0.5	71.4
TX <sub>x</sub> (°C)	18.7	9.1	-9.6	51.3
TX <sub>n</sub> (°C)	-1.3	-9.5	-8.2	-630.8
TNx (°C)	6.1	4.6	-1.5	24.6
TN <sub>n</sub> (°C)	-11.2	-12.0	-0.8	-7.1
TX <sub>m</sub> (°C)	9.2	-0.1	-9.3	101.1
TNm (°C)	-2.1	-3.4	-1.3	-61.9
DTR (°C)	11.2	4.4	-6.8	60.7

**Table 2-6: Mean Climpect Index values for the threshold- and value-based indices across all station locations in AR6 region 16 (Northern Europe).**

Climpect Index (unit)	T2m index mean value	LST index mean value	Difference (LST-T2m)	% Difference with respect to T2m (%)
SU (ndays)	12.6	3.7	-8.9	70.6
ID (ndays)	64.0	153.0	89	139.1
TR (ndays)	0.5	4.4	3.9	780.0
FD (ndays)	136.5	188.0	51.5	37.7
TNI <sub>t2</sub> (ndays)	172.3	204.8	32.5	18.9
TNI <sub>tm2</sub> (ndays)	104.0	169.9	65.9	63.4
TNI <sub>tm20</sub> (ndays)	12.1	28.3	16.2	133.9
TX <sub>ge30</sub> (ndays)	1.2	0.2	-1.0	83.3
TX <sub>ge35</sub> (ndays)	0.0	0.0	0.0	N/A
TX <sub>x</sub> (°C)	16.1	7.9	-8.2	50.9
TX <sub>n</sub> (°C)	2.3	-11.5	-13.8	600.0
TNx (°C)	8.5	4.5	-4.0	47.1
TN <sub>n</sub> (°C)	-6.3	-14.9	-8.6	136.5
TX <sub>m</sub> (°C)	9.3	-1.9	-11.2	120.4
TNm (°C)	1.8	-5.2	-7.0	388.9
DTR (°C)	7.3	3.6	-3.7	50.7

N.W.North-America (AR6 id = 1)

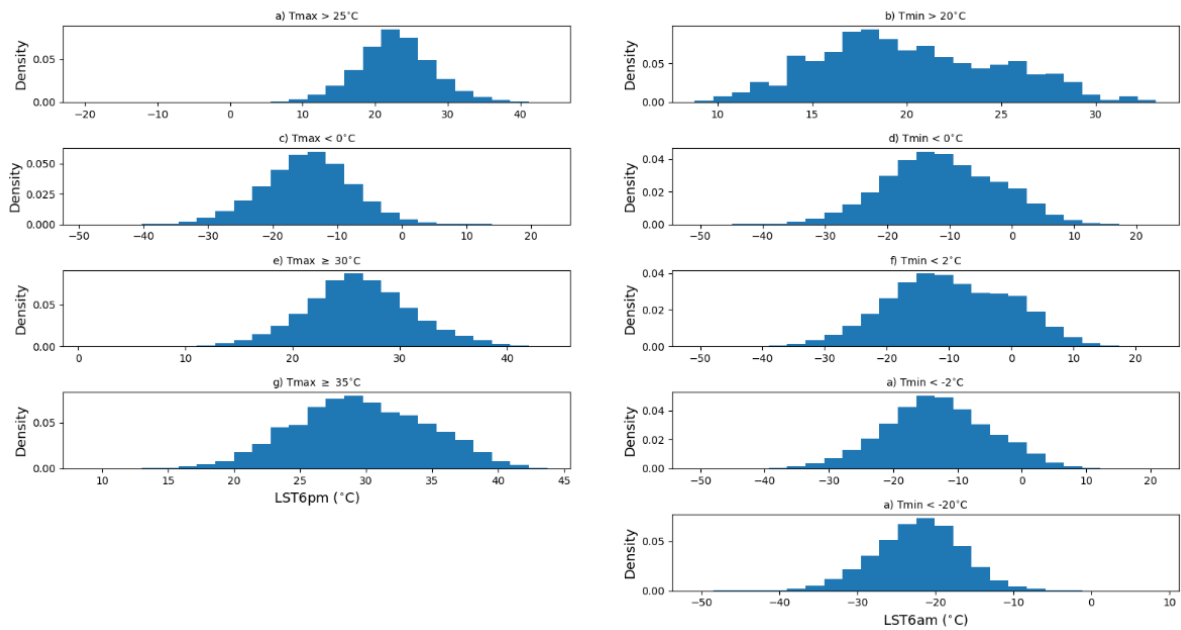


**Figure 2-4: Distributions of LST values for days where the threshold-based indices are triggered by the T2m observations in AR6 region 1 (left: maximum LST or LST at 6pm, right: minimum LST or LST at 6 am).**

N.Europe (AR6 id = 16)

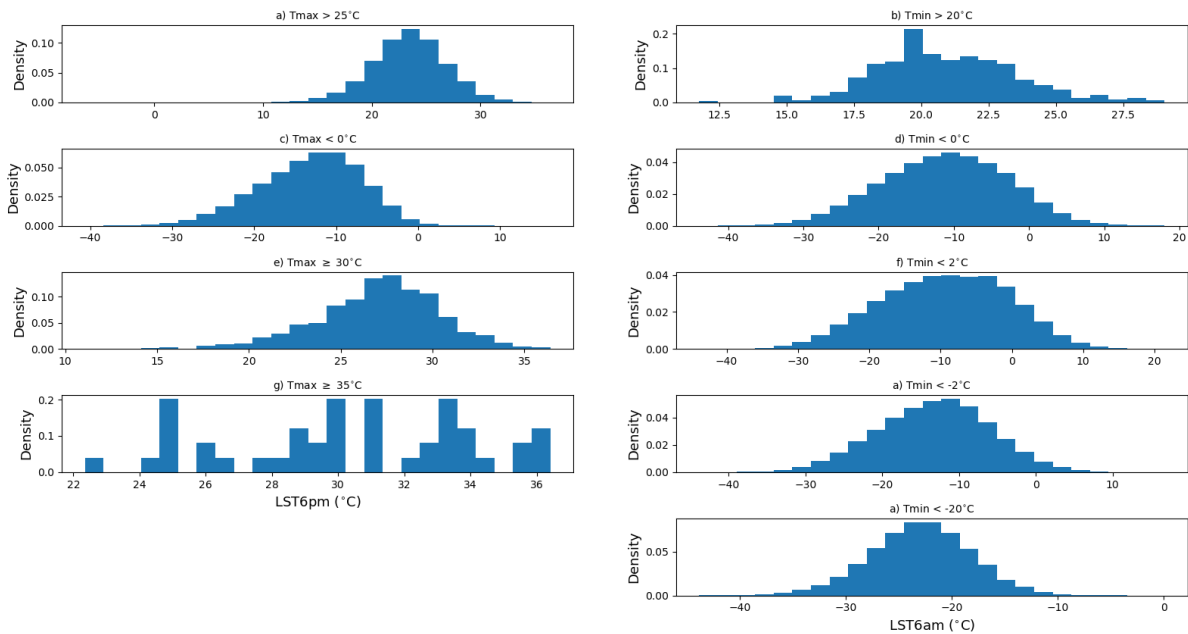


**Figure 2-5: Distributions of LST values for days where the threshold-based indices are triggered by the T2m observations in AR6 region 16 (left: maximum LST or LST at 6pm, right: minimum LST or LST at 6 am).**

The cause of some of these discrepancies between the LST- and T2m-based indices results is illustrated in Figure 2-4 and Figure 2-5, which show the distributions for LST values for each of the threshold-based Climpect indices where the T2m observations have ‘triggered’ the index. For some of the indices, the LST values appear to be well aligned with the T2m observations. For example, for the ID index ( $T_{max} < 0^{\circ}\text{C}$ ; panel c in each Figure), there are almost no LST values that are  $\geq 0^{\circ}\text{C}$ . Similarly, for the four cold Tmin indices (FD ( $T_{min} < 0^{\circ}\text{C}$ ; panel d), TNlt2 ( $T_{min} < 2^{\circ}\text{C}$ ; panel f), TNltm2 ( $T_{min} < -2^{\circ}\text{C}$ ; panel h), TNltm20 ( $T_{min} < -20^{\circ}\text{C}$ ; panel i) most of the LST data also fall below these thresholds in both regions. However, it should be noted that these distributions do not include LST values that have triggered a Climpect index where the index is not triggered by T2m, which also results in some of the apparent differences in LST/T2m index agreement shown in Table 2-5 and Table 2-6.

These results suggest that some indices may yield similar results for both T2m and LST. For the threshold-based indices, it is reasonable to consider that different threshold may be required for LST to account for the inherent physical differences between LST and T2m. This is explored using the bespoke test region, where two statistical methods, Kernel Density Estimation (KDE) and Logistic Regression (LR) are used to estimate new thresholds that could be applied to LST to capture the same events observed in the T2m data. These adjusted thresholds for the bespoke test region are shown in Table 2-7 and the results are shown in Table 2-8. The accuracy metrics ‘precision’ (*pr*) and ‘recall’ (*re*) are used to assess any improvements in the results where:

$$\text{Equation 2-1} \quad Pr = \frac{\text{Hits}}{\text{Hits} + \text{False hits}}$$

$$\text{Equation 2-2} \quad Re = \frac{\text{Hits}}{\text{Hits} + \text{Misses}}$$

Perfect agreement between events captured by the T2m and LST observations would be indicated by precision and recall values of 1.0. However, as both the station T2m and LST data will contain errors, this is unlikely ever to be achieved in practise. The results shown in Table 2-8 suggest that only the indices ID and FD for the MW LST data may be able to achieve comparable results to the indices using station T2m data. However, further work is required to investigated this further, particularly as the number events for both SU and TR is low in the bespoke test region.

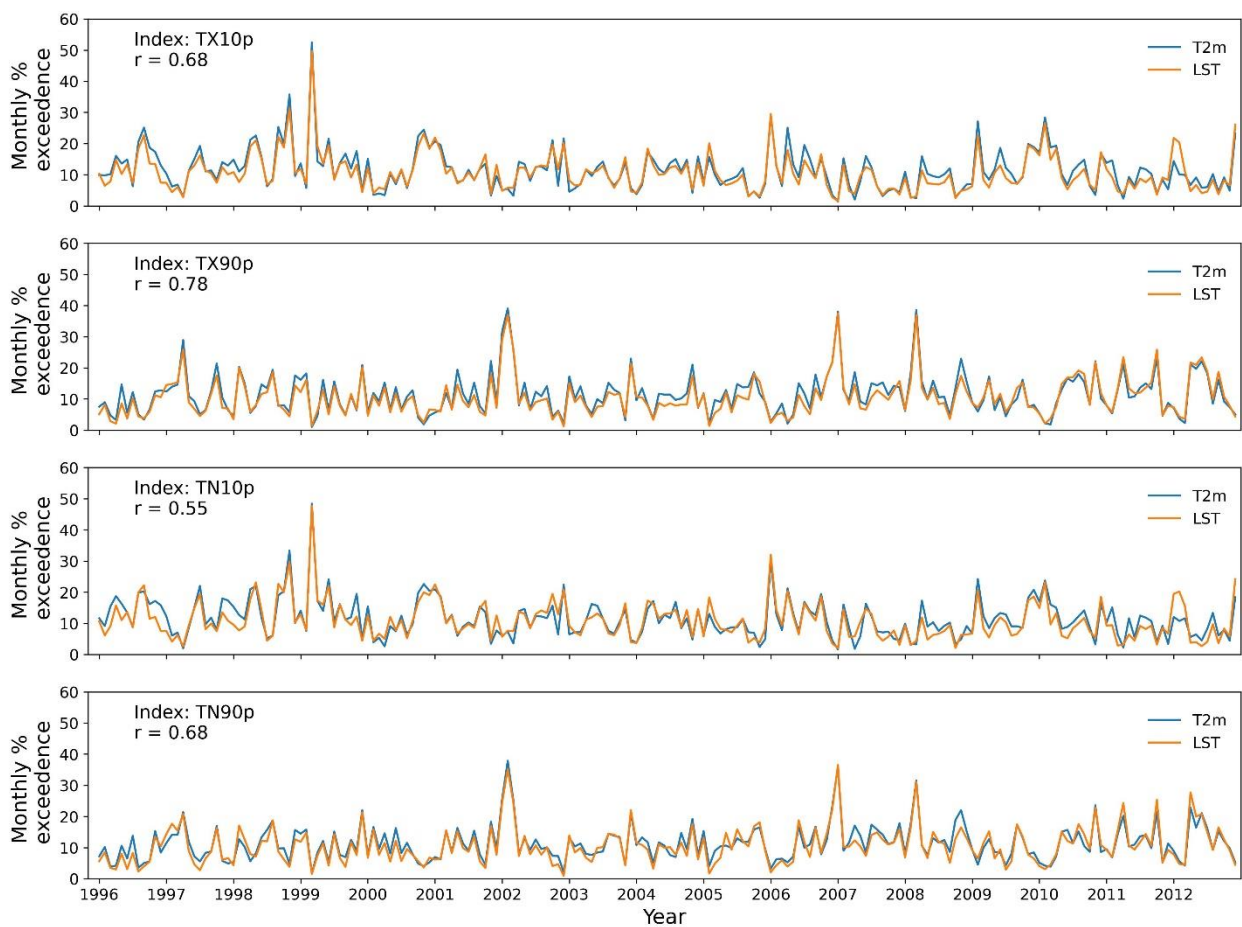
**Table 2-7: Unadjusted and adjusted thresholds for LST for selected threshold-based Climpect indices.**

Climpect Index (unit)	Unadjusted Threshold ( $^{\circ}\text{C}$ )	Kernel Density Estimation LST ( $^{\circ}\text{C}$ )	Logistic Regression LST ( $^{\circ}\text{C}$ )
SU (ndays)	$T_{max} > 25$	$T_{max} > 22.9$	$T_{max} > 16.2$
ID (ndays)	$T_{max} < 0$	$T_{max} < -9.0$	$T_{max} < -6.5$
TR (ndays)	$T_{min} > 20$	$T_{min} > 26.6$	$T_{min} > 15.2$
FD (ndays)	$T_{min} < 0$	$T_{min} < 0.8$	$T_{min} < -0.7$



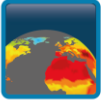
**Table 2-8: Results using unadjusted and adjusted thresholds for LST for selected threshold-based Climact indices for the bespoke test region.**

Climact Index (unit)	T2m results	Unadjusted LST threshold			Kernel Density Estimation LST threshold			Logistic Regression LST threshold		
	<i>n</i> days	<i>n</i> days	Pr	Re	<i>n</i> days	Pr	Re	<i>n</i> days	Pr	Re
SU (ndays)	40	21	0.92	0.49	30	0.83	0.69	67	0.47	0.96
ID (ndays)	215	157	0.79	0.99	195	0.94	0.92	184	0.91	0.96
TR (ndays)	1	10	0.04	0.69	1	0.19	0.10	33	0.01	0.94
FD (ndays)	144	133	0.95	0.93	128	0.93	0.94	137	0.95	0.92



**Figure 2-6: Timeseries of T2m (blue) and LST (orange) mean percentage of days per month that are above (below) the 90th (10th) percentiles averaged over all stations in the bespoke test region. Plots show a) TX10p, b) TX90p, c) TN10p, and d) TN90p (see Table 2-3).**

Figure 2-6 shows the time series of monthly exceedances for the four percentile-based indices tested in the study (Table 2-3) for the bespoke test region. Overall, the time series of T2m- and LST-based indices show a good correlation ( $r = 0.55$  to  $0.78$ ). Extreme events in the T2m indices are also captured well by the LST indices, for example, the extreme cold event in 1999, which is represented by a strong peak in both the T2m and LST time series for the TX10p and TN10p indices. Similarly, the extreme heat event in early 2002 is clearly represented by a peak in both the T2m and LST time series for the TX90p and TN90p

 <b>land surface temperature</b> cci	<b>Climate Assessment Report</b>  <i>WP5.1 – DEL-5.1</i>	Ref.: LST-CCI-D5.1-CAR Version: 3.0 Date: 25-May-2024 Page: 22
--	--	---

indices. Further work is required in order to characterise the behaviour of these indices in full, but in general, it appears that the Climpack percentile indices calculated using MW LST provide very similar results to those obtained using station T2m data.

#### 2.1.2.4. Conclusions

The results of this study suggest that it may be possible to obtain information comparable to T2m-based ‘Climpack’ moderate extremes indices using the LST\_cci MW LST product. However, a major limitation of using the MW LST product is the limited spatio-temporal coverage of the data. Despite being a near all-weather product, near-daily coverage is only achieved above ~50°N so it seems likely that the provision of most, or even all, LST-based indices will be restricted to higher latitudes. Furthermore, this study suggests that it is unlikely all the Climpack indices can be applied to the MW LST data to provide results that are comparable to the T2m-based indices. Further work is required to establish which Climpack indices are most suitable for LST. Future work will also include:

- ❖ a more extensive testing of using LST-specific, adjusted thresholds for the T2m threshold-based indices (i.e. establishing whether a different threshold for the LST data can provide more comparable results to the equivalent T2m-based indices).
- ❖ a more extensive analysis of the percentile-based indices; these indices look most promising in terms of providing T2m-comparable information using the MW LST data.
- ❖ Whether any LST-specific indices can be defined.

#### 2.1.3. Feedback on scientific utility of the LST\_cci products

In general, the SSM/I and SSMIS data are of good quality and are easy to use. However, the documentation is confusing indicating which orbit – ascending/descending – corresponds to the ~6am/pm overpass time.

Provision of some auxiliary data that is already provided in some of the the LST\_cci IR products would be very welcome. For example, ERA5 SKT & T2m temperatures, NDVI and land cover class.

It is suggested that additional information is added in the product documentation regarding the general data availability/coverage. In particular, the impact on observational coverage associated with the “Possibility of inundated land” flag, which refers to flooded ground. Figure 2-7 and Figure 2-8 show seasonal data availability over Asia and the USA, respectively; data availability refers to the percentage of data points in a time series not labelled as “missing” because of either no measurements being taken or having been removed by applying quality flags. There is a clear stippled pattern in the data availability in some regions that may correspond to the locations of rice paddies. This is supported by Figure 2-9, which shows regions of high rice yield in the USA in 2012 that match the locations of the stippling in Figure 2-8.

Finally, in conducting this study, two days of data were found to missing from the data record where there were no files for these days. It would be helpful to include information in the Product User Guide [AD-01] on how missing whole days of data is handled in the LST\_cci products, so users are clear whether these data have been accidentally missed in the processing or are known to be missing days of data.

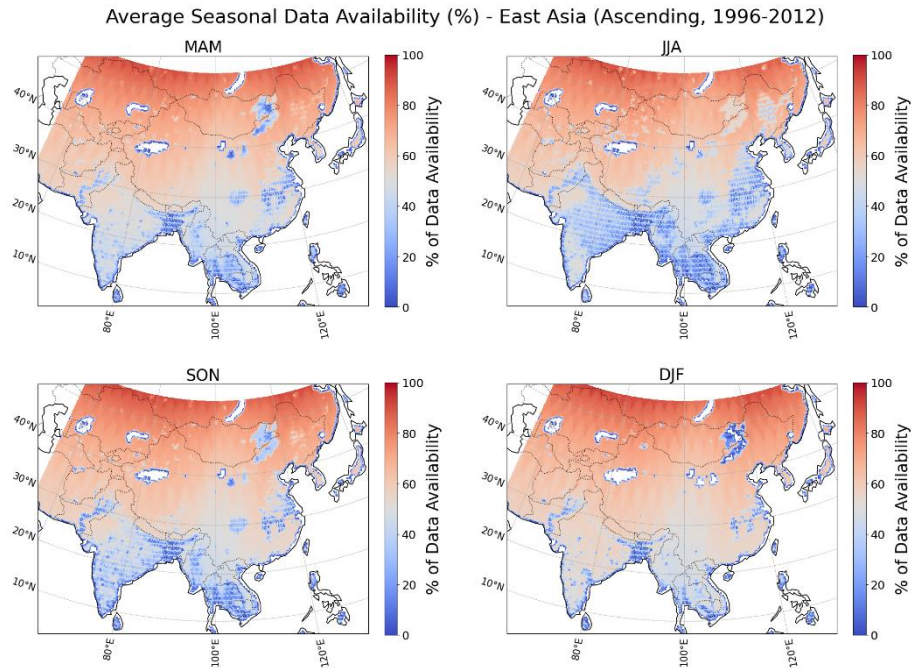


**Figure 2-7: Average seasonal MW LST data availability over Asia as a percentage of the complete timeseries for the ascending overpass between 1996-2012. Data availability refers to the percentage of data points in a time series not labelled as “missing” because of either no measurements being taken or having been removed by applying quality flags. MAM is March/April/May, JJA is June/July/August, SON is September/October/November and DJF is December/January/February.**

Average Seasonal Data Availability (%) - USA (Ascending, 1996-2012)

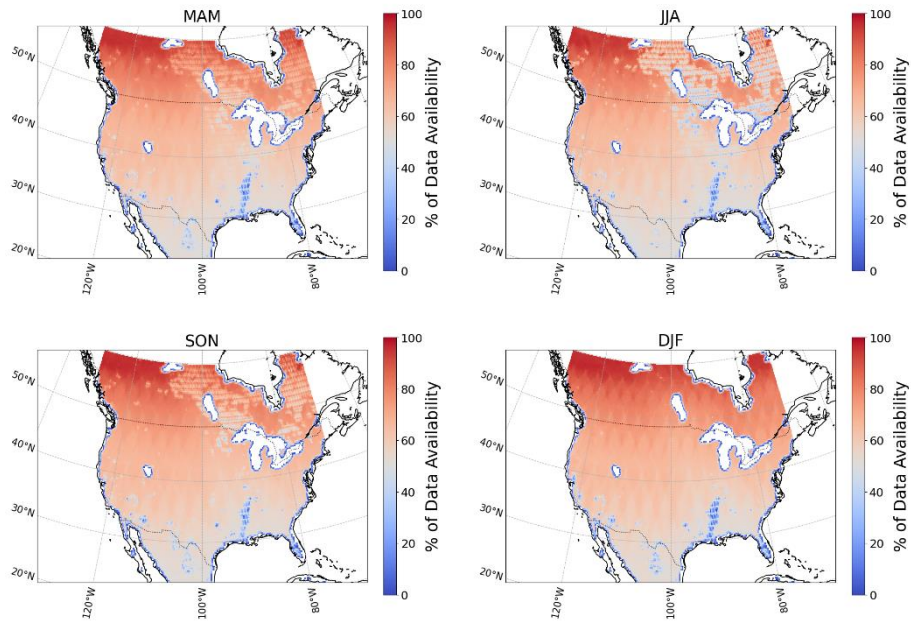


**Figure 2-8: Average seasonal MW LST data availability over the USA as a percentage of the complete timeseries for the ascending overpass between 1996-2012. Data availability refers to the percentage of data points in a time series not labelled as “missing” because of either no measurements being taken or having been removed by applying quality flags. MAM is March/April/May, JJA is June/July/August, SON is September/October/November and DJF is December/January/February.**

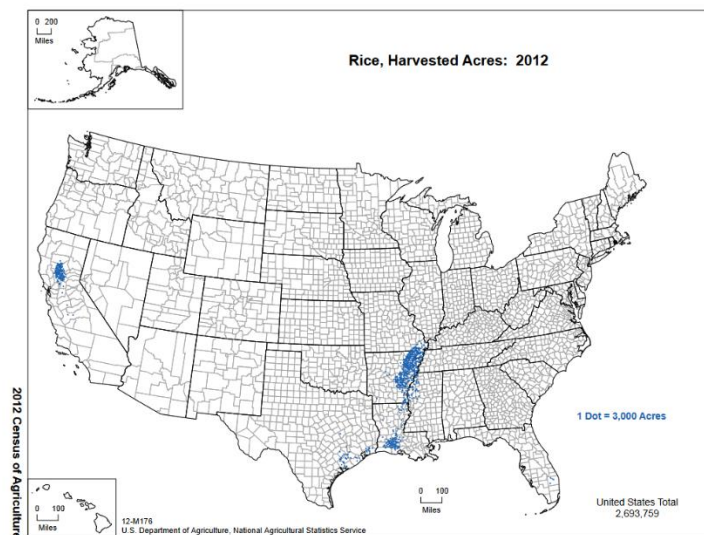


**Figure 2-9: USA rice yields in 2012 for the US Department of Agriculture. Regions of high rice yield show marked similarity to regions with stippled, low data availability in Figure 2-3. (Source: USDA Census of Agriculture Historical Archive - Ag Atlas (census year: 2012) – Crops and Plants – Rice, Harvested Acres. Retrieved at: [https://agcensus.library.cornell.edu/census\\_parts/2012-agricultural-atlas/](https://agcensus.library.cornell.edu/census_parts/2012-agricultural-atlas/). Last access: 29/03/2023).**

## 2.2. UCS#2: Impact of CCI LST IST products from MODIS and SLSTR on the Arctic SST/IST Multi-Year (MY) Product of the Copernicus Marine Service (Ioanna Karagali, Adrien Combelles and Pia Englyst, DMI)

### 2.2.1. Key Messages

- ❖ If a positive impact of ESA LST\_cci MODIS and SLSTR Ice Surface Temperature (IST) products on the Copernicus Marine Service (CMEMS) L4 IST/SST Multi-Year product is identified, it will lead to better characterisation and understanding of the Arctic environment and the complex areas of the marginal ice zone (MIZ).
- ❖ This will enable the future uptake of the ESA LST\_cci IST products in mainstream production chains, e.g. the Copernicus Marine Service Sea Ice Thematic Assembly Centre (TAC) suite of products.

### 2.2.2. Scientific Analysis

#### 2.2.2.1. Aims of the study

The study aims to test the applicability of the LST\_cci MODIS and SLSTR IST products for ingestion in the Arctic SST/IST Multi-Year (MY) Reanalysis product SEAICE\_ARC\_PHY\_CLIMATE\_L4\_MY\_011\_016 ([https://data.marine.copernicus.eu/product/SEAICE\\_ARC\\_PHY\\_CLIMATE\\_L4\\_MY\\_011\\_016/description](https://data.marine.copernicus.eu/product/SEAICE_ARC_PHY_CLIMATE_L4_MY_011_016/description)), generated by the Danish Meteorological Institute (DMI) Optimal Interpolation (DMIOI) system. This product is the first combined sea surface temperature (SST) and sea-ice surface temperature (IST) product for the Arctic Ocean covering the period 1982-2023 at 0.05° and provides a unique dataset for analysis of trends and warming patterns over the last 40 years [RD-05]. It is based on ESA SST\_cci v2.1 (AVHRR, SLSTR, (A)ATSR) and AASTI/C3S IST (AVHRR) input data; although SST information is available from multiple products only one input dataset is currently used for the IST. Therefore, the potential to expand with more IST products is highly relevant and the ESA LST\_cci LST products are potentially suitable and highly relevant for this purpose.

To assess the applicability of the ESA LST\_cci LST MODIS and SLSTR IST products, they will be ingested in the DMIOI system for the test year 2021 (selected due to the discontinuity of MODIS products) to produce a new SST/IST L4 dataset than can be directly compared to the reference SST/IST L4 dataset (only using AASTI information for IST) and to in situ observations.

A positive impact of the ESA LST\_cci IST from MODIS and SLSTR on the CMEMS L4 IST/SST Multi-Year (MY) product will result in better characterization and understanding the Arctic environment and the complex areas of the marginal ice zone. This will also demonstrate the future applicability of ESA LST\_cci IST products in mainstream production chains, e.g. Copernicus Marine Service Sea Ice TAC suite of products.

#### 2.2.2.2. Data and methods

In situ observations used for the validation of the ESA LST\_cci MODIS and SLSTR IST products are obtained from the Sea Ice Mass Balance (SIMB3) buoys measuring air temperature at different heights (typically around 1.2 m above the surface) depending on e.g. snow accumulation, snow drift and snow melt. The data are available at the Cryosphere Innovation website, <https://www.cryosphereinnovation.com/data/>.



It is important to clarify that the use of air measurements to validate IST will introduce a difference due to the vertical stratification in the near surface temperature.

A summary of the LST\_cci products used for this case study is available in Table 2-9. All available daily L2P files are pre-processed with the DMIOI system to produce daily L3C (collated) single sensor files on a 0.05° latitude-longitude grid for the area of interest, i.e. north of 58°N. Only sea-ice is of interest, so the land cover class flag is set to 230 and only quality flags (QF) 4 and 5 are used. The daily L3C files were validated directly using in situ observations from the Seasonal Ice Mass Balance Buoy 3 (SIMB3) sea-ice buoys to provide error characteristics of the single sensor products. When pixels are classified as being covered by sea-ice, a minimum of 50% sea ice concentration is assumed. Nonetheless, the sea ice concentration is not considered during the retrieval of IST in the MODIS and SLSTR L2P data.

Validation was performed using L3C files, rather than the L2P files, in order to assess the performance of the data that will be ingested into the DMIOI system directly. The procedure for creating the match-ups between the in situ buoys and the L3C products is performed such that the buoy temperature is averaged over the day and since these are drifting stations, the mean of all reported positions is used to match a given grid cell of the L3C products.

**Table 2-9: A summary of LST\_cci products used in this study.**

Product String and version	Sensor type	Resolution	Data availability	Local time of ascending node
AQUA MODIS L2P v4.aa	IR	1 km at nadir	January 2021 – December 2021	13:30
TERRA MODIS L2P v4.aa	IR	1 km at nadir	January 2021 – December 2021	22:30
Sentinel 3A SLSTR L2P v4.aa	IR	1 km at nadir	January 2021 – December 2021	22:00
Sentinel 3B SLSTR L2P v4.aa	IR	1 km at nadir	January 2021 – December 2021	22:00

An overview of the DMIOI production chain, which integrates individual, single sensor, swath-based SST and IST observations to a multi-sensor interpolated (gap-free) field, is shown in Figure 2-10. The OI Sea Ice Concentration (SIC) field is used as input to identify the different surface types (i.e. ocean, sea ice and the Marginal Ice Zone (MIZ)) for each day during the record. The surface is considered as open water when Sea Ice Concentration (SIC) ≤ 15%, ice covered when SIC > 70% and as MIZ when 15 < SIC ≤ 70%. Together with the land mask the SIC is used to construct a dynamic surface mask. This dynamic surface mask is used during the pre-processing of the input L2 + L3 IST/SST to L3 Super-collated (L3S) data. The surface mask is also used during the derivation of the error statistics and covariances for each surface type, which are used in the OI method for analysis of the observations. In the end, the OI method produces the daily L4 SST/IST and the corresponding uncertainties.

DMIOI L4 Processing System

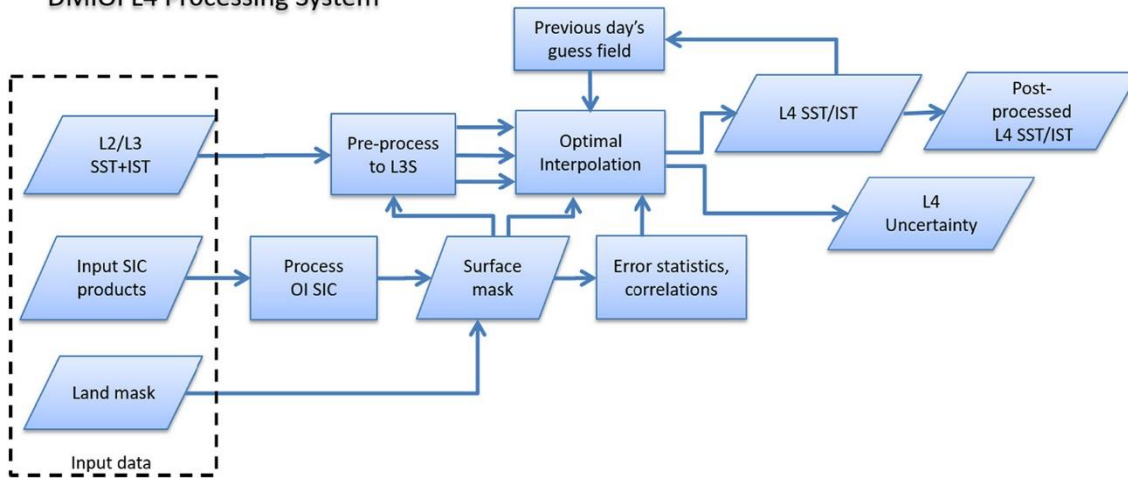


Figure 2-10: Schematic diagram illustrating the processing steps of the DMIOI L4 Processing System.

2.2.2.3. Results

Tests on producing the gridded L3C (collated) single sensor files from MODIS and SLSTR IST products are ongoing. Initial validation results of the MODIS and SLSTR IST L3C files using in situ observations from the SIMB3 buoys for the year 2021 (data availability shown in Figure 2-11) are available in Table 2-10, together with validation results of the AASTI dataset (currently used in the L4 SST/IST MY product). The validation of the IST is generally limited by the sparse number of in situ observations as well as increased in situ uncertainties in the ice-covered regions compared to the open ocean.

Overall, all assessed metrics (mean and median bias, standard and robust standard deviation and root mean square (RMS)) indicate that IST from MODIS/Aqua & Terra and SLSTR/S-3 & S-B is colder compared to the in situ stations by approximately 5 K while the cold bias for AASTI and the L4 MY product is in the order of 2 to 3 K. Standard deviation and robust standard deviation values are also higher for IST from MODIS/Aqua & Terra and SLSTR/S-3 & S-B compared to those found for AASTI and the L4 MY product.

Table 2-10: Validation results for 2021 between ESA LST\_cci products from MODIS and SLSTR for IST and in situ stations. The metrics for the AASTI v2.1 IST dataset and the L4 SST/IST MY product are also shown for reference.

Note that the in situ data represent T2m while the satellite data are IST. Therefore, a non-zero difference is expected in this comparison due to the inherent differences between IST/LST and T2m (see text).

Product	Mean Bias	Standard Deviation	RMS	Median	Robust Standard Deviation	No. Match-ups
MODIS/Aqua	-4.70	4.31	6.38	-3.99	4.44	1238
MODIS/Terra	-4.02	4.55	6.07	-3.12	4.46	1095
SLSTR/S3-A	-4.99	4.56	6.76	-4.15	4.56	1248
SLSTR/S3-B	-4.97	4.56	6.74	-3.96	4.42	1253
AASTI v2.1	-2.38	3.03	3.85	-2.03	2.94	989
L4 MY SST/IST	-2.75	2.94	4.02	-2.58	3.07	1280



**Figure 2-11: In situ observation data obtained during 2021 used in the study.**

The existing L4 SST/IST MY product has been reported by [RD-05] to be colder than in situ measurements from ice buoys that typically report 2m air temperatures (T2m; Section 2.2.2.2). [RD-06] found an average IST-T2m difference of  $-1.25$  °C during all-sky conditions over sea ice. This IST-T2m difference is a real temperature difference between the snow surface and the air above it and therefore the non-zero ‘Mean Bias’ reported in Table 2-10 is expected. These results suggest that the LST\_cci IST data may be on average  $\sim 1.5$ - $3.5$  K too cold, while the AASTI and L4 MY SST/IST data are  $\sim 1.0$ - $1.5$  K too cold.

When examining the spatial differences between the various products, shown in Figure 2-12, it can be seen that MODIS/Aqua is warmer compared to MODIS/Terra in some regions while colder in others (top left), MODIS/Aqua & Terra are slightly warmer compared to AASTI (top middle and right) in some parts of the central Arctic Ocean, Laptev Sea, parts of the East Siberian Sea and Beaufort Sea (more pronounced for MODIS/Terra) while they are significantly colder in Kara Sea, Barents Sea, Greenland Sea, Bering Sea, Labrador, Baffin and Hudson Bay. In a similar manner, SLSTR has almost zero biases between the A and B platforms (bottom left). SLSTR/S3-A shows similar warmer/colder biases compared to AASTI as the MODIS products (bottom middle) and a comparison between SLSTR/S3-A and MODIS/Terra (bottom right) indicates overall negative biases, i.e. warmer MODIS/Terra IST values (similar to Table 2-10, although the coverage of the in situ data is very limited to the Beaufort Sea according to Figure 2-11).



Mean temperature difference between products

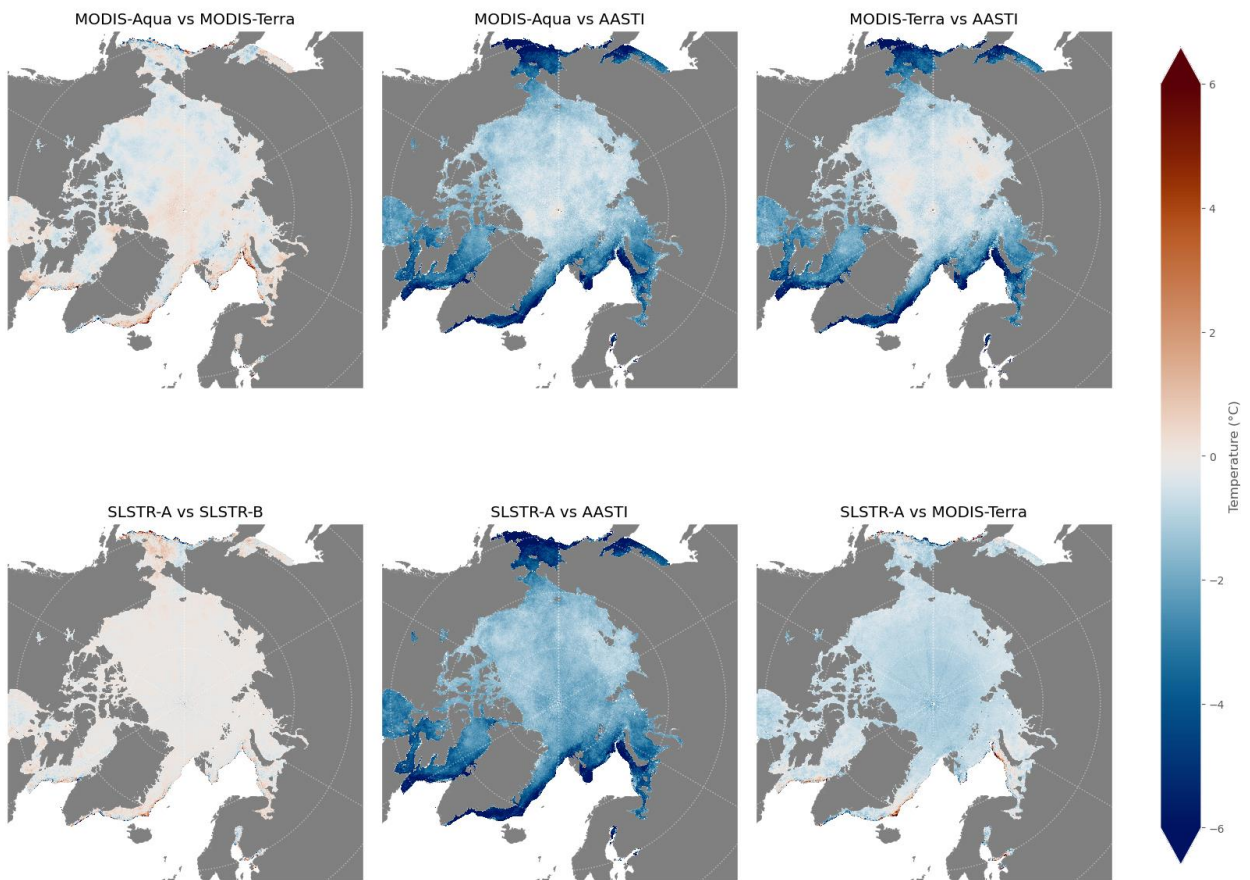


**Figure 2-12: 2-d plots of the mean bias between various IST products: MODIS/Aqua minus MODIS/Terra on top left, MODIS/Aqua minus AASTI on top middle, MODIS/Terra minus AASTI on top right, SLSTR/S3-A minus SLSTR/S3-B on bottom left, SLSTR/S3-A minus AASTI on bottom middle and SLSTR/S3-A minus MODIS/Terra on bottom right. All spatially averaged biases are for 2021.**

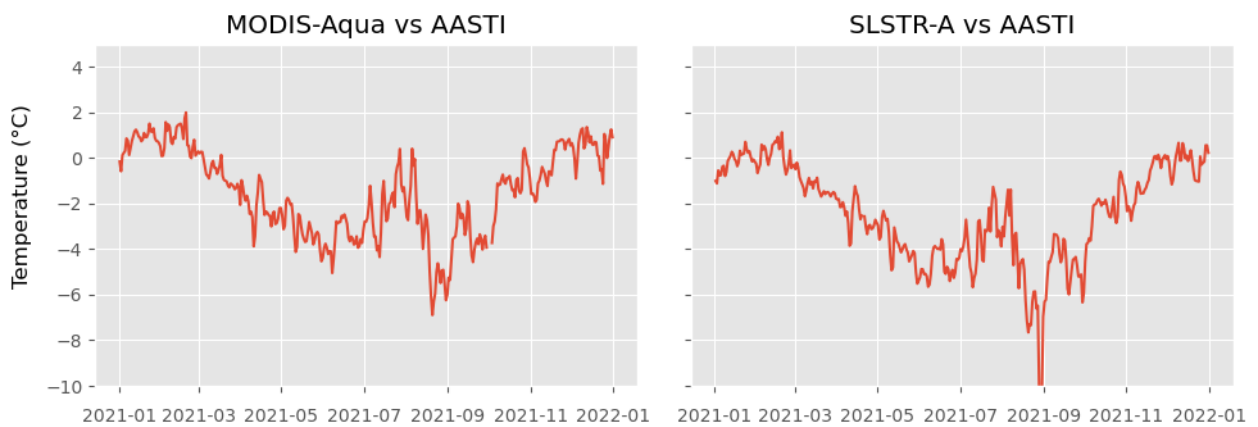


**Figure 2-13: Time-series of mean daily biases between MODIS/Aqua and AASTI (left) and SLSTR/S3-A and AASTI (right) for 2021.**

When examining the averaged mean bias during the entire year, shown in Figure 2-13, it is found that both MODIS/Aqua and SLSTR/S3-A show a positive bias compared to AASTI in winter which decreases and becomes largely negative in spring and summer. Especially between July and August, there appears to be some tendency for the bias to decrease again.

When examining the daily spatial averages of the mean temperature from the different products, shown in Figure 2-14 (top left), it is found that all products agree well from January until mid-April and from mid-November to end of December. Starting from mid-April and especially during summer, AASTI is warmer compared to all MODIS and SLSTR products which also appear to have an offset between them. The same pattern is observed when the median daily temperature is examined (top right). The standard deviation of the mean daily temperature (bottom left) indicates higher variability for AASTI until mid-April compared to the MODIS and SLSTR products, which then decreases to lower values during summer and early autumn. The number of observations used, shown in the bottom right panel, indicated that AASTI always has less available observations – particularly lower in spring and summer – compared to the MODIS and SLSTR products. Notice also a period in June when no MODIS/Terra data are available.

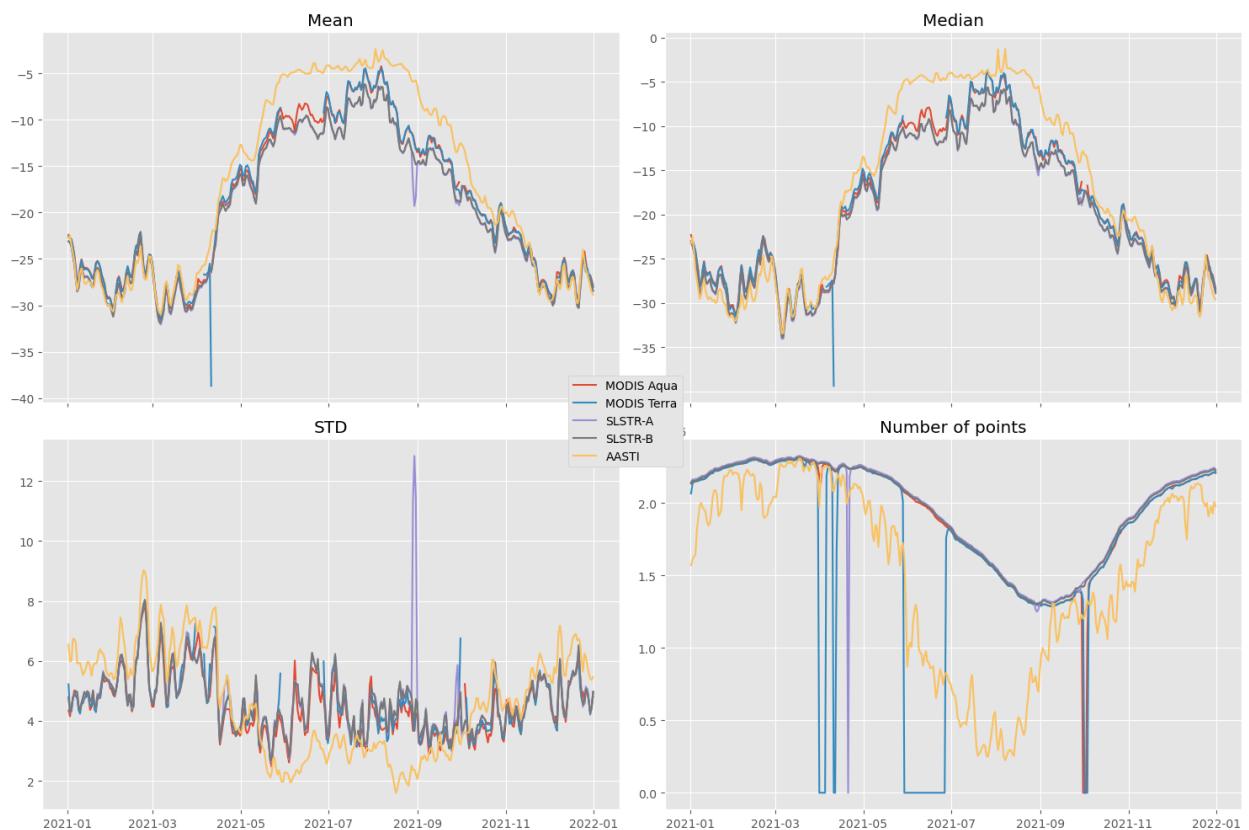


**Figure 2-14: Time-series of spatially averaged daily mean temperature (top left), median temperature (top right), standard deviation of the temperature (bottom left) and number of points used in the spatial averaging (bottom right) for MODIS/Aqua (red), MODIS/Terra (blue), SLSTR/S3-A (magenta), SLSTR/S3-B (grey) and AASTI (yellow) for 2021.**

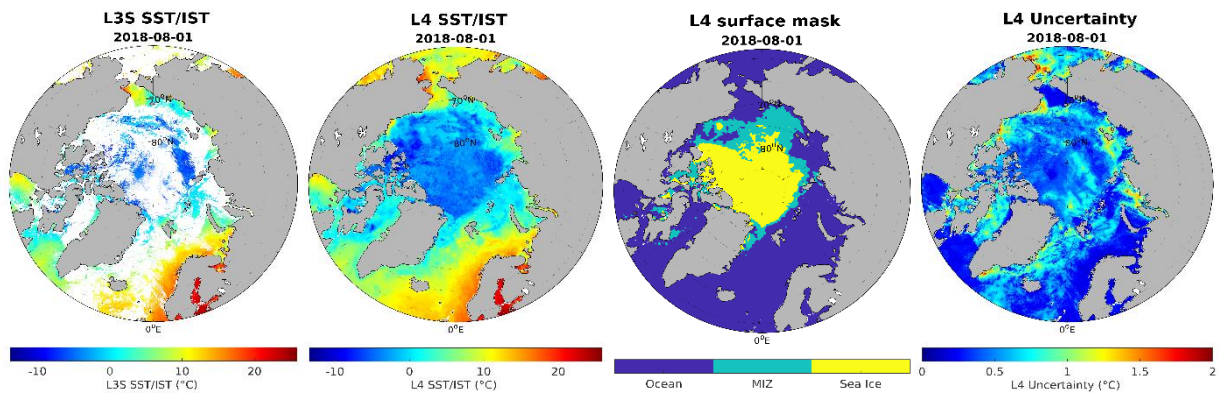


**Figure 2-15: Example of L3S and L4 OI IST/SST product along with the surface mask and uncertainty estimates. Observed stability:  $-0.0001$  °C/year and  $0.0047$  °C/year against drifters (SST) and North Pole (NP) drifting buoys (IST) observations.**

#### 2.2.2.4. Conclusions

From initial analyses conducted so far it has been found that all four LST\_cci IST products for 2021 are cold biased compared to in situ observations, the AASTI IST CDR and the L4 SST/IST MY product.

Reasons for the overall cold biases will be investigated further during the remaining part of the study. A potential explanation can be linked to the percentage of sea ice concentration allowed to exist for a pixel to be characterised as sea ice, which in the case of the MODIS and SLSTR products is 50%. Large parts of the Marginal Ice Zone can therefore be excluded, while for AASTI, sea ice concentrations above 15% are used for a pixel to be characterised as partial sea-ice. This is supported by the fact that biases are most intense in the marginal areas of the domain and during summer when the Marginal Ice Zone has a large extent. The apparent cold biases in the LST\_cci products may also be due to cloud contamination, which would result in colder ISTs, which may, at least in part, account for the overall cold bias observed in the LST\_cci data. It should be noted that the IST data used in this study are a prototype and therefore the cloud masking algorithm over sea ice is in its infancy and requires further development.

As such the products cannot be directly ingested in the L4 MY SST/IST processing chain. A potential benefit from having more IST observations is expected if the cold biases can be corrected.

#### 2.2.3. Feedback on scientific utility of the LST\_cci products

In general, the MODIS/Aqua & Terra and SLSTR/S3-A & -B L2P products are easy to use and preprocess to L3C single-sensor products.

The quality of the temperature retrieval over sea-ice (IST) appears to be challenging in these early versions of the products. It remains to be seen if the reported cold biases can be adjusted so that the products can be ingested in the L4 MY SST/IST processing chain.

## 2.3. UCS#3: Global SUHI Trend Analysis (Panagiotis Sismanidis, RUB)

### 2.3.1. Key Messages

- ❖ The nighttime LST of urban areas has been increasing on global level by about  $0.06 \pm 0.02$  K/year.
- ❖ Continental cities are warming the fastest by about 0.08 K/year.
- ❖ Cities in the Northern Hemisphere are warming faster than cities in the Southern Hemisphere.
- ❖ The cities where the LST increased the most are all located in Middle East.
- ❖ The MODIS LST trends agree reasonably well with those from ERA5.

### 2.3.2. Scientific Analysis

#### 2.3.2.1. Aims of the study

Cities are generally warmer than their surroundings. This phenomenon is known as the Urban Heat Island (UHI) and is one of the clearest examples of human-induced climate modification. UHIs increase the cooling energy demand, aggravate the feeling of thermal discomfort, and influence air quality. As such, they impact the health and welfare of the urban population and increase the carbon footprint of cities. The root cause of an UHI is the transformation of the natural landscape to a corrugated, mostly manufactured, and less vegetated surface. The radiative, aerodynamic, thermal, and moisture properties of man-made surfaces are fundamentally different to natural ones, leading to reduced evapotranspiration and the uptake, storage, and release of more heat. The relative warmth of the urban atmosphere, surface, and substrate leads to four distinct UHI types that are governed by a different mix of physical processes. These four types are the canopy layer, boundary layer, surface, and subsurface UHI. Surface UHIs (SUHI) result from modifications of the surface energy balance at urban facets, canyons, and neighbourhoods. They exhibit complex spatial and temporal patterns that are strongly related to land cover and are usually estimated from remotely-sensed LST data. This UCS aims to investigate how the LST of cities has changed over the last ~20 years (2002-2019) using nighttime data from MODIS/Aqua. The study focuses on nighttime conditions when the agreement between the LST and the near-surface air temperature over cities is strongest [RD-07]. The research questions the UCS aims to answer are:

- ❖ How fast the LST of urban areas increases across the globe?
- ❖ How do the LST trends vary among cities in different climate zones?
- ❖ How well do the MODIS trends agree with those derived from ERA5 data?

#### 2.3.2.2. Data and methods

This work uses 19 years (2002-2021) of global, daily, nighttime LST data from the LST\_cci MODIS/Aqua v.4.aa product (Table 2-11). MODIS/Aqua is a multispectral sun-synchronous satellite instrument that crosses the equator at 13:30 (local solar time) in the descending orbit and 01:30 in the ascending orbit and views almost the entire surface of the Earth every day. The spatial resolution of the employed data is  $0.01^\circ$  (approx. 1 km). This LST\_cci dataset was selected for the study following [RD-04], who demonstrated that these data are sufficiently stable to be used for time-series analysis, whereas other LST\_cci datasets, including MODIS/Terra, suffer from some non-climatic discontinuities.

**Table 2-11: The LST\_cci products used for this study.**

Product String and version	Sensor type	Resolution	Data availability	Local time of ascending node
Aqua MODIS L3C Daily Night v4.aa	TIR	0.01°	July 2002 – December 2021	~13:30

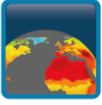
The study workflow comprises four steps, namely (i) delineating the cities for which the LST trends will be calculated; (ii) calculating, for each city, the 2002-2021 daily nighttime LST means; (iii) calculating the corresponding LST uncertainties; and (iv) applying the trend analysis. To delineate the cities that will be included in the analysis, the study uses land cover (LC) data from the CCI Land Cover project. This data product provides annual high-resolution (300 m) LC maps that classify the global surface in 37 classes according to the United Nations Land Cover Classification System (UNLCCS) with an overall accuracy of 75.4%. To process the LC data, they are first resampled to the 0.01°× 0.01° LST grid by calculating the LC fractions of each grid cell. Then, for each year from 2002 to 2021, a binary urban mask of all the grid cells is created where an urban classification is assigned to cells where the urban fraction is at least 95%, the water fraction is equal to 0%, and the cell is more than ~2 km away from the coastline. To eliminate single grid cells and small urban areas from the resulting masks, a morphological operator is applied that removes any objects with eight or fewer connected grid cells. Finally, the filtered masks are segmented into clusters that correspond to cities and each city is labelled with a unique ID (same over the years). Next, for each city, appropriate rural grid cells are selected using the Boundary Generation Algorithm (BGA) that iteratively expands a rural buffer around each city until its size is approximately that of the urban area. To ensure consistency over time, a single rural buffer per city is created that is representative for all the years from 2002 to 2021. The employed implementation of the BGA, does not use all the grid cells in each new ring, but filters them according to the following rules: the rural LC fraction of each candidate grid cell is at least 95% for every year between 2002 and 2021; the corresponding urban and water LC fractions are equal to 0%; and the elevation of each candidate grid cell does not differ by more than ±200 m from the median elevation of the corresponding city. To ensure that only rural grid cells adjacent to each city are selected, the search zone of the BGA is limited to within 30 grid cells from the city boundary.

Next, the urban and rural masks are used to sample the LST image data from each day and calculate, using only clear-sky grid cells, the nighttime LST arithmetic mean, the LST standard deviation (SD), the uncertainty of the LST mean, the percentage of clear-sky grid cells (CC-%), and the median satellite view zenith angle. Equation 2-3 is used to calculate the total uncertainty of the LST mean ( $u_{total}$ ), where  $u_c$  is the uncertainty of the arithmetic mean considering the errors for individual grid cells are fully correlated and  $u_{su}$  is the subsampling uncertainty (SU) due to missing grid cells.

$$\text{Equation 2-3} \quad u_{total} = \sqrt{u_c^2 + u_{su}^2}$$

Because  $u_{su}$  cannot be estimated from the data, it is modelled using the approach proposed in [RD-08] for SST\_cci. To do this, the cities are first split into groups according to their size (in km<sup>2</sup>). Selecting only the days with no missing grid cells, and for each size group and day, the subsampling error E — adjusted for the LST uncertainty— is calculated iteratively for different percentages of missing grid cells, e.g., 10%,



 <b>land surface temperature</b> cci	<b>Climate Assessment Report</b>  <i>WP5.1 – DEL-5.1</i>	Ref.: LST-CCI-D5.1-CAR Version: 3.0 Date: 25-May-2024 Page: 34
--	--	---

20%, ..., 90%. The resulting distributions are then used to calculate the subsampling uncertainty  $u_{su}$  as a function of city size ( $s$ ), clear-sky grid cells percentage (CC), and SD using Equation 24, similarly to [RD-08].

$$\text{Equation 2-4} \quad u_{su}(s, CC, SD) = \sqrt{\text{var}(E)}$$

Where  $\text{var}(E)$  is the variance of the subsampling error distribution.

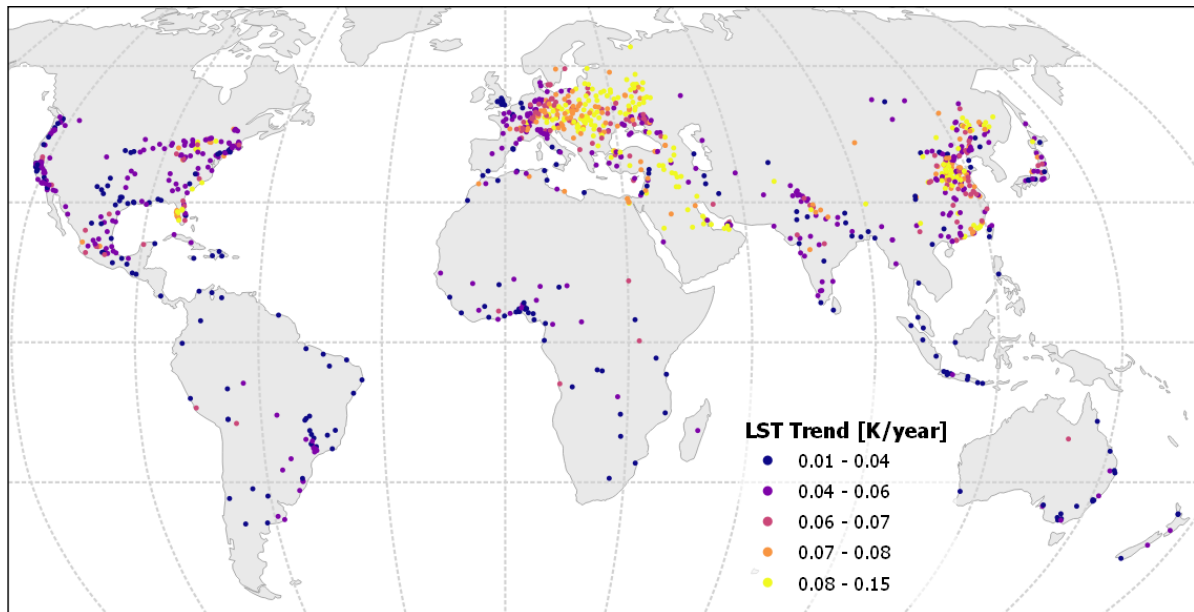
To assess each city’s LST trend, the three-step approach proposed in [RD-09] is followed. This approach starts by creating—for each city—a time series of de-seasoned monthly means that will be used in the trend analysis. To create the de-seasoned time series, the Theil-Sen (TS) slope estimator [RD-10] is first used to calculate the overall linear trend of the daily LST data. The TS slope is then used to de-trend the daily LST data and calculate the climatological monthly and annual means for each city (using  $\frac{1}{u_{total}^2}$  as weights). Next, the monthly adjustments that are necessary for generating the de-seasoned data are calculated by subtracting the climatological annual mean from the climatological monthly means. The de-seasoned monthly mean time-series is then obtained by subtracting the LST monthly adjustments from the corresponding time-series of monthly means, which has not been de-trended (derived from the daily LST data).

For assessing the 2002-2021 LST trend of each city, two approaches are used: a weighted least squares linear (WLS) regression model with Newey-West standard errors to account for heteroskedasticity and autocorrelation, and a TS estimator. As weights for the WLS, the LST uncertainty of the monthly means are used, which are calculated as  $\frac{1}{n} \sum_i^n u_{total, i}$ . In addition to the trend of each city, the WLS trend standard error, the WLS trend significance (at the 95% confidence level), the WLS and TS 95% confidence intervals, and the Trend Detection Time (TDT) from [RD-11] are also calculated.

In the next section, the LST trends calculated using the TS estimator are presented.

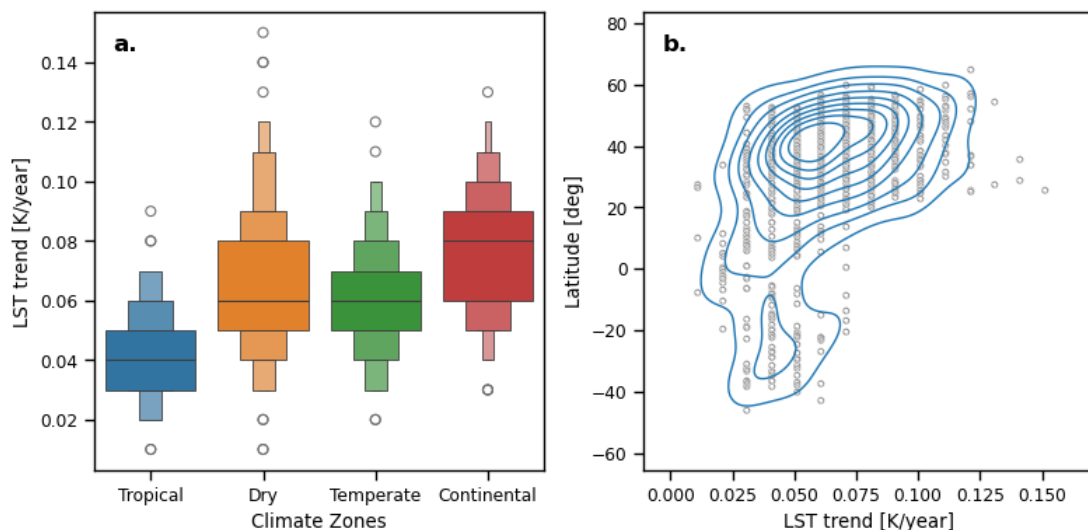
### 2.3.2.3. Results

Figure 2-16 presents the LST trends for all the cities ( $n=1070$ ) covered by this study. The analysis includes only cities with a data span of 19 years (2002-2021) and where the trend is statistically significant at the 95% confidence level. The observed trends vary from 0.01 K/year to 0.15 K/year. The mean (and the median) for all 1070 cities is 0.06 K/year with a standard deviation (SD) of 0.02 K/year. Among these, tropical cities ( $n=122$ ) show the least pronounced trends with a median of 0.04 K/year (Figure 2-17a), while continental cities ( $n=374$ ) exhibit the most pronounced trends with a median of 0.08 K/year. For both dry ( $n=189$ ) and temperate ( $n=385$ ) cities, the median LST trend is 0.06 K/year. Figure 2-17a also indicates that the LST trends of cities in dry and continental climates exhibit the greatest variation with a SD of 0.25 K/year and 0.19 K/year, respectively.



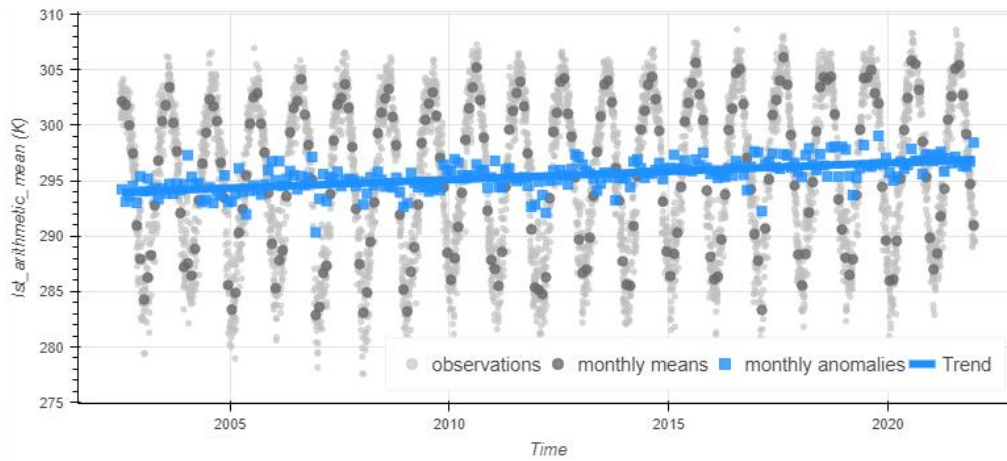
**Figure 2-16: The distribution of nighttime LST trends (2002-2021) across the globe.**

In the Southern Hemisphere ( $n = 95$ ), the trends range from 0.01 to 0.07 K/year, with a median value of 0.04 K/year, while on the Northern Hemisphere ( $n = 975$ ), from 0.01 to 0.15 K/year, with a median value of 0.06 K/year (Figure 2-17b). This is anticipated given that most of the Earth's population resides in the Northern Hemisphere, where the largest urban centres are also located (i.e. the strongest warming trends are expected in northern cities, because the sample (i.e., number of cities) is larger). Figure 2-17b also indicates, that in the Northern Hemisphere, cities located at higher latitudes have experienced a slightly faster increase in nighttime LST between 2002 and 2021 compared to those in mid and low latitudes.

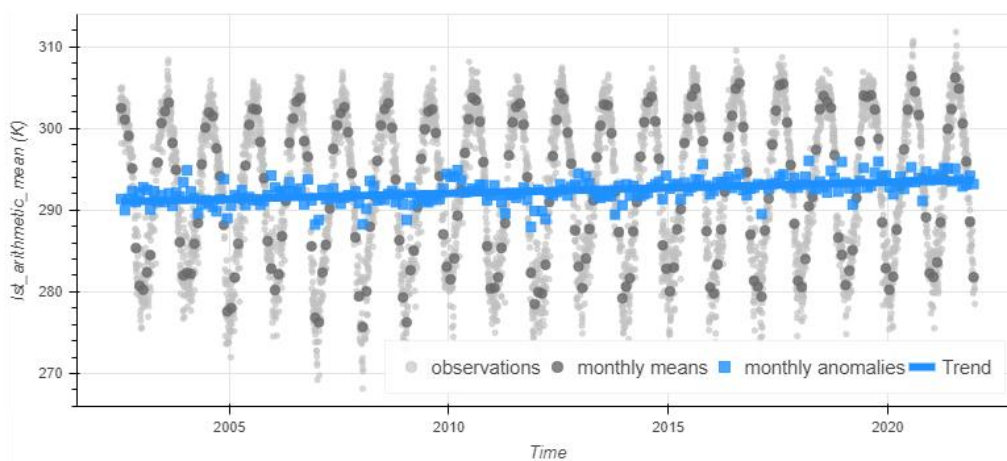


**Figure 2-17: The distribution of the LST trends per climate zone (a) and as function of latitude (b).**

A. Doha, Qatar (LST Trend: 0.15 K/year, CI95: 0.13 - 0.17 K/year)



B. Hafar Al Batin, Saudi Arabia (LST Trend: 0.14 K/year, CI95: 0.11 - 0.17 K/year)



C. Kirkuk, Iraq (LST Trend: 0.14 K/year, CI95: 0.11 - 0.17 K/year)

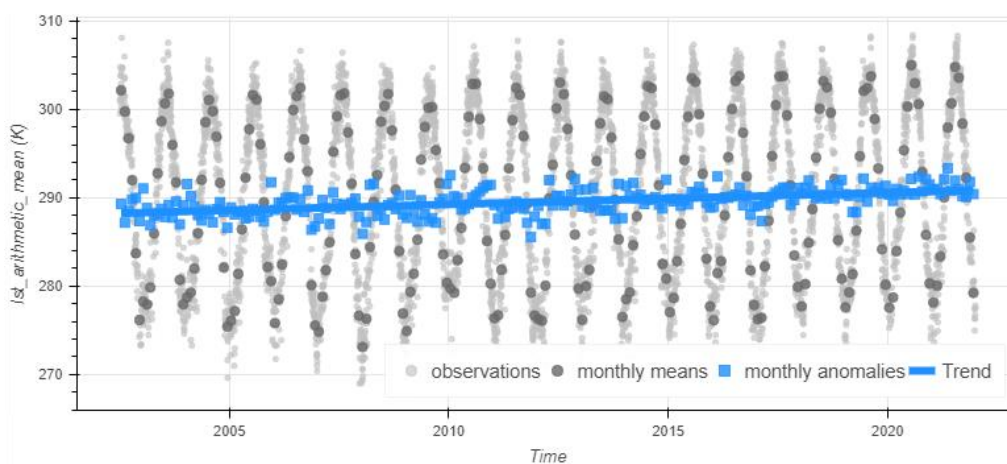


**Figure 2-18: The LST observations, monthly means, monthly anomalies, and Thei-Sen slope (trend) for a) Doha, Qatar; b) Hafar Al Batin (Saudi Arabia); and c) Kirkuk, Iraq.**



Based on the data presented in Figure 2-16, three regions can be identified where the LST trends are particularly pronounced. These regions are the Middle East, Eastern Europe, and specific provinces in China (Shaanxi, Shanxi, and Henan). From 2002 to 2021, the average nighttime LST in these areas has increased by  $0.08 \pm 0.03$  K/year,  $0.09 \pm 0.01$  K/year, and  $0.08 \pm 0.02$  K/year, respectively. The cities with the most pronounced LST trends are also all located in Middle East. These include Doha in Qatar (Figure 2-18a), with a trend of 0.15 K/year (95% confidence interval, CI95: 0.13 - 0.17 K/year); Hafar Al Batin in Saudi Arabia (Figure 2-18b), with a trend of 0.14 K/year (CI95: 0.11 - 0.17 K/year); and Kirkuk in Iraq (Figure 2-18c), with a trend of 0.13 K/year (CI95: 0.11 - 0.17 K/year). The difference in the heating trends (mean  $\pm$  SD) between eastern and western Europe is also particularly striking— $0.09 \pm 0.01$  K/year vs.  $0.06 \pm 0.02$  K/year, respectively—and partly related to the different climates (the climate in eastern Europe is continental, while in western Europe it is temperate).

In Figure 2-19, the trends between the MODIS LST are compared with the corresponding near-surface air temperature (Tair) and skin temperature (SKT) trends derived from ERA5 data [RD-12]. To calculate the ERA5 trends, the method described in the previous section is used. The datasets agree quite well, with a correlation coefficient of 49.0% (p-value < 0.001) between the LST and Tair data, and 60.0% (p-value < 0.001) between the LST and SKT data. Overall, the Tair and SKT trends are lower than that of the LST. In tropical cities, the mean ( $\pm$  SD) trends for Tair and SKT are  $0.02 \pm 0.02$  K/year and  $0.03 \pm 0.02$  K/year, respectively. In dry climate cities, these values are  $0.04 \pm 0.03$  K/year and  $0.05 \pm 0.03$  K/year, respectively, while in temperate cities  $0.04 \pm 0.02$  K/year and  $0.05 \pm 0.02$  K/year, and in continental cities  $0.06 \pm 0.02$  K/year and  $0.07 \pm 0.02$  K/year. Some differences are expected since ERA5 does not model local urban effects, and because the spatial resolution of the ERA5 data is much coarser than that of MODIS data (~31 km vs. ~1 km). In addition, ERA5 is derived from an evolving observation system and therefore will contain some non-climatic discontinuities, for example when satellite data input transitions from one instrument to the next. Therefore, trends calculated from ERA5 may also not represent the truth.

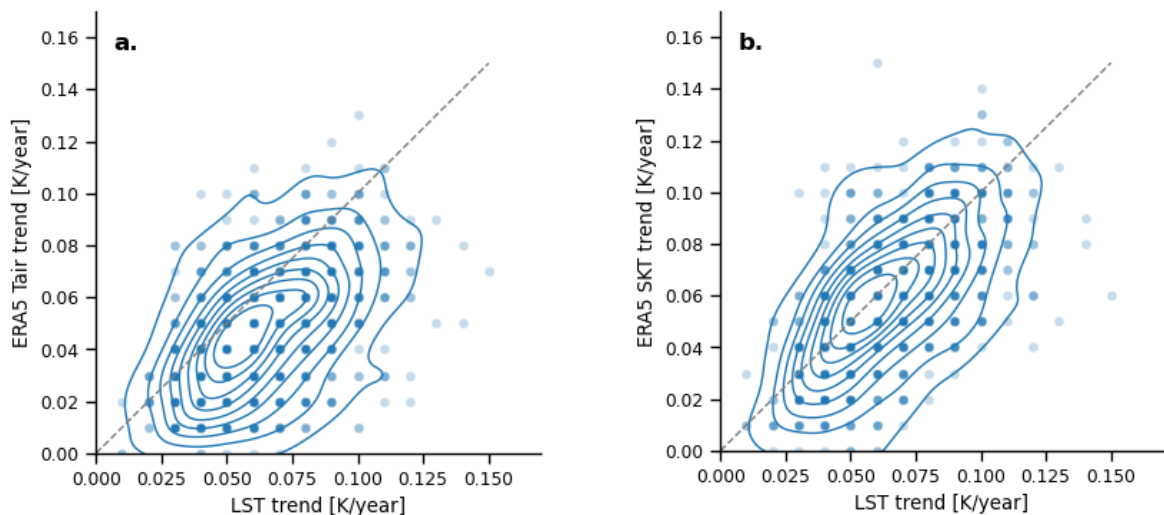


**Figure 2-19: Agreement between the 2002-2021 nighttime LST, Tair (a) and SKT (b) trends for the urban areas included in this analysis. The dashed line is the  $y=x$ . The dots are plotted with the same hue of blue and some level of transparency; darker blues imply that several dots overlap.**

#### 2.3.2.4. Conclusions

This UCS investigates the long-term LST trends in 1070 cities across the globe using 19 years (2002-2021) of nighttime LST data from the LST\_cci MODIS/Aqua product. The focus is on nighttime conditions, when shortwave radiation fluxes are zero, and the agreement between the LST and the near-surface air temperatures is strongest. The results reveal a consistent warming trend across all cities, that is on average ( $\pm$  SD) equal to  $0.06 \pm 0.02$  K/year. Cities located in continental climates exhibit the most pronounced warming, of about 0.08 K/year, while those in tropical climates the least ( $\sim 0.04$  K/year). The results also suggest that the cities with the strongest increase in nighttime LST are all concentrated in Middle East, where the estimated trends as high as 0.15 K/year (Doha, Qatar). Moving forward, this study will investigate the LST trends of the rural areas surrounding each city and explore the relationship between the LST trends and the city size.

#### 2.3.3. Feedback on scientific utility of the LST\_cci products

- ❖ **LST Data Usability and Quality:** The LST data are user-friendly and of high-quality.
- ❖ **Simplified Data Processing:** Compared to v1.0, the provision of LST data as a single NetCDF file per day and overpass has streamlined their processing.
- ❖ **Resolved Cloud Contamination:** The MODIS/Aqua cloud contamination issues identified during LST\_cci Phase-1 have been successfully addressed.
- ❖ **Incorporating LST Uncertainties:** The availability of LST uncertainties enables these data to be incorporated into the analysis effectively and update them with the subsampling uncertainty (i.e. the uncertainty due to missing grid cells).
- ❖ **Enhanced User Experience:** Providing the corresponding ERA5 Tair and SKT data, along with the MODIS NDVI, in the same grid as the LST data facilitates the data analysis and improves the overall user experience.

### 2.4. UCS#5: Evaluating the Surface Urban Heat Island Intensity using the SENTINEL3x\_SLSTR\_L3C\_0.01 products (Sorin Cheval, Alexandru Dumitrescu and Dana Micu, MeteoRomania):

---

#### 2.4.1. Key Messages

- ❖ The LST\_cci is strongly correlated with the 2m air temperature (T2m) retrieved at weather stations placed in World Meteorological Organization (WMO) standard conditions.
- ❖ The correlation and the differences between LST\_cci and T2m are consistent with previous findings, and they are strongly influenced by altitude and topography.
- ❖ The links between LST\_cci and the underlying land cover did not return reliable results and further analysis is required using the new version of the product (v4.00)
- ❖ Quality control is strongly recommended before the extended use of the LST\_cci products.

## 2.4.2. Scientific Analysis

### 2.4.2.1. Aims of the study

The study aims at (i) comparing the LST\_cci and T2m, (ii) analysing the relationship between the LST\_cci and land cover in selected urban areas, and (iii) developing a web-based application to visualise and analyse the Surface Urban Heat Island Intensity (SUHII). The comparison between LST\_cci and T2m addresses a complex topography environment which is characteristic for the Romanian territory, including almost equal share between mountains, hills and plains, woodland, crop land and a variety of urban areas (e.g., one city with over 2 million inhabitants, and 6 cities with about 300,000 inhabitants).

### 2.4.2.2. Data and methods

In this investigation, an analysis was conducted on version 4.aa of the L3C-LST-SLSTRA-0.01deg and L3C-LST-SLSTRB-0.01deg products (Table 2-12). Only LST values with uncertainty of less than 1 Kelvin degree have been used ( $lst\_uncertainty < 1$ ).

**Table 2-12: A summary of LST\_cci products used in this study.**

Product String and version	Sensor type	Resolution	Data availability	Local time of ascending node
L3C-LST-SLSTRA-0.01deg (v4aa)	SLSTR	0.01° lat-long	01/May/2015 –31/Dec/2022	22:00 local observation time
L3C-LST-SLSTRB-0.01deg (v4aa)	SLSTR	0.01° lat-long	17/Nov/2018 –31/Dec/2022	22:00 local observation time

The T2m data used in the study comprise hourly air temperatures collected at 2-m above the ground at 156 weather stations from the National Meteorological Network (Romania) (Figure 2-20).

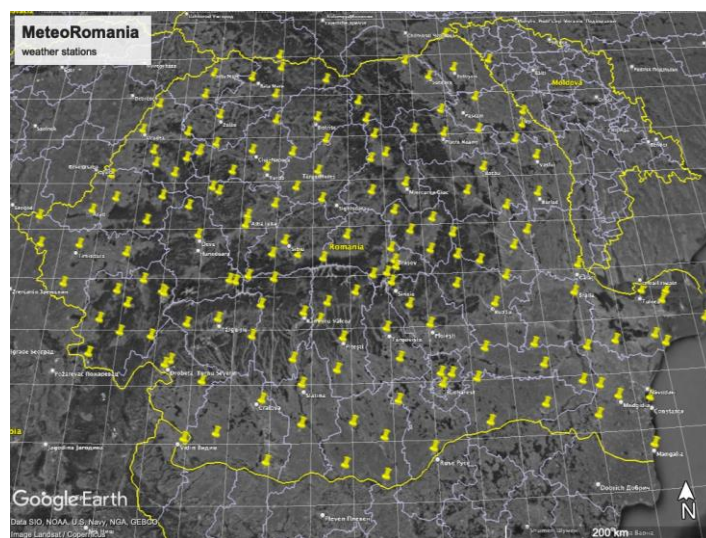


**Figure 2-20:: Location of the 156 weather stations of the National Meteorological Network delivering T2m values.**

The Land cover classes (LCC) retrieved for 41 urban areas, using the LCC data within the above mentioned LST\_cci products (L3C-LST-SLSTRA-0.01 and L3C-LST-SLSTRB-0.01), were also used in the study.

For the validation with in-situ data (air temperature measured at 2 m above ground level – T2m), the LST values were extracted from the pixels corresponding to the coordinates of each weather station. Using the two-time series (LST and T2m), the Pearson’s coefficient of correlation (COR) and mean absolute error (MAE) were computed as accuracy metrics for each product and stations across five altitude steps (0 - 500 m, 501 – 1000 m, 1001 – 1500 m, 1501 – 2000 m, 2001 – 2500 m). Summary statistics of both datasets (LST and T2m) were also compared using box plots, which illustrate how values are distributed within a dataset by dividing it into four quartiles.

### 2.4.2.3. Results

The LST values were averaged at monthly scale for the periods May 2016 – December 2022 (L3C-LST-SLSTRA-0.01deg) and November 2018 – December 2022 (L3C-LST-SLSTRB-0.01deg) over Romania and the neighbouring territory. These monthly syntheses were performed to assess the spatio-temporal coherence of the product. Figure 2-21 illustrates the average monthly LST in 2020.

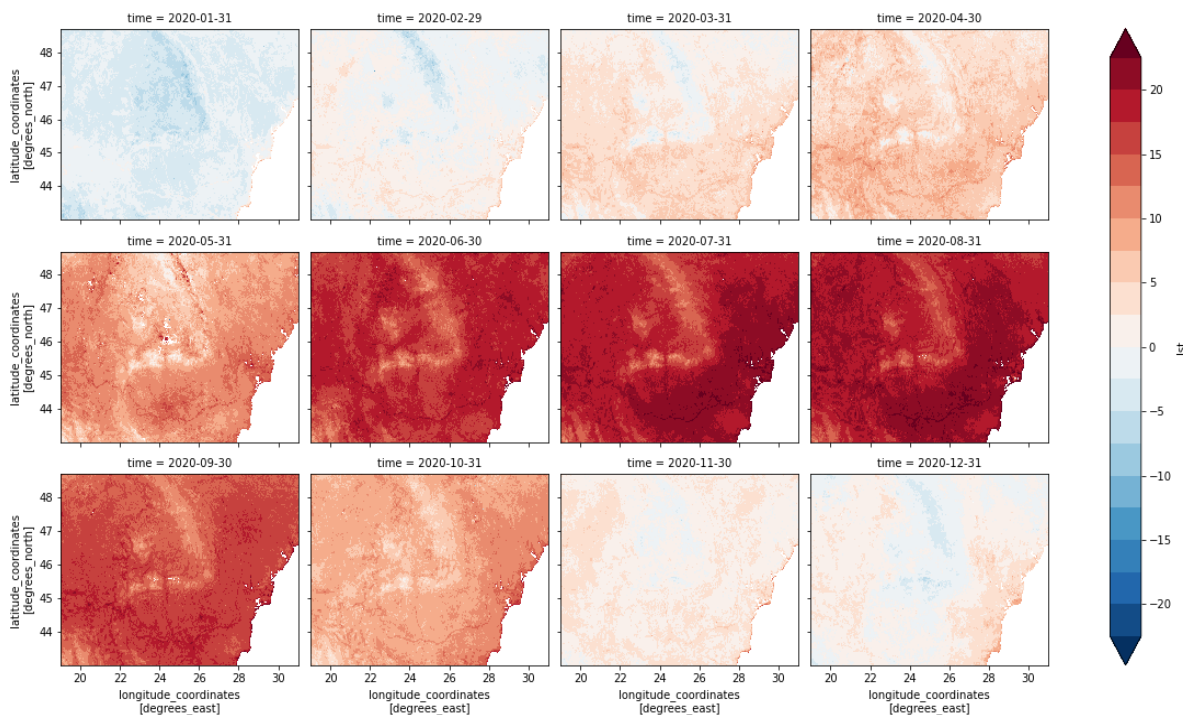


**Figure 2-21: Average monthly night-time LST (°C) over Romania in 2020, derived from L3C-LST-SLSTRA-0.01.**

The LST\_cci data and T2m are very highly correlated (i.e., in general, the Pearson’s correlation coefficients exceed 0.9), and the mean differences range between 2.3 and 3.5°C, which is consistent with previous studies focusing on the urban areas of Romania [RD-13] (Figure 2-22 and Figure 2-23). The very strong link between the two variables is also illustrated by the summary statistics presented in the Figure 2-24 and Figure 2-25. The LST\_cci data have higher median, lower, and upper quartile values, as well as a more extended range than the T2m, because of the near-surface radiative processes specific to the land-



atmosphere interactions, i.e. the land surface can be much warmer during the daytime, and the surface temperature reach higher and lower extremes than the air temperature on most terrestrial land cover categories.

Both the correlations and differences between the LST\_cci and T2m are clearly influenced by the altitude and topography. The correlation coefficients decrease, and the mean absolute errors increase with altitude (Figure 2-22 and Figure 2-23). The low-altitude plains trigger (i) higher correlations, due to the higher landscape homogeneity, and (ii) higher mean absolute errors than the highlands mountainous areas, due to more open regional-scale horizon (Figure 2-26 and Figure 2-27).

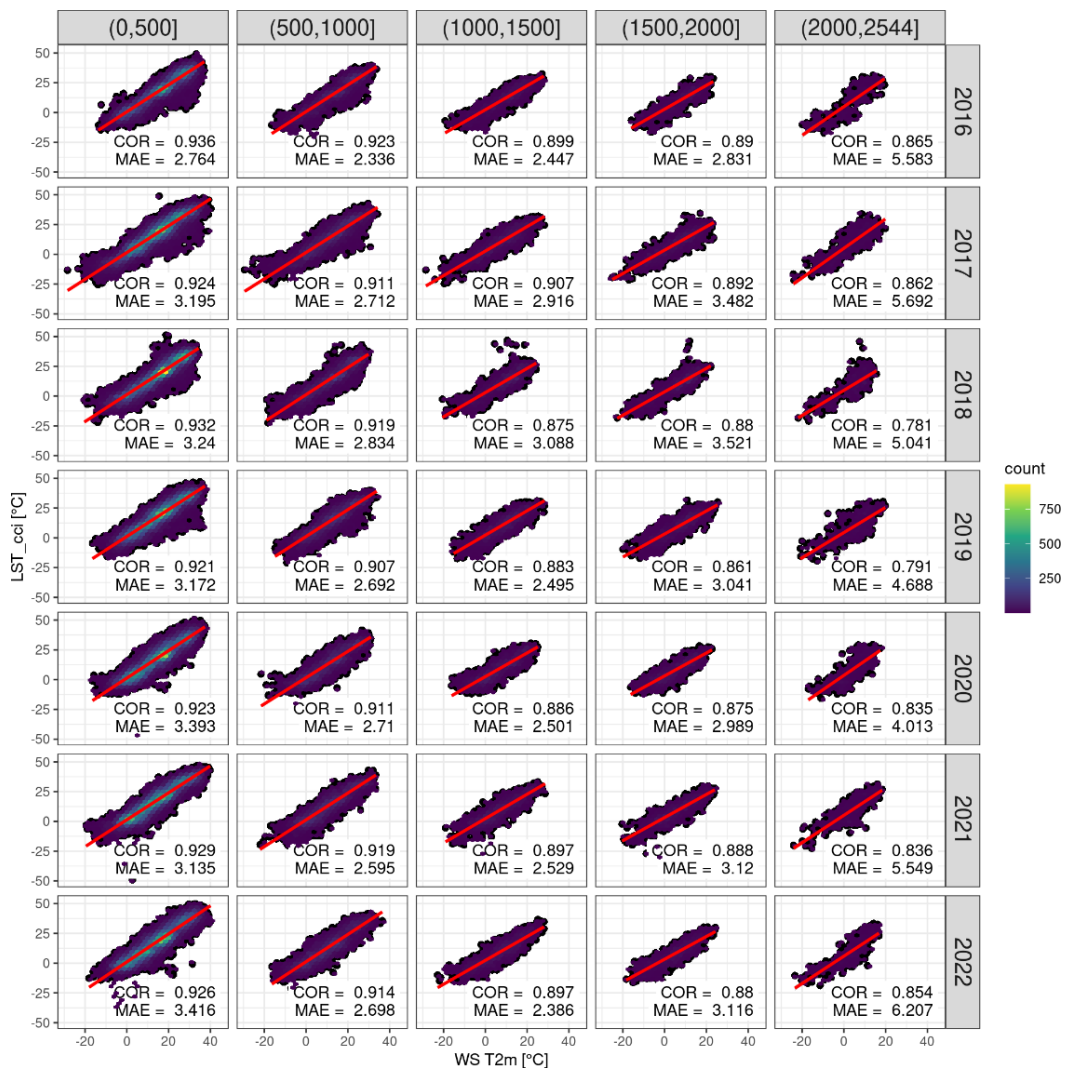
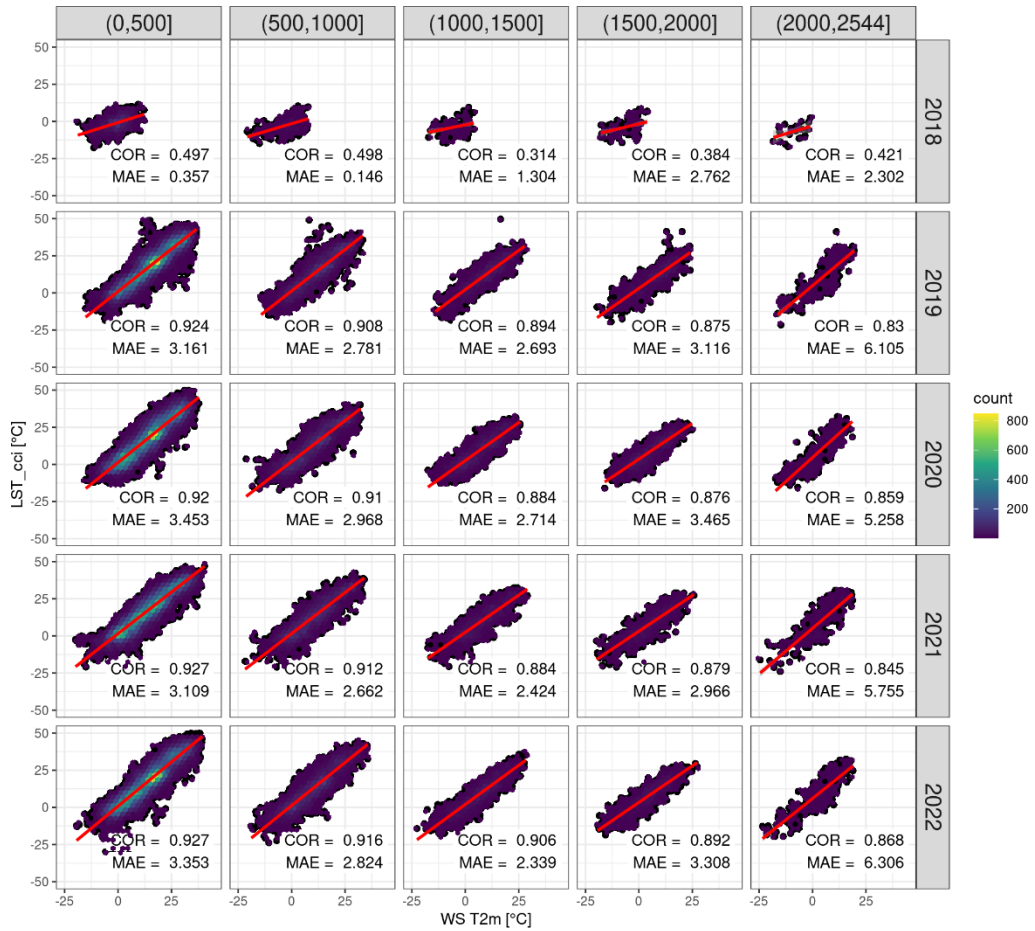
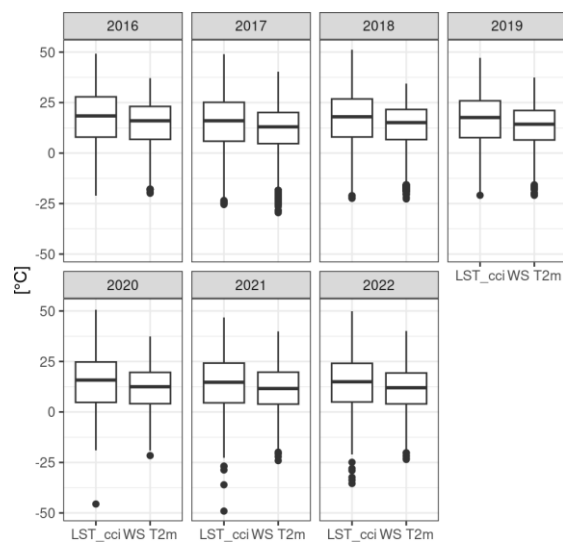


Figure 2-22: Correlation (COR) and Mean Absolute Errors (MAE) between L3C-LST-SLSTRA-0.01deg and weather station air temperature (WS T2m) for the different altitude categories (top of each column, in m above sea level).



**Figure 2-23: Correlation (COR) and Mean Absolute Errors (MAE) between LST\_cci retrieved from L3C-LST-SLSTRB-0.01deg and weather station air temperature (WS T2m) for the different altitude categories (top of each column, in m above sea level).**



**Figure 2-24: Summary statistics for LST\_cci retrieved from L3C-LST-SLSTRB-0.01 and weather station air temperature (WS T2m) for each year.**

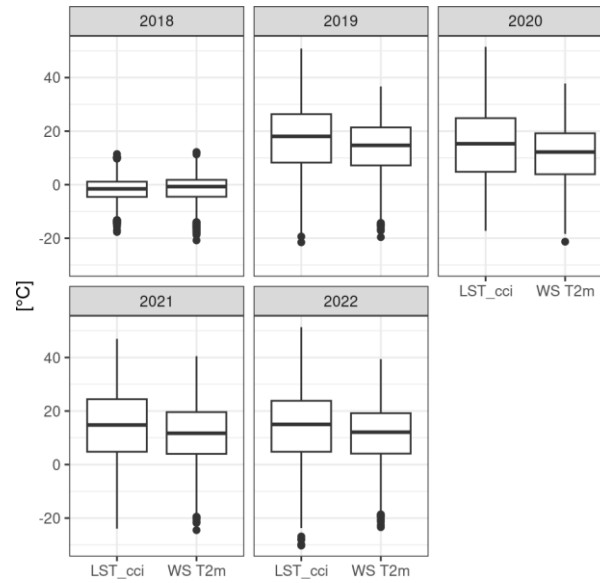


Figure 2-25: Summary statistics for LST\_cci retrieved from L3C-LST-SLSTRB-0.01 and weather station air temperature (WS T2m) for each year.

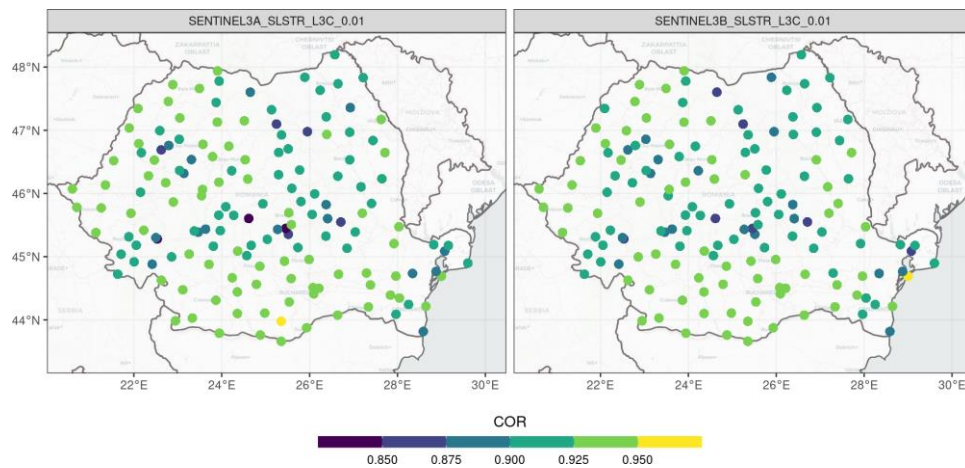


Figure 2-26: Spatial distribution of the correlation coefficients (COR) between the LST\_cci retrieved from L3C-LST-SLSTRx-0.01 and weather station air temperature (WS T2m).

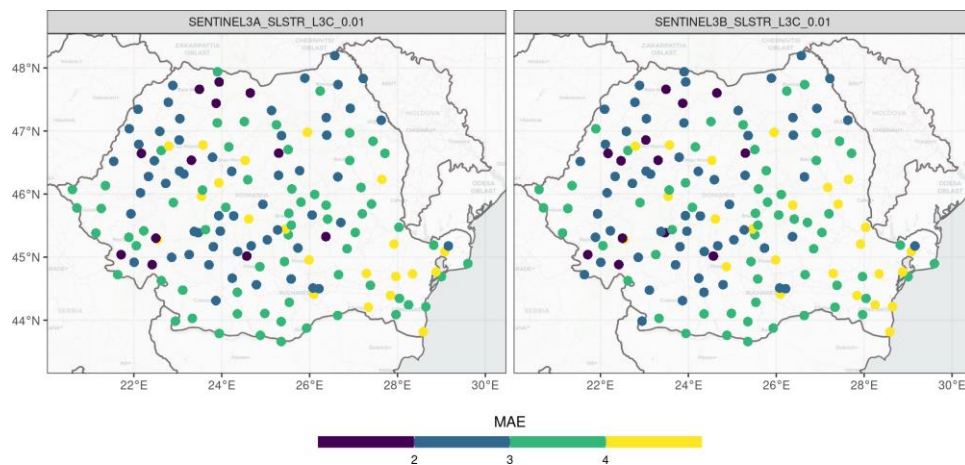
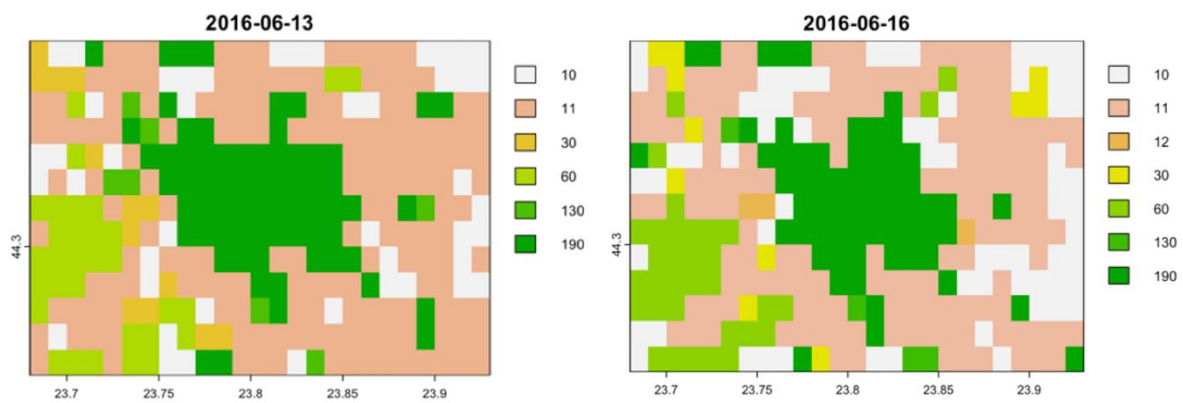
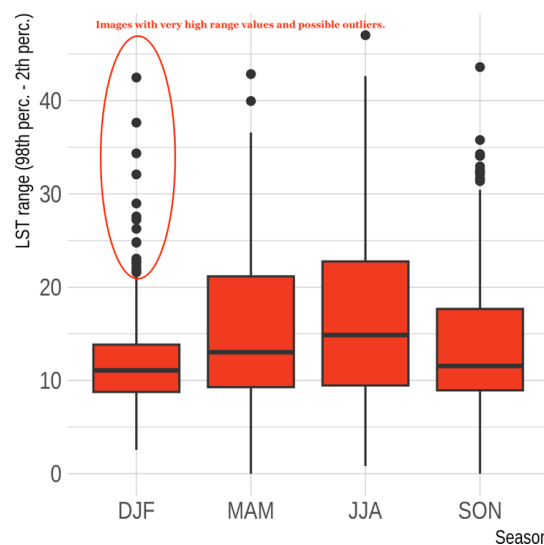


Figure 2-27: Spatial distribution of the mean absolute error (MAE) between the LST\_cci retrieved from L3C-LST-SLSTRx-0.01, and weather station air temperature (WS T2m).

The LST\_cci values were also analysed against the LCC retrieved from the L3C-LST-SLSTRA-0.01 and L3C-LST-SLSTRB-0.01 over 41 urban areas, i.e. Bucharest and the capital cities of the districts of Romania (Nomenclature of territorial units for statistics - NUTS 3; <https://ec.europa.eu/eurostat/web/nuts>). Figure 2-28 provides an example showing the LCC over Craiova city in two different days from June 2016. The differences between 13 and 16 June 2016 are noticeable. For example, the changes observed in the categories 130 (grassland) and 190 (urban) are not credible within such a short period, and this requires a substantial quality revision of the L3C-LST-SLSTRA-0.01 and L3C-LST-SLSTRB-0.01. Moreover, the daily amplitude of the LST\_cci suggests several possible outliers in all the seasons, requiring additional quality checks, including the LCC data (Figure 2-29).



**Figure 2-28: Land Cover Classes over Craiova city (Romania) retrieved from the L3C-LST-SLSTRA-0.01 product, for 13 June 2016 and 16 June 2016. The figures in the legend stand for: 10 - cropland\_rainfed, 11 - cropland\_rainfed\_herbaceous\_cover, 12 - cropland\_rainfed\_tree\_or\_shrub\_cover, 30 - mosaic\_cropland, 60 - tree\_broadleaved\_deciduous\_closed\_to\_open, 130 - grassland, 190 - urban.**



**Figure 2-29: Daily range of the L3C-LST-SLSTRA-0.01 and L3C-LST-SLSTRB-0.01 at the country level in each season.**



The LST\_cci data retrieved from the L3C-LST-SLSTRx-0.01 product have been used to compute the Surface Urban Heat Island Intensity (SUHII) over the 41 urban areas of Romania considered in this study. The SUHII was computed as the difference between the LST\_urban and LST\_rural, using the Equation 2-5 [RD-13].

$$\text{Equation 2-5} \quad SUHII = LST\_cci_{urban} - LST\_cci_{rural}$$

Where (see Figure 2-30)

LST\_cci<sub>urban</sub> is the LST computed over the pixels within the administrative perimeter of an urban area, including only artificial surfaces and associated areas.

LST\_cci<sub>rural</sub> is the LST computed over pixels from the buffer extended up to ½ × average distance between the city centroid and nodes of the urban administrative perimeter, including the LCCs except for urban and water.

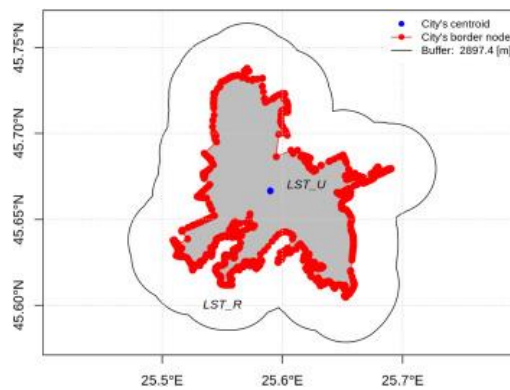


**Figure 2-30: Delimitation of areas for computing LST\_cci<sub>urban</sub> and LST\_cci<sub>rural</sub>. The example is for Braşov City (Romania). The rural buffer is drawn at ½ \* average distance between the city centroid (blue dot) and nodes of the urban administrative perimeter (red dots).**

The results were integrated in a web-based platform (<http://193.26.129.95:3838/synuhi/>) designed to supply free information on the seasonal characteristics of the SUHII of the selected cities (Figure 2-31), including the spatial and annual variation, to a wide range of potential users (i.e., municipalities, urban planners, citizens, research & academia). The web-based platform is designed to support the implementation of the national project *Synergies between Urban Heat Island and Heat Wave Risks in Romania: Climate Change Challenges and Adaptation Options* (SynUHI), funded by the Ministry of Research, Innovation and Digitization, Romania, CCCDI – UEFISCDI.

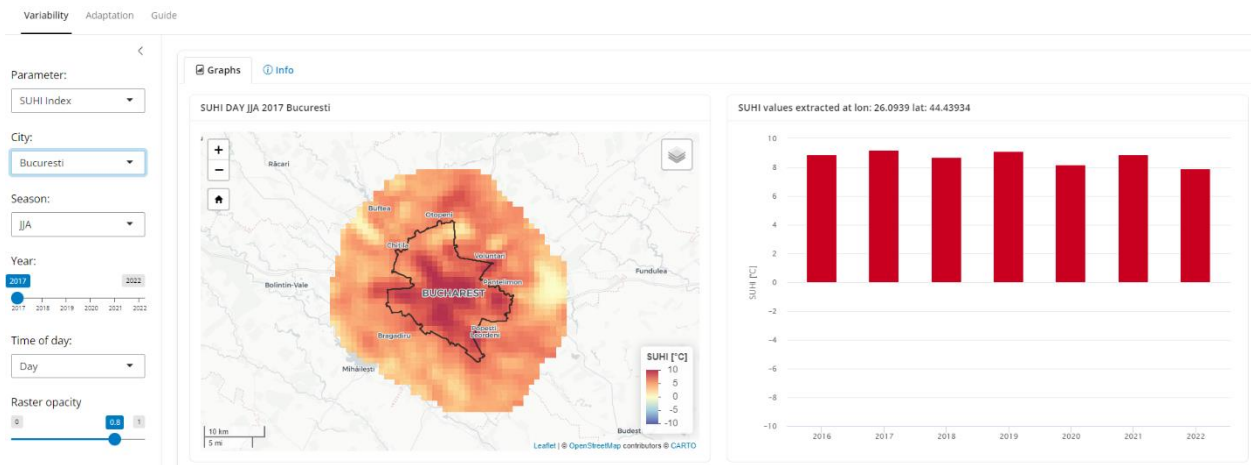


Figure 2-31: Web-based interface for visualising and analysing the SUHI of the Bucharest city.

#### 2.4.2.4. Conclusions

The LST\_cci may be used in a variety of applications but a proper quality control is required prior further in-depth analyses. The high correlation between the LST\_cci and T2m pledges for the development of composite products combining the two variables which can extend the field of applications.

#### 2.4.3. Feedback on scientific utility of the LST\_cci products

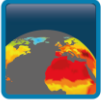
- ❖ **LST Data Usability and Quality:** The LST\_cci products are user-friendly and of a very high quality and can be used in a variety of applications.
- ❖ **Data Processing:** The provision of LST data as a single NetCDF file per diurnal cycle and satellite overpass presents challenges in processing, particularly when analysing national-scale regions of interest. The possibility to process the data on the Jasmin infrastructure may overcome this issue.
- ❖ **Cloud Contamination:** Some outliers were identified in version 4.aa of the L3C-LST-SLSTRx-0.01 products, probably due to cloud contamination. The same validation will be performed on the new version of the product (v4.00) to verify if this issue persists.
- ❖ **Auxiliary data:** By including ERA5 T2m alongside the LCC information in the same grid as the LST data, it streamlines data analysis and enhances the user experience. However, the changes observed from day to day in the LCC categories 130 (grassland) and 190 (urban) are not credible within such a short period. This issue will be checked in the new version of the product (v4.00).

## 3. Other CRG Study Reports

### 3.1. Evaluation of v4 LST\_cci products and study of LST trends in Spain (R. Niclòs, M. Perelló, S. Arribas, & J. Puchades, University of Valencia)

#### 1.1.1 Key Messages

- ❖ TERRA\_MODIS\_L3C / AQUA\_MODIS\_L3C 0.01° or 0.05° LST\_cci products (versions v1 to v4) were evaluated against ground data at the Valencia Test Site to test accuracies for meteorological and climate studies within the University of Valencia's research projects.
- ❖ SENTINEL3A\_SLSTR\_L3C / SENTINEL3B\_SLSTR\_L3C 0.01° LST\_cci products (version v4) were also evaluated against ground data at the Valencia Test Site.
- ❖ Evaluation of the MODIS operational LST products (MOD/MYD11\_L2 and MOD/MYD21) and Sentinel-3A/B SLSTR operational LST product were also performed using the same ground data as reference data. An alternative emissivity-dependent split-window algorithm was also evaluated for Sentinel-3A/B SLSTR for comparison purposes.
- ❖ Systematic uncertainties of around 1.5-2 K and random uncertainties from 1.0 K to 1.5 K are shown for v2, v3 and v4 of the LST\_cci MODIS L3C products, leading to total uncertainties (RMSD) around 2 K (unlike the uncertainties of 4 K obtained for the v1 ones).
- ❖ The v4 LST\_cci MODIS L3C product still overestimates ground LSTs both for EOS-Aqua and EOS-Terra at the Valencia Test Site, but the results for v2-v4 are much better than those for v1 products. Further evaluation could be carried out by analysing the results for v4 LST\_cci MODIS L2P products, if provided for the site.
- ❖ Using the same ground dataset, lower systematic uncertainties are shown for the MODIS operational products (negligible in the case of MYD/MOD11\_L2 products), with similar random uncertainties, leading to total uncertainties from <1 K to 1.5 K, within the GCOS recommended uncertainty thresholds.
- ❖ The remaining overestimation of v4 LST\_cci MODIS L3C product is due to differences between product emissivities and ground-measured emissivities at the site. The product emissivities are underestimated at the site, and the emissivity underestimation ranges from 0.007 for full vegetation cover to 0.03 for flooded soils (water).
- ❖ The v4 LST\_cci SLSTR L3C product also overestimates ground LSTs, with bias of around 1.5 K and RMSD of 2K both for Sentinel-3A and Sentinel-3B data. The product emissivities again show an underestimation at the site that leads to the LST overestimation.
- ❖ Similar biases are observed for the operational product at the site, which are close to those shown at other sites by the ESA team. However, negligible biases and RMSD of around 1.5 K are shown for the alternative emissivity-dependent split-window algorithm.
- ❖ The analysis of LST trends with the complete v4 AQUA MODIS L3C 0.01° LST\_cci dataset over the Iberian Peninsula (Spain) show significant trends in 22% of the area with a mean value of 0.1 K/year for daytime observations, while the area with significant trends is 34% with a mean value of 0.07 K/year at nighttime.

 <b>land surface temperature</b> cci	<b>Climate Assessment Report</b>  <i>WP5.1 – DEL-5.1</i>	Ref.: LST-CCI-D5.1-CAR Version: 3.0 Date: 25-May-2024 Page: 48
--	--	---

## 1.1.2 Scientific Analysis

### 1.1.2.1 Aims of the study

Versions 1 to 4 of the TERRA\_MODIS\_L3C / AQUA\_MODIS\_L3C products (i.e., MODIS LST\_cci 0.01° or 0.05° products both for EOS-Terra and EOS-Aqua overpasses, respectively) were evaluated against ground data at the Valencia Test Site [RD-14, RD-15, RD-16, RD-17, RD-18], from 2014 to 2019, to test the accuracies of these LST products for meteorological and climate studies within the research projects lead by the University of Valencia (e.g., project PID2020-118797RB-I00 (Tool4Extreme) funded by MCIN/AEI/10.13039/501100011033). The Valencia Test Site is a uniform and thermally-homogeneous rice paddy area, with very different land covers through the year due to crop phenology (i.e., water surfaces (in case of flooded soils), full vegetation cover and bare soil).

The MODIS operational products (MOD/MYD11\_L2 and MOD/MYD21 at versions v006 and v061) were also evaluated using the same ground data as reference data for comparison. These products are obtained with the generalized split-window (SW) algorithm [RD-19, RD-20] and the temperature-emissivity separation (TES) algorithm [RD-21, RD-22], respectively, and are disseminated through the NASA's Earth Data Search website ([search.earthdata.nasa.gov](https://search.earthdata.nasa.gov)).

In addition, version 4 of the SENTINEL3A\_SLSTR\_L3C / SENTINEL3B\_SLSTR\_L3C products (i.e., SLSTR LST\_cci 0.01° products both for Sentinel-3A and Sentinel-3B overpasses, respectively) were evaluated with ground data at the Valencia Test Site (from 2021 to 2022). The operational SLSTR LST product [RD-23] was also evaluated with the same ground data for comparison, but additionally an alternative emissivity-dependent, and also viewing-angle dependent, split-window algorithm (E-SWA) proposed in [RD-18], based in the algorithm previously proposed in [RD-16].

The objective of this validation was to contribute feedback to the LST\_cci project, to generate more accurate LST products for climate applications, but also to quantify the uncertainties of the LST\_cci products for the Iberian Peninsula region with the aim of using them for analysing trends potentially associated with climate change.

Finally, LST trends were analysed over the Iberian Peninsula using twenty years of the version 4 AQUA\_MODIS\_L3C product series (from 2002 to 2021).

### 1.1.2.2 Data and methods

The data used for the study is summarized in Table 3-1.

**Table 3-1: A summary of LST\_cci products used for this study.**

Product String and version	Sensor type	Resolution	Data availability / Data used	Local time of descending node
TERRA_MODIS_L2P (v1)	TIR	1 km swath	2000-2021 / 2016-2018	~10:10-11:50
AQUA_MODIS_L2P (v1)	TIR	1 km swath	2002-2021 / 2016-2018	~12:40-14:00
TERRA_MODIS_L3C (v1-v4.aa)	TIR	0.01° or 0.05°	2000-2021 / 2014-2019	~10:10-11:50
AQUA_MODIS_L3C (v1-v4.aa)	TIR	0.01° or 0.05°	2002-2021 / 2002-2021	~12:40-14:00
SENTINEL3A_SLSTR_L3C (v4.aa)	TIR	0.01°	2016-2022 / 2020-2022	~10:15-10:45
SENTINEL3B_SLSTR_L3C (v4.aa)	TIR	0.01°	2018-2022 / 2020-2022	~10:15-10:45

Ground TIR measurements were performed at the Valencia Test site concurrently with Terra/Aqua MODIS overpasses using hand-held Cimel Electronique CE-312 radiometers. Measurements were acquired along predetermined transects over the test site in cloud-free conditions. The number of radiometers used ranged from 2 to 4 depending on the day. Radiometers were calibrated in the laboratory (each year) and within international campaigns in which the calibration uncertainty was estimated [RD-24, RD-25, RD-26].

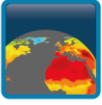
The ground measurements acquired along transects followed the methodology described in [RD-14, RD-17] for cloud-free days from 2016 to 2018 (daytime only). The CE-312 radiometers measured the surface radiance within a spectral band  $i$ ,  $L_{surf,i}$ , which depends on the surface emissivity,  $\epsilon_i$ , as follows:

$$\text{Equation 3-1} \quad L_{surf,i} = \epsilon_i B_i(T) + (1 - \epsilon_i) L_{i,a,hem}^{\downarrow}$$

where  $B_i(T)$  is the channel Planck's function for a temperature  $T$  (here  $T$  being the LST).  $L_{i,a,hem}^{\downarrow}$  is the atmospheric downwelling irradiance divided by  $\pi$  [RD-15, RD-17].  $L_{i,a,hem}^{\downarrow}$  was measured using an Infragold Reflectance Target (IRT-94-100) made by Labsphere [RD-27], which is a highly diffuse gold panel with a reflectivity close to 0.92 in the 8 – 14  $\mu\text{m}$  region.

The reference ground LSTs were obtained using the mean of the LST measurements performed by all ground radiometers within five minutes of each overpass time.

As just a few measurements were acquired along transects concurrently with Sentinel-3A and Sentinel-3B overpasses, ground data acquired from a fixed station at the Valencia Test site from 2020 to 2022 were used to evaluate the SENTINEL3A\_SLSTR\_L3C and SENTINEL3B\_SLSTR\_L3C products. Apogee SI-121 radiometers were set up at the station to acquire surface and atmosphere radiances in the 8 – 14  $\mu\text{m}$  region and Equation 3-1 was also used to retrieve LSTs from these data.

 <b>land surface temperature</b> cci	<b>Climate Assessment Report</b>  <i>WP5.1 – DEL-5.1</i>	Ref.: LST-CCI-D5.1-CAR Version: 3.0 Date: 25-May-2024 Page: 50
--	--	---

Additionally, emissivities for the different land covers were measured at the site, and not assumed or estimated from threshold methods or databases. Emissivity measurements were taken using the TES method [RD-21, RD-28], applied to the ground data measured by the CE-312 radiometers, and also the Box Method [RD-15].

LST trends in the Iberian Peninsula were then obtained from the AQUA\_MODIS\_L3C LST\_cci products from 2002 to 2021, removing the grid cells with satellite zenith angles larger than 55° and total uncertainties above 2.5K. This data filtering was motivated by a previous analysis of grid cell quality in the region. Only the AQUA\_MODIS\_L3C data were used following the study of [RD-04], who found that TERRA\_MODIS\_L3C suffers from some non-climatic discontinuities, and also due to the AQUA overpass times at the site, which are closer to the times of minimum/maximum daily temperatures in the study region.

To detect trends in the LST time series, the Mann-Kendall (MK) non-parametric seasonal test was used [RD-29]. The null hypothesis for the test is that the data are independent and randomly ordered in each season. The null hypothesis was tested using a significance level of  $\alpha = 0.05$  (i.e., confidence level of 95%). If the data are not randomly ordered (meaning that the null hypothesis is rejected), the magnitude of the trend is calculated with the Sen-slope estimator [RD-10].

Trends were calculated for each grid cell of the study region for the minimum, mean and maximum LST data of each season (using ‘actual’ LSTs rather than anomalies, with one LST value for each season). For the seasons, two groupings were used: the 12 months of the year and the 4 “meteorological” seasons. Once the trend for each grid cell was obtained, the mean and its deviation for the entire region was calculated, obtaining a result for both daytime and nighttime Aqua MODIS overpasses for each season separately and also for the whole year.

To apply the explained methods, the *sktt* and *ktaub* Matlab functions were used.

### 1.1.2.3 Results

#### 3.1.2.3.1. Terra/Aqua MODIS evaluation

This section shows the results of the evaluation of the above-mentioned MODIS LST\_cci and operational LST products using the described ground data as reference. Table 3-2 to Table 3-5 show the statistical differences of the product LSTs minus ground LSTs in terms of bias, standard deviation (SD) and root-mean-square differences (RMSD). Table 3-2 shows the results for versions 1 to 4 AQUA\_MODIS\_L3C together with those for version 1 AQUA\_MODIS\_L2P (2016-2018). Table 3-3 shows the results for the operational MYD11\_L2 and MYD21 products (v006 and v061, respectively). Table 3-4 shows the results for versions 1 to 4 TERRA\_MODIS\_L3C together with those for version 1 TERRA\_MODIS\_L2P. Table 3-5 shows the results for the MOD11\_L2 and MOD21 products (v006 and v061, respectively). No v006 MOD21 scenes were available for the study period. Results are also shown in Figure 3-1 and Figure 3-2 for Aqua MODIS and Terra MODIS, respectively. Average LSTs weighted by the inverse of the squared distance to the site coordinates were obtained for the 2 × 2 closest pixels or grid cells for evaluating the 0.01° or 1 km LST\_cci products, respectively, and the operational products.

**Table 3-2: Results of the evaluation of the different versions of the AQUA MODIS LST\_cci products.**

	LST_CCI_L3C_0.01_v4 – LST_ground (K)	LST_CCI_L3C_0.01_v3 – LST_ground (K)	LST_CCI_L3C_0.05_v2 – LST_ground (K)	LST_CCI_L3C_0.05_v1 – LST_ground (K)	LST_CCI_L2P_v1 – LST_ground (K)
BIAS	1.9	1.7	1.9	4.4	3.5
SD	1.2	1.1	1.1	1.7	1.1
RMSD	2.2	2.1	2.2	4.7	3.3
N. EVENTS	22	22	22	18	13

**Table 3-3: Results of the evaluation of the operational v006 and v061 products for EOS Aqua - MODIS.**

	LST_MYD11_v006 – LST_ground (K)	LST_MYD11_v061 – LST_ground (K)	LST_MYD21_v006 – LST_ground (K)	LST_MYD21_v061 – LST_ground (K)
Bias	-0.1	0.0	0.9	1.1
SD	0.8	0.8	1.1	1.1
RMSD	0.8	0.8	1.5	1.5
N. EVENTS	19	19	19	19

**Table 3-4: Results of the evaluation of the different versions of the TERRA MODIS LST\_cci products.**

	LST_CCI_L3C_0.01_v4 – LST_ground (K)	LST_CCI_L3C_0.01_v3 – LST_ground (K)	LST_CCI_L3C_0.05_v2 – LST_ground (K)	LST_CCI_L3C_0.05_v1 – LST_ground (K)	LST_CCI_L2P_v1 – LST_ground (K)
Bias	1.6	1.8	2.1	3.5	3.1
SD	1.5	1.4	1.5	1.4	1.4
RMSD	2.2	2.3	2.5	3.7	3.4
N. EVENTS	31	31	31	31	31

**Table 3-5: Results of the evaluation of the operational v006 and v061 products for EOS Terra - MODIS. No v006 MOD21 product was available for the study period.**

	LST_MOD11_v006 – LST_ground (K)	LST_MOD11_v061 – LST_ground (K)	LST_MOD21_v061 – LST_ground (K)
Bias	-0.2	-0.3	0.8
SD	1.6	1.5	1.5
RMSD	1.6	1.6	1.6
N. EVENTS	28	27	27

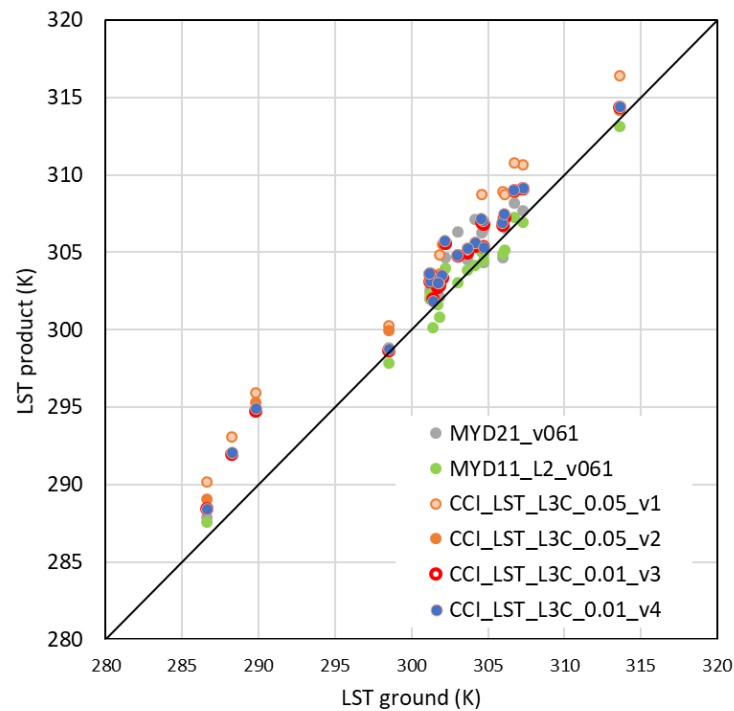


**Figure 3-1: Comparison of LSTs obtained for the Valencia Test site coordinates from the EOS Aqua – MODIS products against ground LSTs. Results for versions 1 to 4 AQUA\_MODIS\_L3C products and v061 MYD11\_L2 and MYD21 operational products are shown for daytime only, when ground measurements along transects were acquired.**

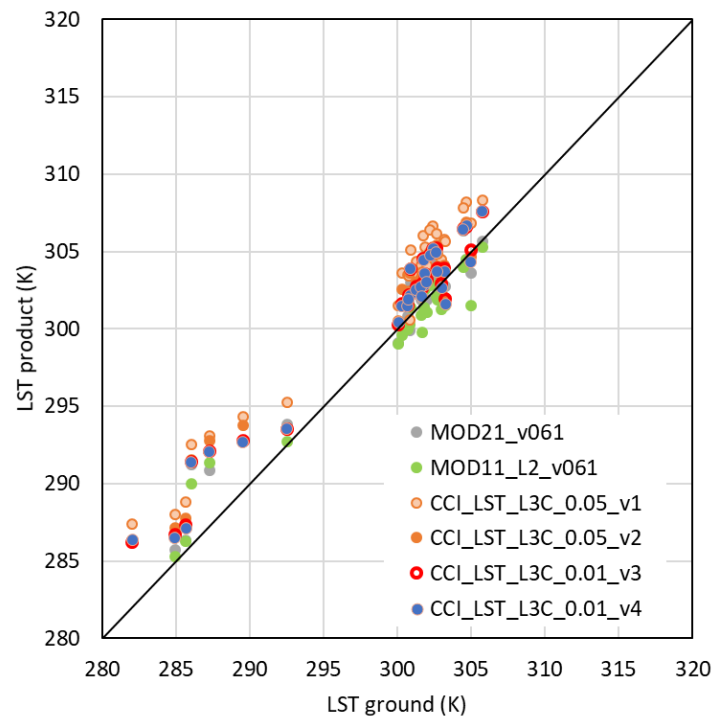


**Figure 3-2: Comparison of LSTs obtained for the Valencia Test coordinates from the EOS Terra – MODIS products against ground LSTs. Results for versions 1 to 4 TERRA\_MODIS\_L3C products and v061 MOD11\_L2 and MOD21 operational products are shown for daytime only, when ground measurements along transects were acquired.**



Biases from 1.6 K to 2.1 K and SDs up to 1.5 K are shown for versions 2 to 4 LST\_cci MODIS L3C products, with respect to the ground observations, leading to RMSDs of 2.2 K for AQUA\_MODIS\_L3C and up to 2.5 K for TERRA\_MODIS\_L3C (unlike the biases and RMSDs from 3.1 K to 4.7 K shown for version 1 LST\_cci MODIS products). Lower biases are shown for the operational products (e.g., negligible biases were obtained for MYD11\_L2 and MOD11\_L2 products), with similar SDs, leading to RMSDs lower than 1.6 K in all cases (and even lower than 1 K in the case of MYD11\_L2).

Emissivities are provided for each grid cell in version 4 LST\_cci products. These emissivities were analysed for the site, and the remaining LST overestimation in v4 MODIS LST\_cci products can be attributed to differences between emissivities used in the product for the Valencia test site and ground-measured emissivities, which sharply varied because of the rice paddy land cover changes. The v4 LST\_cci product emissivities are underestimated at the site, and the emissivity underestimation ranges from 0.007 for full vegetation covers up to 0.03 for flooded soils (water), which can explain the reported overestimations in terms of LSTs.

The LST\_cci products provide 3 additional cloud-free overpasses compared with the operational products in each case, suggesting that the cloud screening in the operational products may be overzealous.

### 3.1.2.3.2. S3A/S3B SLSTR evaluation

This section shows the validation results for the SENTINEL3A\_SLSTR\_L3C and SENTINEL3B\_SLSTR\_L3C LST\_cci products, and for the operational LST product and the alternative E-SWA, using the described ground data as reference. Table 3-6 shows the results for the LST\_cci product, the operational product and the alternative E-SWA for the SLSTR data from Sentinel-3A. Table 3-7 shows equivalent results for Sentinel-3B. Average LSTs weighted by the inverse of the squared distance to the site coordinates were obtained for the 2 × 2 closest grid cells to evaluate all the products.

**Table 3-6: Results of the evaluation of the SENTINEL3A\_SLSTR\_L3C LST\_cci product and the operational one together with the alternative E-SWA proposed for the SLSTR data in Sentinel-3A.**

	LST_CCI_L3C_0.01_v4 – LST_ground (K)	LST_operational – LST_ground (K)	LST_E-SWA – LST_ground (K)
<b>Bias</b>	1.5	1.6	-0.1
<b>SD</b>	1.4	1.3	1.4
<b>RMSD</b>	2.0	2.0	1.4
<b>N. EVENTS</b>	95	95	95

**Table 3-7: Results of the evaluation of the SENTINEL3B\_SLSTR\_L3C LST\_cci product and the operational one together with the alternative E-SWA proposed for the SLSTR data in Sentinel-3B.**

	LST_CCI_L3C_0.01_v4 – LST_ground (K)	LST_operational – LST_ground (K)	LST_E-SWA – LST_ground (K)
<b>Bias</b>	1.5	1.7	0.0
<b>SD</b>	1.5	1.7	1.7
<b>RMSD</b>	2.1	2.4	1.7
<b>N. EVENTS</b>	89	89	89

Similar results were obtained for the LST\_cci and the operational product, with biases from 1.5 to 1.7 K and RMSDs from 2 K to 2.4 K, with respect to the ground data. These results agreed with those shown by the ESA SLSTR Expert Science Laboratory team, which showed absolute accuracies (i.e., average of absolute biases for the different stations) of 1.5 K and 1.7 K at daytime for Sentinel-3A and Sentinel-3B, respectively, and 1.2 K at night-time. However, much better results were obtained for the alternative E-SWA, with negligible biases and RSMD of 1.4 K and 1.7 for Sentinel-3A and Sentinel-3B, respectively.

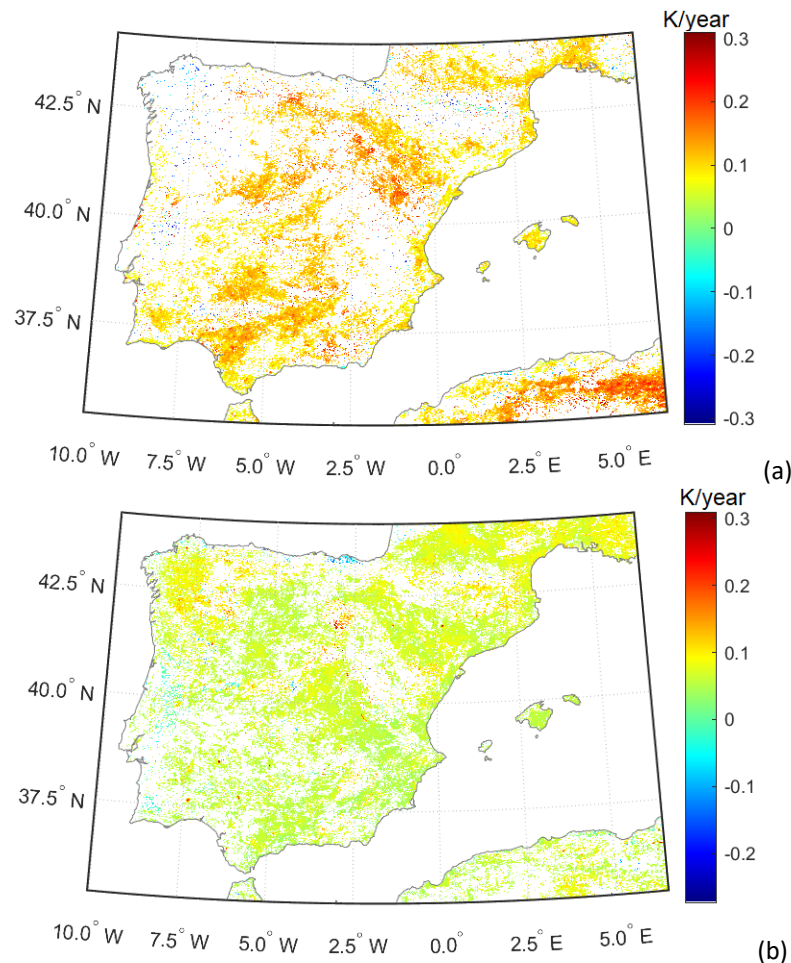
The biome assigned at the rice paddy site by the operational product is irrigated cropland (biome 1). In the case of the LST\_cci product, emissivities do not reproduce the site emissivity changes and LST\_cci emissivities are also underestimated at the site. This fact again explains the observed LST overestimation for the LST\_cci products.

### 3.1.2.3.3. LST trends in the Iberian Peninsula

Trends results for the whole year, obtained using version 4 MODIS/Aqua LST\_cci data, are shown in Table 3-8. The area with significant trends is higher for the monthly analysis, which means that seasonal analysis is more restrictive as the periods considered are longer. The results for the mean LST and the maximum LST show similar values, with a larger area with significant trends and higher trends than for the minimum LST. In addition, the nighttime trends are lower than the daytime ones. In all cases, a wide interval should not be understood as an invalid result but as an indicator of the variability of trends over the Iberian Peninsula.

**Table 3-8: LST trends results obtained for the whole year using the full v4 AQUA MODIS LST\_cci dataset.**

			Area with significant trends (%)	Mean trend (K/year)	Interval (K/year)
<b>Mean</b>	<b>Day</b>	<b>Seasons</b>	22	0.10	[-0.01, 0.20]
		<b>Months</b>	31	0.06	[-0.07,0.20]
	<b>Night</b>	<b>Seasons</b>	34	0.07	[0.02,0.11]
		<b>Months</b>	53	0.05	[0.00,0.10]
<b>Max</b>	<b>Day</b>	<b>Seasons</b>	23	0.14	[0.04,0.24]
		<b>Months</b>	30	0.08	[-0.06,0.22]
	<b>Night</b>	<b>Seasons</b>	39	0.10	[0.04,0.16]
		<b>Months</b>	43	0.06	[0.00,0.12]
<b>Min</b>	<b>Day</b>	<b>Seasons</b>	5	0.04	[-0.35,0.44]
		<b>Months</b>	15	0.04	[-0.19,0.26]
	<b>Night</b>	<b>Seasons</b>	7	0.03	[-0.19,0.25]
		<b>Months</b>	43	0.06	[-0.03,0.14]

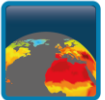


**Figure 3-3: Annual AQUA MODIS LST\_cci v4 trends in the Iberian Peninsula for (a) daytime and (b) nighttime mean seasonal temperatures.**

If the results for seasonal mean LST analysis are taken as reference (Figure 3-3a for daytime and Figure 3-3b for nighttime), a trend is observed in the 22% of the area with a mean value of 0.1 K/year at daytime while the area is increased to 34% with a mean value of 0.07 K/year at nighttime. Similar trend values were found in [RD-30] and over Europe by [RD-04].

#### 1.1.2.4 Conclusions

The results show that the version 4 of LST\_cci MODIS L3C 0.01° products still overestimate ground LSTs at the Valencia Test site (with bias and RMSD of around 2 K) both for EOS Aqua - MODIS and EOS Terra – MODIS. However, the overestimates have decreased as compared to those for version 1 products (of around 4 K). Using the same ground dataset, lower systematic uncertainties are shown for the operational products (negligible in the case of MYD/MOD11\_L2 products), with similar random uncertainties, leading to total uncertainties from <1 K to 1.5 K, within the GCOS recommended uncertainty thresholds. The remaining overestimation of v4 LST\_cci MODIS L3C product is due to differences between emissivities used in the product and ground-measured emissivities at the site. The product emissivities are

 <b>land surface temperature</b> cci	<b>Climate Assessment Report</b>  <i>WP5.1 – DEL-5.1</i>	Ref.: LST-CCI-D5.1-CAR Version: 3.0 Date: 25-May-2024 Page: 56
--	--	---

underestimated at the site, and the emissivity underestimation ranges from 0.007 for full vegetation covers to 0.03 for flooded soils (water).

Version 4 of LST\_cci SLSTR L3C 0.01° products also overestimates ground LSTs (with bias of 1.5 K and RMSD of 2 K) both for Sentinel-3A and Sentinel-3B. The analysis of the product emissivities again shows an underestimation at the site, which can explain the LST overestimation. Similar overestimates are observed for the operational product at the site, with bias values of 1.6-1.7 K close to those reported by the ESA SLSTR Expert Science Laboratory team at other sites. However, when the alternative E-SWA [RD-18] is used (with band emissivities appropriate for the site land covers), negligible biases and RMSD of 1.4 K and 1.7 are obtained for Sentinel-3A and Sentinel-3B, respectively.

Finally, the analysis of LST trends with the complete v4 LST\_cci AQUA MODIS L3C 0.01° dataset over the Iberian Peninsula shows significant trends in the 22% of the area with a mean value of 0.1 K/year at daytime, while the area with significant trends is 34% with a mean value of 0.07 K/year at nighttime.

### 1.1.3 Feedback on scientific utility of the LST\_cci products

The following summarises the experience with the LST\_cci products in this study:

- ❖ L3C products were accessible and easy to use since they are provided in the standard NetCDF format.
- ❖ Emissivity values are underestimated in the v4 LST\_cci MODIS L3C product at the Valencia Test site (and they do not reproduce correctly the land cover changes at the site) and thus the corresponding LSTs are overestimated.
- ❖ LST\_cci products for other satellite sensors (e.g., MetOp-A/B/C AVHRR/3 and S-NPP/JPSS1 VIIRS) could also be interesting.
- ❖ To study trends with v4 LST\_cci AQUA MODIS L3C data, data filtering was required in terms of total uncertainties, since they have increased in this version compared to those in v3. Total uncertainties of up to 4-5 K were observed in the Iberian Peninsula. It might be interesting to investigate whether these uncertainties are overestimated.

## 3.1. SUBDROUGHT: Subseasonal-to-seasonal drought and heatwave evolution via land-atmosphere interactions (Bethan Harris, ESA CCI fellowship, UK Centre for Ecology & Hydrology/National Centre for Earth Observation)

---

### 3.1.1. Scientific Analysis

#### 3.1.1.1. Aims of the study

The aim of this study is to use daily-resolution Earth Observation datasets to create a global characterisation of land-atmosphere feedback during drought events that develop on a subseasonal-to-seasonal timescale (“flash droughts”). An improved understanding of these processes is necessary to tackle the challenge of predicting flash droughts in subseasonal-to-seasonal forecasts, with the overall aim of reducing their impact on agriculture and water resources.

### 3.1.1.2. Data and methods

Flash drought events are identified globally by using ESA CCI Soil Moisture data to detect the rapid development of drought conditions. The evolution of land-atmosphere interactions during the events is then explored by compositing standardised anomalies of various surface energy budget components around the dates of flash drought onset. The difference between LST and 2m air temperature (from ERA5 [RD-12]) is used as a proxy for sensible heat flux. Latent heat fluxes are taken from the Global Land Evaporation Amsterdam Model (GLEAM) and the net surface radiation from Clouds and the Earth’s Radiant Energy System (CERES).

Two different products from LST\_cci are tested to compare the results: the microwave product and the single-sensor MODIS/Aqua product. The local overpass time of MODIS/Aqua (~13.30) is preferred for studying land-atmosphere interactions, but assessing against the microwave record enables a further understanding of the possible impacts of cloud cover on the conclusions.

**Table 3-9: A summary of LST\_cci products used for this study.**

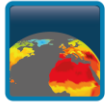
Product String and version	Sensor type	Resolution	Data availability	Local time of ascending node
SSMI/SSMIS L3C Daily v2.33	MW	0.25°	January 1996 – December 2020 (Use 2000–2020 only)	~17:30-19:30 but corrected to 18:00
MODIS Aqua L3C daily v4.aa (beta)	IR	0.01°	July 2002-December 2021 (use July 2002-December 2020 only)	~13:30

### 3.1.1.3. Results

The study provides a consistent picture of the surface energy budget between the observational products studied. Figure S-1, focusing on flash drought events in rainfed cropland during the growing season, shows that very similar results are obtained when computing the sensible heat flux with either the MODIS/Aqua LST or the SSMI/SSMIS microwave LST. This provides reassurance that the results are not sensitive to the choice of product. During the peak of the drought conditions, the net radiation at the surface decreases, but the sensible heat flux continues to increase. This is an indicator of water-limited soil conditions, which is corroborated by the concurrent decrease in latent heat flux. Therefore, these observational datasets are suitable for detecting evaporative regime changes during drought development. Subsequent work in this project will investigate the resulting feedbacks to atmospheric temperature and circulation.

### 3.1.2. Feedback on scientific utility of the LST\_cci products

The availability of both IR and microwave products strengthened the assessment of the surface energy budget, demonstrating consistency across datasets that are observed with different spatial resolutions, at different times of day and with different sensitivity to cloud cover. In particular, the coarser resolution of the microwave product was useful for easily drawing comparisons with other datasets such as ESA CCI Soil Moisture and GLEAM evaporation, which are produced at 0.25°, without the need to regrid.



The inclusion of ERA5 2m temperatures interpolated to the satellite overpass time/location in the beta version of the MODIS/Aqua product was extremely convenient for computing the sensible heat flux anomalies. This is also likely to be useful for many future studies focusing on land-atmosphere interactions, in which the sensible heat flux proxy LST-T2m is a useful indicator of the surface energy budget partitioning.

## 4. Non-CRG Study Reports

### 4.1. Downscaling Daily Land Surface Temperature (Shaerdan Shataer, University of Reading)

#### 4.1.1. Scientific Analysis

##### 4.1.1.1. Aims of the study

To downscale daily LST to CHUK grid resolution (~100m) using either: LST\_cci Sentinel-3A/3B, 1km daily LST or atmospheric temperature data from HadUK-Grid (the Met Office UK collection of gridded climate variables, such as 2m air temperature, precipitation and sunshine duration, see <https://www.metoffice.gov.uk/research/climate/maps-and-data/data/haduk-grid/haduk-grid>).

##### 4.1.1.2. Data and methods

Data: HadUK-Grid [RD-31], SLSTR SENTINEL-3A/3B L3C (Table 4-1), other

Method: Deep Neural Networks, Machine Learning

**Table 4-1: A summary of LST\_cci products used for this study.**

Product String and version	Sensor type	Resolution	Data availability	Local time of ascending node
SENTINEL3B_SLSTR LST DAILY L3C v3.00	SLSTR	0.01°	January 1996 – December 2020	22:00

##### 4.1.1.3. Results

Gap-filling step proven to be challenging and unsatisfactory, due to heavy cloud coverage and some cloud contamination in the level 3 dataset. Changed strategy to use HadUK-Grid atmospheric data instead.

#### 4.1.2. Feedback on scientific utility of the LST\_cci products

Cloud coverage and contamination has been a major issue (Figure 4-1). The group have been advised that the reprocessed SENTINEL3B\_SLSTR LST DAILY L3C data will be better in terms of cloud contamination and artifacts. They will return to use it for the downscaling task at some point after the reprocessing is completed and assessed.



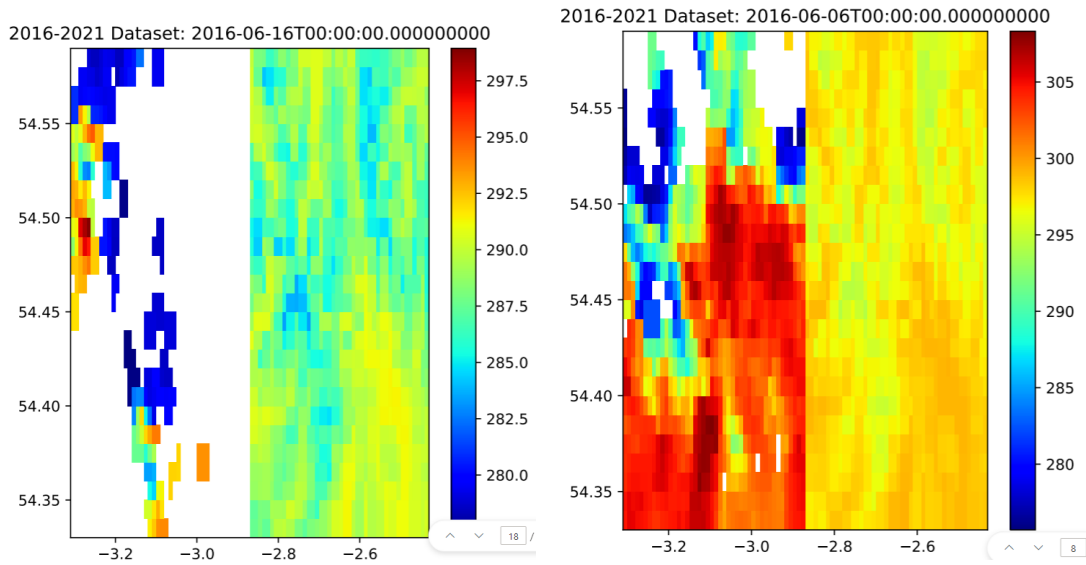


**Figure 4-1:** *LST (left half of each image above) and maximum daily T2m from the HadUK-Grid dataset [RD-31] (right half of each image shown) showing data scarcity (white space) and cloud contamination (cold temperatures shown in blue) in the LST data.*

## 4.1. 25 years assessment of Hot and Dry Weather Compound Events in Europe (Elody Fluck, ESA)

### 4.1.1. Scientific Analysis

#### 4.1.1.1. Aims of the study

To establish a consistent catalogue of hot and dry weather compound events using long-term Earth Observation (EO) data over Europe

#### 4.1.1.2. Data and methods

The LST\_cci microwave LST product was used to identify heatwaves through Europe on a monthly basis (Table 4-2).

**Table 4-2: A summary of LST\_cci products used for this study.**

Product String and version	Sensor type	Resolution	Data availability	Local time of ascending node
ESACCI-LST-L3C-LST-SSMI13/ ESACCI-LST-L3C-LST-SSMI17 monthly (v2.23)	MW	0.25°	January 1996 – December 2020	~18:00, monthly

**Equation 4-1** 
$$LST_{month\_anom} = LST_{month\_observed} - LST_{month\_climatology}$$

The presence of heatwaves is determined if *LST\_month\_anom* is great than or equal to 2 standard deviations compared to the climatology.

#### 4.1.2. Feedback on scientific utility of the LST\_cci products

The original plan was to use LST\_cci data on daily basis over Europe and compute a mean daily temperature (Ex using: ESACCI-LST-L3C-LST-SSMI13-0.25deg\_1DAILY\_DES-20011128000000-fv2.23.nc with the ASC mode) with the highest possible resolution; but due to some swath coverage scarcities over Europe, this was not possible (see Figure 4-2). Instead, the monthly resolution was used. It would be fantastic to have a daily mean worldwide product of LST to better assess heatwaves / heat hotspots for climatological studies.

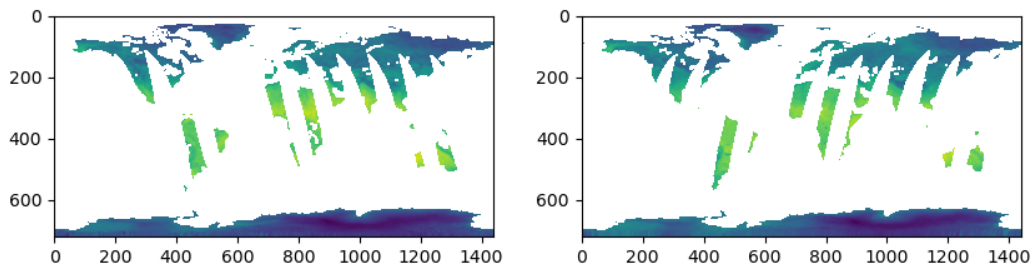


**Figure 4-2: Example of the LST\_cci MW LST product for a day in 1996 in ASC and DES mode. Some regions in Europe are covered twice by the swaths; but some other regions in Europe are not covered at all.**

## 4.2. AI4GHEObs: Ground Heat Flux from satellite data (Francisco José Cuesta Valero, Helmholtz-Centre for Environmental Research – UFZ)

### 4.2.1. Scientific Analysis

#### 4.2.1.1. Data and methods

1. The temperature correction provided within each dataset is implemented (Table 4-3).
2. Both ASC and DES files are merged by calculating the mean of both files for each month.
3. All months are combined to have a continuous time series.
4. Data from Greenland and Antarctica are removed.
5. The annual mean is estimated.
6. The global mean is estimated.

**Table 4-3: A summary of LST\_cci products used for this study.**

Product String and version	Sensor type	Resolution	Data availability	Local time of ascending node
ESACCI-LST-L3C-LST-SSMI13/ ESACCI-LST-L3C-LST-SSMI17 monthly (v2.33)	MW	0.25°	January 1996 – December 2020	Monthly ~17:30-19:30 but corrected to 18:00
ESACCI-LST-L3S-LST-IRMGP (v1.0)	IR	0.05°	January 2009 - December 2020	3-hourly

#### 4.2.2. Feedback on scientific utility of the LST\_cci products

- ❖ IRMGP monthly product version 1.00
- ❖ Some time steps include valid LST data in the ocean around the American continent; this may also be a problem in other areas (Figure 4-3).
- ❖ SSMI-SSMIS monthly product version 2.33.
- ❖ The magnitude of the global trend in actual (i.e. absolute LST values rather than anomalies with respect to a climatology) LST data is smaller than expected and therefore may indicate some errors or problems with the dataset (Figure 4-4 top). Moreover, the spatial distribution of trends is also considered to be unrealistic, with negative trends obtained for most of Africa, India, S.E. Asia, Australia and for parts of the Americas.

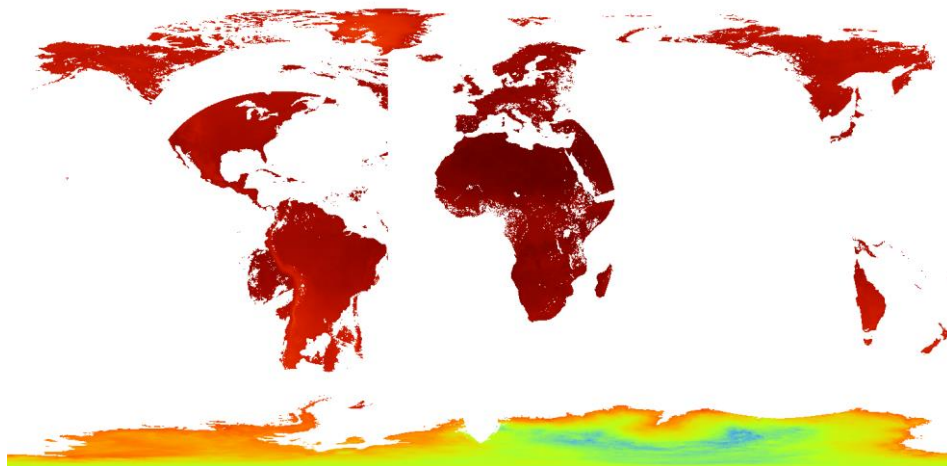


**Figure 4-3: Plot of ESACCI-LST-L3S-LST-IRMGP\_-0.05deg\_1MONTHLY-20180701120000-fv1.00.nc showing valid LSTs in the ocean off the coast of S. America.**

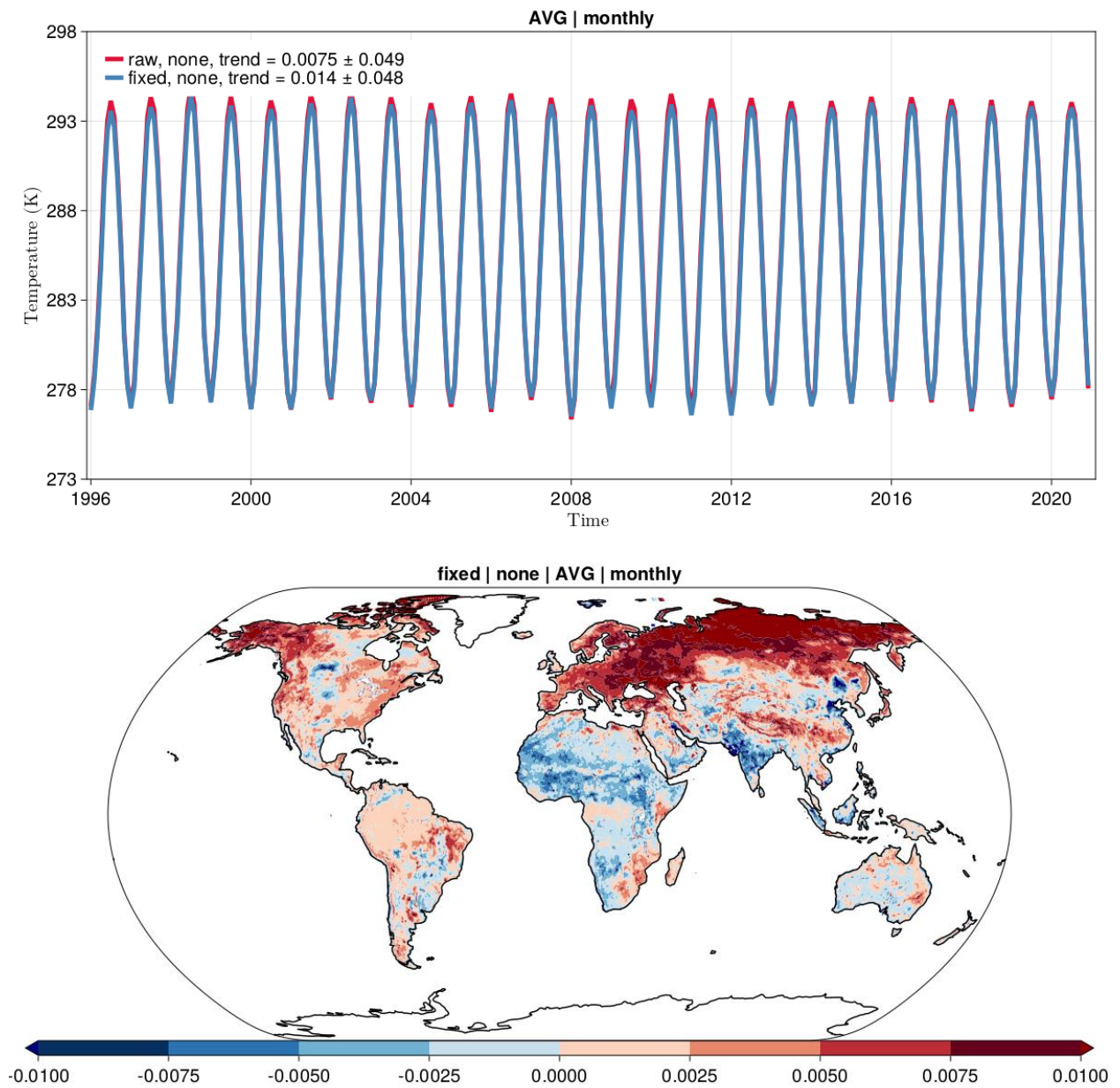


**Figure 4-4: (Top) Time series of mean global monthly actual LST from the MW LST\_cci product v2.33. The numerical values of the trends are also shown on the plot where ‘raw’ refers to the MW LST data without applying the LST correction for orbital drift and ‘fixed’ refers to the MW LST data where the orbital drift LST correction has been applied. (Bottom) Geographical distribution of trends in the actual MW LST monthly data where the orbital drift LST correction has been applied. Red indicates positive trends and blue negative trends in the data. The units of the trend are in K per month.**

### 4.3. Evaluating heat extremes in the Sahel using LST\_cci data (Amina Maroini, ESA Graduate Trainee project)

#### 4.3.1. Scientific Analysis

##### 4.3.1.1. Aims of the study

The overall goal of this study is to investigate if LST\_cci All-Weather Microwave Land Surface Temperature (LST) products provide consistent information on spatial patterns and temporal trends of heat extremes in the Sahel. For this, a range of heat extremes are computed quantifying the intensity, duration of heat extreme events, and the human perception of heat, respectively: the monthly Maximum day temperature (TX), the Number of Hot days (NHD) for the year 2010 with respect to the 1996-2020 baseline and Thom’s Discomfort Heat Stress Index (DI\_Thoms).

##### 4.3.1.2. Data and methods

###### Data

###### 1. Daily ESA Land Surface Temperature LST\_cci SSM/I-SSMIS CDR version 2.23

The Microwave Land Surface Temperature (MW LST) product is used in this study (Table 4-4). Although this product is at a coarser resolution than the Infrared product (0.25x0.25), the LST from Microwave (LST-MW) provides estimates for clear-sky as well as cloudy conditions, since MW can penetrate clouds to a larger extent. Given there are observations of MW LST\_CCI only twice a day, and the focus on indices reliant on maximum temperature, daily LST\_cci at 6PM as a proxy of daily maximum temperature is used.

**Table 4-4: A summary of LST\_cci products used for this study.**

Product String and version	Sensor type	Resolution	Data availability	Local time of ascending node
SSM/I-SSMIS L3C Daily v2.33	MW	0.25°	January 1996 – December 2020	~17:30-19:30 but corrected to 18:00

###### 2. Daily ERA5 2m temperature data

Reanalysis data is used to compare spatial maps of anomalies of indices computed from LST\_cci data. Daily ERA5 surface air temperature (T2m) is used in this study [RD-12]. The daily maximum temperature is computed from hourly data. ERA5 2m dew point temperature is also used to compute the heat stress index. Both datasets are available on an hourly scale for a 0.25x0.25 grid.

###### 3. NOAA Global Summary Of the Day data (GSOD NOAA)

Global Surface Summary Of the Day (GSOD) is derived from The Integrated Surface Hourly (ISH) dataset. The ISH dataset includes global data obtained from the United States Air Force (USAF) Climatology Center. The latest daily summary data are normally available 1-2 days after the date-time of the observations

used in the daily summaries. In the Sahel region, as delimited in this study, for the time period 1996-2020, 75 stations are listed for the variable of interest: Tmax.

Monthly LST-day (ESA CCI LST - SSMI7) in 04 / 2010

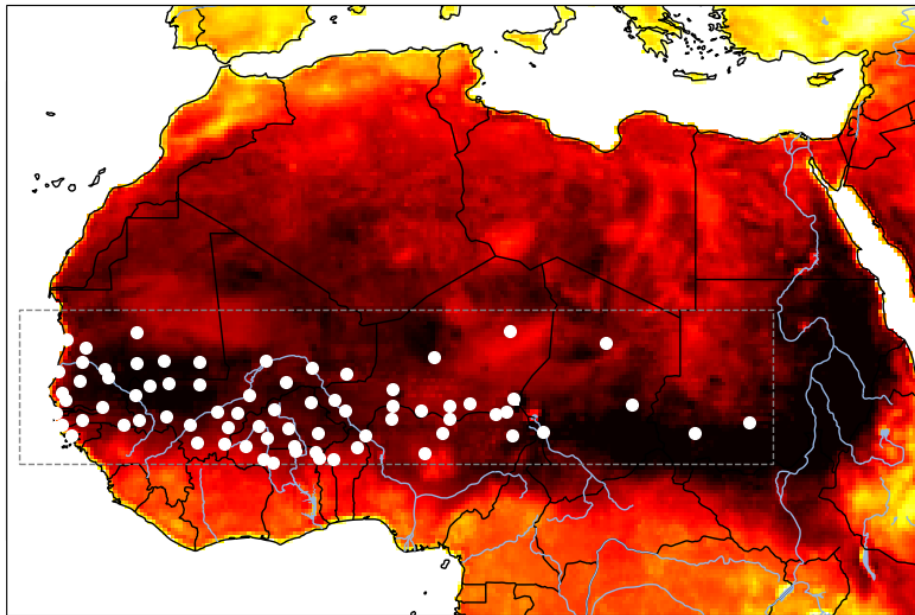


*Figure 4-5: Distribution of the 75 GSOD NOAA stations in the Sahel region.*

## Methods

### 1. TX: Monthly maximum value of daily maximum temperature

To evaluate the intensity of heat, the monthly maximum temperature index is computed. This is representative of the hottest day of the month. The monthly maximum of daily maximums (TX monthly) is first computed for the baseline (1996-2020), and then the monthly anomalies of TX are calculated for the year 2010 with respect to the baseline of 1996-2020. This choice of a 25-year baseline was made dependant on LST\_cci data availability and to encompass a sufficient number of years to provide a robust baseline for detecting changes in extremes. That baseline is retained for the calculation of anomalies for all heat extreme metrics.

For the LST-based metric, LST at 6PM (ascending orbit) is used as a proxy of maximum daily temperature, while for ERA5, the daily maximum temperature is first computed from the daily T2m datasets.

### 2. NHD: Monthly Number of hot days

The number of monthly hot days of year YY is calculated considering the number of monthly days in year YY exceeding the 90th percentile of daily maximum temperature values of each month in the considered baseline period. To avoid inhomogeneity in percentile-based indices, it is necessary to consider a fixed time days window when computing the 90th percentile baseline.

### 3. Thom's discomfort Index

To fully grasp the impact of heat on populations, it is essential to use metrics that not only consider temperature but also factor in relative humidity as the interaction between high temperatures and increased humidity levels creates a challenge for the body's cooling process, maintained through evapotranspiration. Beyond a specific thermodynamic threshold, the body faces limitations in effectively cooling.

For this study, the Thom's discomfort index [RD-32, RD-33] is chosen due to its high correlation with Wet Bulb Globe Temperature (WBGT) and its technical simplicity. It includes air temperature and relative humidity only and is defined as follows:

$$\text{Equation 4-2 } DI = (T2m - 273.15) - 0.55 * (1 - 0.01 * RH) * (T2m - 273.15 - 14.5)$$

Where:

- ❖ - RH is the relative humidity
- ❖ - T2m is the 2m air temperature

For the LST-built metric T2m is replaced with LST in Equation 4-2.

Different risk levels are associated with different values of this discomfort index.

#### **4.3.1.3. Results**

##### **1. Characterisation of the exceptionality of the 2010 Sahelian heatwave**

Sahelian observations of LST\_cci MW data indicate that the months of April and May 2010 were the 4th and 5th hottest months on land in record, respectively by 1.42°C and 1.31°C compared to the 1996-2020 climatology. The year 2010 is the first year on record for which highest values of LST are observed for at least two consecutive months. Moreover, examination of the LST-built index reveals that the Sahelian band endured extreme heat stress during this time. The risk levels derived computed from LST\_cci data align closely with those derived from the ERA5 built index, corroborating the severity of the heatwave.

##### **2. Climatology of indices**

Tx: The Maximum temperature measured by LST (Tx-LST) values are below maximum temperature captured by ERA5 T2m (Tx-T2m) during the winter months (October, November, December, January), apart from the eastern part of the Sahel (Sudan, Chad). The cooler Tx-LSTs during winter months can be explained by the lower insolation, whereas Tx-T2m is higher because the air has passed over warmer SSTs. From February a warmer trend emerges in the western part of the Sahel as well, this lasts until May. During the monsoon period (June, July, August, September) values of Tx-LST are lower than Tx-T2m apart from parts of northeastern Sahel.

Number of Hot Days (NHD): The average number of hot days exceeding the 90th percentile of each monthly baseline is higher for ERA5 (~4 days) than for LST (between 1.5 and 2.5 days). For ERA5 the highest NHD is found during the summer months as well as in December and January. While the lowest is



found in February. For LST the lowest values are found in February as well, while highest NHD are found in the coldest months (December, January, and March).

### 3. Anomalies of indices

During January and February, both ERA5-Tx and LST-Tx anomalies depict higher-than-average conditions across the entire Sahel region. This trend is mirrored in the number of hot days (NHD), with high anomalies of around +7 days observed except in parts of Mali and eastern Niger. A gradient of temperature anomalies emerges in March, with lower-than-average conditions in the eastern Sahel and higher-than-average conditions in the western part, particularly along the coast.

This pattern is consistent with the number of hot days, with elevated anomalies except in parts of central Niger, Chad, and Sudan according to ERA5 data. While this gradient persists for LST data in April, ERA5 indicates below-average conditions along the coast and above-average conditions moving northeast. Correspondingly, high anomalies in the number of hot days are observed across the Sahel, except in parts of the eastern Sahel according to LST data.

From May to September, both datasets indicate positive anomalies of Tx in the northern Sahel and highest anomalies in the western south Sahel, with cooler-than-average conditions in the southeastern Sahel. Similar patterns are observed in the number of hot days, with lower-than-average values in the western part of the Sahel and higher conditions in the northeastern part.

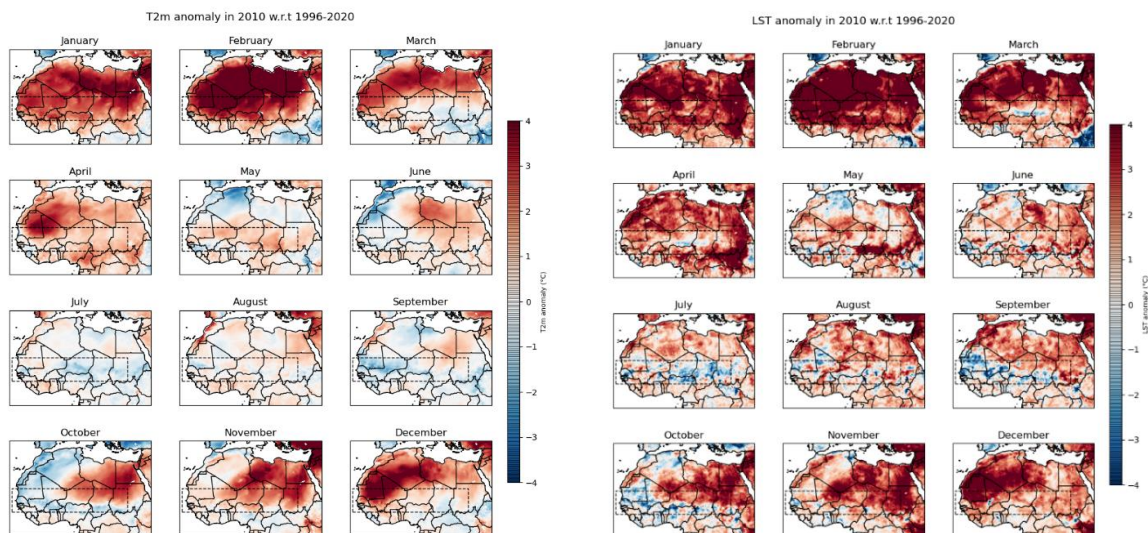


**Figure 4-6: Monthly anomalies of Tx during 2010 with respect to the 1996-2020 baseline for ERA5 T2m (left) and MW LST\_cci (right)**

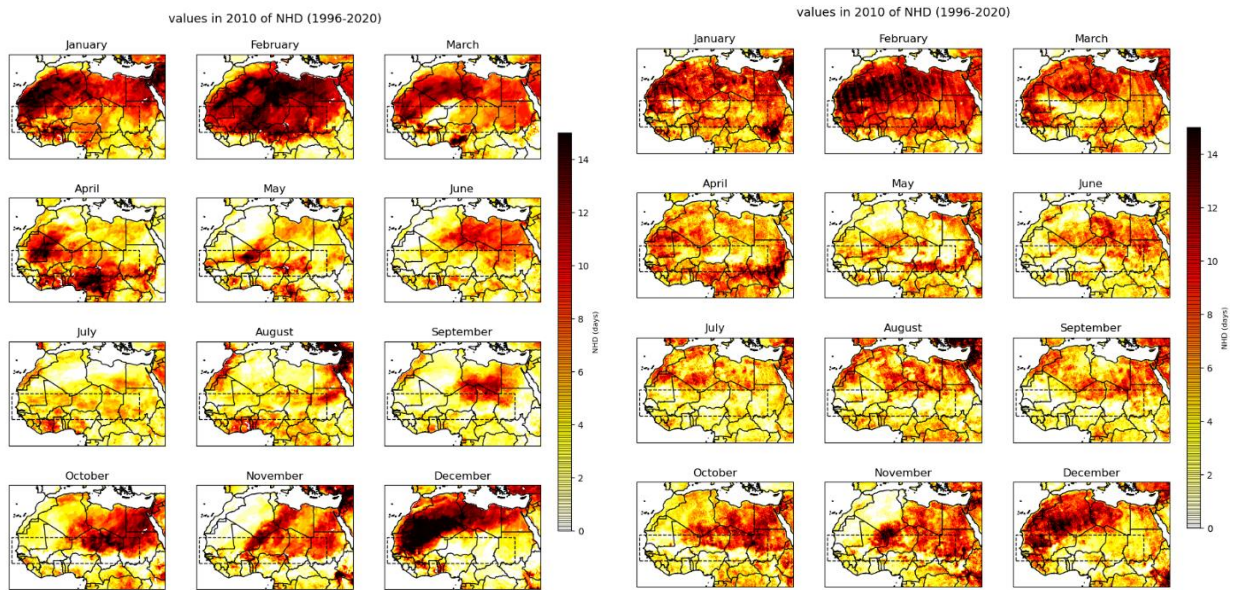


**Figure 4-7: Monthly climatology of the Number of Hot Days (NHD) over the Sahel for the period 1996-2020 using ERA5 data (left) and using MW LST\_cci data (right).**

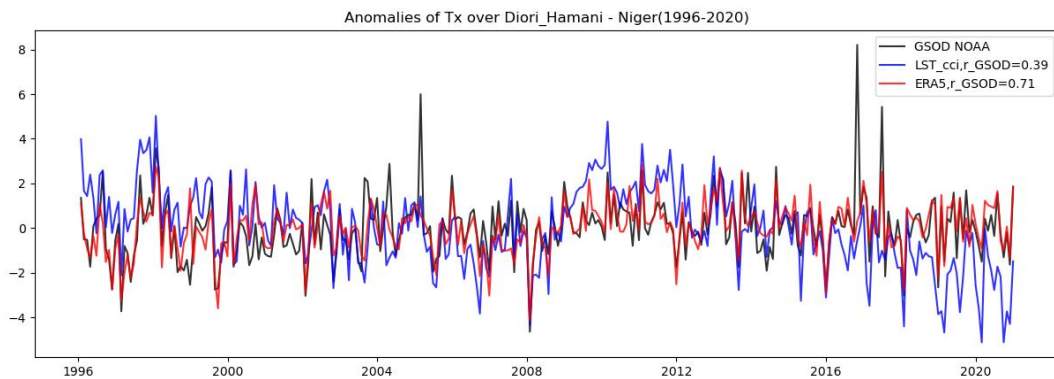


**Figure 4-8: Monthly anomaly of maximum temperature (TX) over Diiori Hamani (Niger) station for the period 1996-2020**

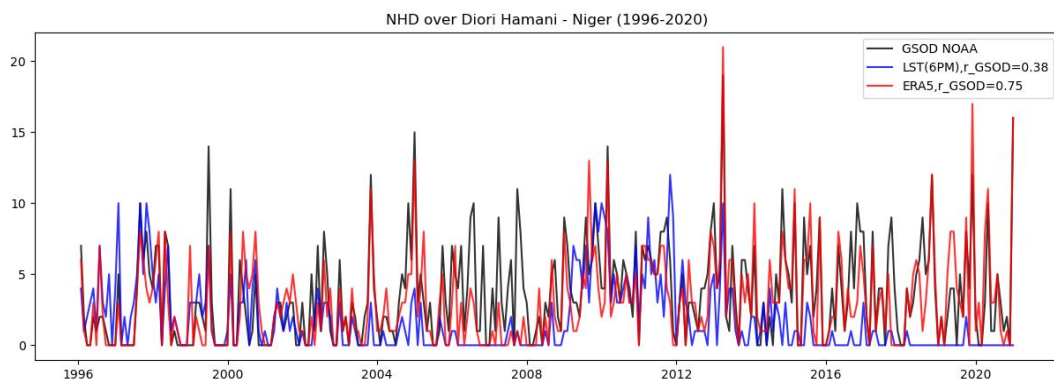


**Figure 4-9: Monthly Number of Hot Days (NHD) over Diiori Hamani (Niger) station for the period 1996-2020**

While LST\_cci and ERA5 show good coherence between the spatial patterns of anomalies during the heatwave year of 2010, results from in-situ stations show poor correlations for time series of monthly heat extreme indices computed from CCI data. As an example, the time series of anomalies of Tx and NHD plotted for Diiori Hamani station in Niger show correlations of respectively 0.38 and 0.39, while ERA5 data correlate better with station data (0.75 and 0.71).

#### 4.3.1.4. Conclusions

This study finds that the metrics computed from LST\_cci data capture well the spatial patterns of high anomalies as depicted by ERA5 reanalysis during the extreme event year. However, when it comes to comparing metrics computed from Sahelian stations of the GSOD database, results show poor correlations. For future work, this study proposes to investigate another approach as conducted by [RD-34] which consisted of computing indices in the band grouping the Sahelian stations instead of computing each index over the closest grid point to the station.

#### 4.3.2. Feedback on scientific utility of the LST\_cci products

---

The data are very easy to use but the classification of ascending/descending for day/night is not systematically explicit in the LST\_cci documentation.

It was not easy to find information on the signification of the quality flags for the MW data.

## 5. Summary of User Feedback and Response from the Science Team

This section synthesises the outcomes from the studies presented in Section 2, 3 and 4 regarding the suitability of the LST\_cci products for climate applications. The following sub-sections summarise the feedback on the utility of the LST\_cci datasets across all studies. Where appropriate, the response or course of action proposed by the LST\_cci project Science Team is also included.

### 5.1. General Feedback

The provision of multiple LST datasets in a common format and source is a major strength of the LST\_cci project. In particular, one study reports that the availability of both IR and microwave products strengthened the analysis performed and made this easier. In general, users are very positive about the LST\_cci products and find them to be of high quality and suitable for many climate applications.

Users are also very positive about the provision of auxiliary data in some LST\_cci products, including ERA5 T2m & SKT, land cover class and NDVI data, and it is suggested this provision is extended to other LST\_cci products as it may increase their uptake.

- ❖ *Response from the Science Team: The feasibility of adding these additional fields to other LST\_cci products will be assessed by the Science Team.*

Several users have reported problems in their analysis due to sparse data availability (or coverage), both due to missing data due to cloud and other quality flags, and due to the gaps between swaths. Whilst this is an inherent problem with satellite data that cannot be resolved without gap-filling, it would be useful to find a way to communicate this 'issue' to users so they are more aware of the spatial/temporal limitations of each dataset. Helpful examples of each product are provided in the Product User Guide (PUG) [AD-01] but perhaps adding some statistics for typical data availability for different latitude bands or showing a plot that indicates the % of coverage with latitude/longitude may make this clearer. In addition, there is no information in the PUG [AD-01] on how missing whole days of data are handled in the LST\_cci project and this should be added to the documentation.

- ❖ *Response from the Science Team: Information on how missing whole days of data are handled in the LST\_cci project will be added to the PUG. With the support of the LST\_cci CRG, the Science Team will also consider how additional information on data availability for each LST\_cci product could be added to the PUG in a way that is useful to users.*

### 5.2. Product-Specific Feedback

#### 5.2.1. MODIS/Aqua v4.aa

Four studies in this CAR v1 report using the LST\_cci MODIS/Aqua products; three studies use the v4.aa 0.01° latitude-longitude data, while one study uses the L2P v4.aa data. At the time of writing, no users report using the LST\_cci regridding tool to reproject these data onto a different grid resolution. User feedback on these data is as follows:



- ❖ **Product Usability and Quality:** In general, the LST data are user-friendly and of high-quality. The provision of data in NetCDF format is appreciated. One study reports that compared to earlier versions of this dataset, the provision of LST data as a single NetCDF file per day and overpass has streamlined their processing.
- ❖ **Product Accuracy:** Issues related to an incorrect emissivity being used at a test site in Valencia, Spain have been reported by one study, which results in an overestimation of LST at this location by ~2 K. In addition, one study finds that the prototype Ice Surface Temperature (IST) retrievals in the North Atlantic are cold-biased by up to 4 K when compared with in situ T2m observations from buoys.
  - *Suggested Action for the Science Team: Investigate whether improved emissivity data can be used in the IR LST\_cci products. Investigate whether the accuracy of the IST retrievals can be significantly improved.*
    - ◆ *Response from the Science Team: This emissivity issue is a known problem that the team have uncovered with the CAMEL emissivity datasets that are used to generate the product. LST\_cci v3 used CAMEL V2, and LST\_cci v4.aa used CAMEL V3. Both are unstable in time and do not represent some surface types accurately, such as the Valencia test site. In the short-term, the CAMEL V2 climatology will be used in v4.00 (noting this is worse at the Valencia site) because the stability in the climatology is preferable compared to the unstable CAMEL V3. Long-term, an optimal estimation approach will be used for MODIS to retrieve LST and emissivity per pixel. The team will also continue to work on improvements to the sea-ice temperature data, noting that this is first version of these data in LST\_cci and therefore these data represent a prototype that is still under development.*
- ❖ **Cloud Contamination:** The MODIS/Aqua cloud contamination issues identified during LST\_cci Phase-1 appear to have been successfully addressed.
- ❖ **LST Uncertainties:** The availability of LST uncertainties enables these data to be incorporated into the analysis effectively and update them with the subsampling uncertainty (i.e. the uncertainty due to missing grid cells). Provision of uncertainties is also useful to enable users to filter-out LSTs with particularly high uncertainties. However, it was noted in one study that the uncertainties in v4.aa are much larger over in Iberian Peninsula compared to the values provided in earlier versions of the product, which is confusing for users.
  - *Suggested Action for the Science Team: Check whether the uncertainties (up to 5 K) over the Iberian Peninsular (and potentially other regions) are as expected and update documentation to communicate to users the expected range of uncertainty values.*
    - ◆ *Response from the Science Team: The increase in LST uncertainty over the Iberian Peninsula (and potentially elsewhere) is related to the change in version of the CAMEL emissivity database used in the retrieval (as noted above).*
- ❖ **Provision of Auxiliary Data:** At least two studies noted that the provision of auxiliary data in the files, e.g. ERA5 T2m & SKT, and NDVI, on the same grid as the LST data has been very useful.

### 5.2.2. SLSTR/Sentinel-3B v3.0

Only one study reports using the LST\_cci SLSTR-B/Sentinel-3 v3.0 product. At the time of writing, no users report using the LST\_cci regridding tool to reproject these data onto a different grid resolution. User feedback for these data is as follows:

- ❖ **Cloud Coverage and Contamination:** The unavailability of data due to cloud coverage and the presence of significant cloud contamination in this product has prevented the data from being used in one study.
- *Suggested Action for the Science Team: Improve cloud screening in the SLSTR products and update product documentation with more detailed information data availability (coverage) that users can expect (also see 'General Feedback' in Section 5.1).*
  - ◆ *Response from the Science Team: The cloud screening has been improved in v4.00 of this product (recently added to the Jasmin public folder). With the support of the LST\_cci CRG, the Science Team will also consider how additional information on data availability for each LST\_cci product could be added to the PUG in a way that is useful to users (also see Section 5.1).*

### 5.2.3. SLSTR/Sentinel-3A & -B v4.aa

Three studies report using the LST\_cci SLSTR-B/Sentinel-3 v4.aa product. Two studies use the 0.01° data, while one study uses the L2P product. At the time of writing, no users report using the LST\_cci regridding tool to reproject these data onto a different grid resolution. User feedback on these data is as follows:

- ❖ **Product Usability and Quality:** The LST\_cci products are user-friendly and of a very high quality. Provision in NetCDF format is appreciated. However, one study reports that the provision of LST data as a single NetCDF file per diurnal cycle has made processing the data more challenging due to the large data volumes.
- *Suggested Action for the Science Team/ESA/CEDA: Investigate whether it is possible to provide data regionally, i.e. using user-defined cut-outs, rather than only as global products.*
  - ◆ *Response from the Science Team: Sub-setting of the data can be performed by the regridding tool provided by the LST\_cci project ([https://climate.esa.int/en/projects/land-surface-temperature/#\\_about-tab](https://climate.esa.int/en/projects/land-surface-temperature/#_about-tab)). Unfortunately, different regional datasets cannot be supported by the ODP.*
- ❖ **Product Accuracy:** As for the MODIS/Aqua v4.aa LST\_cci products, issues related to an incorrect emissivity being used at a test site in Valencia, Spain have been reported by one study, which results in an overestimation of LST at this location by ~1.5 K. In addition, one study finds that the prototype Ice Surface Temperature (IST) retrievals in the North Atlantic are cold-biased by up to 4 K when compared with in situ T2m observations from buoys.
- *Suggested Action for the Science Team: Investigate whether improved emissivity data can be used in the IR LST\_cci products. Investigate whether the accuracy of the IST retrievals can be improved significantly.*
  - ◆ *Response from the Science Team: This emissivity issue is a known problem that the team have uncovered with the CAMEL emissivity datasets that are used to generate the product. LST\_cci v3 used CAMEL V2, and LST\_cci v4.aa used CAMEL V3. Both are unstable in time and do not represent some surface types accurately, such as the Valencia test site. In the short-term, the CAMEL V2 climatology will be used in v4.00 (noting this is worse at the Valencia site) because the stability in the climatology is preferable compared to the unstable CAMEL V3. Long-term, an optimal estimation approach will be used for MODIS to retrieve LST and emissivity per pixel. The team will also continue to work on improvements to the sea-ice temperature data, noting that this is first version of these data in LST\_cci and therefore these data represent a prototype that is still under development.*

- ❖ **Cloud Contamination:** As noted for v3.0, there are notable outliers in the v4.aa product, which are likely due to cloud contamination.
  - *Suggested Action for the Science Team: Improve cloud screening in the SLSTR products and update product documentation with more detailed information data availability (coverage) that users can expect.*
    - ◆ *Response from the Science Team: The cloud screening has been improved in v4.00 of this product (recently added to the Jasmin public folder). Some of the outliers observed may also be due to issues with the SLSTR input L1 data. There is no systematic filtering of bad datafiles (such as during decontaminations, blackbody crossover tests, etc) in the online quality control from the ground segment. This is a known issue, and a fix has now been implemented moving forward. Thus, it is currently an entirely manual process to try to filter out these bad datafiles. The Science Team will investigate how the post-filtering of the L1B can be improved.*
- ❖ **Provision of Auxiliary Data:** As for the MODIS LST\_cci products, inclusion of auxiliary data from ERA5 (e.g. T2m) and land cover classification on the same grid as the LST data has been very useful. However, unrealistic changes in land cover classification between neighbouring days have been observed in one user case study that need investigating by the Science Team.
  - *Suggested Action for the Science Team: Check the land cover classifications in the LST\_cci products for unrealistic changes over very short periods of time and correct as appropriate.*
    - ◆ *Response from the Science Team: This is caused by a variable swath (within a repeat cycle) using a nearest neighbour approach to select the land cover classification from a static map. As the orbit progresses, the cells selected from the static land cover classification map can vary from day to day, with the same pattern of changes occurring with each repeat orbit cycle. A potential solution to this problem would be to use a 'spatially static regrided' land cover classification map in the final L3C product that matches the L3C LST spatiotemporal resolution. (Note that 'spatially static regrided' data in this context refers to land cover data that have been regrided onto a regular grid that matches the relevant L3C LST grid, but still includes realistic dynamic land cover changes, e.g. from one month to the next.) Updating the land cover classification auxiliary data in the LST\_cci files in this way will be considered for future versions of the product.*

#### 5.2.4. IRMGP v1.00

Only one study has utilised the IRMGP product. At the time of writing, no users report using the LST\_cci regridting tool to reproject these data onto a different grid resolution. User feedback is as follows:

- ❖ **Product Quality:** Some time steps include valid LST data in the ocean around the American continent; this may also be a problem in other areas and appears to affect multiple files.
  - *Suggested Action for the Science Team: Check for occurrences of valid LSTs over the ocean and correct as required.*
    - ◆ *Response from the Science Team: This is a known legacy issue from an earlier version of this product where there was an error in the regriding process. It is thought some files with this regriding error from an earlier version of this dataset were erroneously included in the official v1.00 product release. The dataset will be corrected and updated as soon as possible.*



### 5.2.5. SSM/I & SSMIS MW product v2.33

In LST\_cci Phase-1, only one study utilised the MW LST\_cci product. However, there has been good uptake of these data since Phase-1 and this report includes five separate studies that have utilised the v2.33 product, which is available on both the ESA ODP, CEDA and Jasmin public folder. No studies have yet trialled the v4.11 SSM/I & SSMIS product, or the new AMSR-E/AMSR-2 product, which are only available via the Jasmin public folder. However, some of the feedback below will also be relevant to these products. At the time of writing, no users report using the LST\_cci regridding tool to reproject these data onto a different grid resolution.

- ❖ **Product Usability and Quality:** In general, users report that the product is easy to use and provides useful data.
- ❖ **Product Documentation:** At least two users report that the documentation is unclear in indicating which orbit, i.e. ascending or descending, corresponds to the nominal ~6am or pm overpass times. Information on the significance (recommended utility) of the product quality flags is also hard to find. In particular, use of the flag ‘Possibility of inundated land’ flag results in stippled data availability in some regions, that users may find questionable/not understand. Users are also finding that even though this product is ‘all sky’, the data availability (or coverage) is still quite low in some regions due to filtered data and the gaps between adjacent swaths. Finally, it is not clear in the documentation how missing days of data are handled in the LST\_cci products (e.g. two whole days of data are missing in the MW LST product archive) and this should be included in the documentation.
  - *Suggested actions for the Science Team: Update documentation to indicate ascending/descending orbit times more clearly, provide advice on how users should best utilise the quality flags and provide more detailed information on data availability (coverage), so users know what to expect, including how missing whole days of data are handled (also see ‘General Feedback’ in Section 5.1). Some information, e.g. overpass times for ascending/descending orbits, could also be included in the NetCDF files global attributes.*
- ❖ **Product Accuracy:** One user study has obtained unrealistic trends using these data (based on all available years of data), where 1) the global trend is too close to zero (i.e. too small) and 2) large regions appear to have unrealistic negative trends. This result for the global trend contradicts similar results obtained by the LST\_cci project team.
  - *Suggested actions for the Science Team/CRG: Liaise with the user to better understand this result (obtained by the user) and how/why the analysis appears to contradict the same type of results obtained by the Science Team/CRG.*
- ❖ **Auxiliary Data:** Unlike for the IR LST\_cci products, there are no auxiliary data provided in the MW LST files. Provision of e.g. ERA5 T2m & SKT, land cover class and NDVI would be useful to users.
  - *Suggested actions for the Science Team: Provide ERA5 T2m & SKT, land cover class and NDVI (as per the LST\_cci IR products) in the MW LST products.*
    - ◆ *Response from the Science Team: As stated above, the feasibility of adding these additional fields to other LST\_cci products in future will be considered by the Science Team. However, it should be noted that adding these additional fields into the MW LST products is more complex than for the IR products. Auxiliary ERA5 and NDVI data are used in the retrieval and production of the IR LST datasets and can consequently be written to the LST data files quite easily. As these auxiliary data are not part of the MW LST data processing, it would therefore require a substantial update the processing software to add these data to the MW LST data files.*



***End of document***